FIGURE 5–6
The hydrologic cycle.

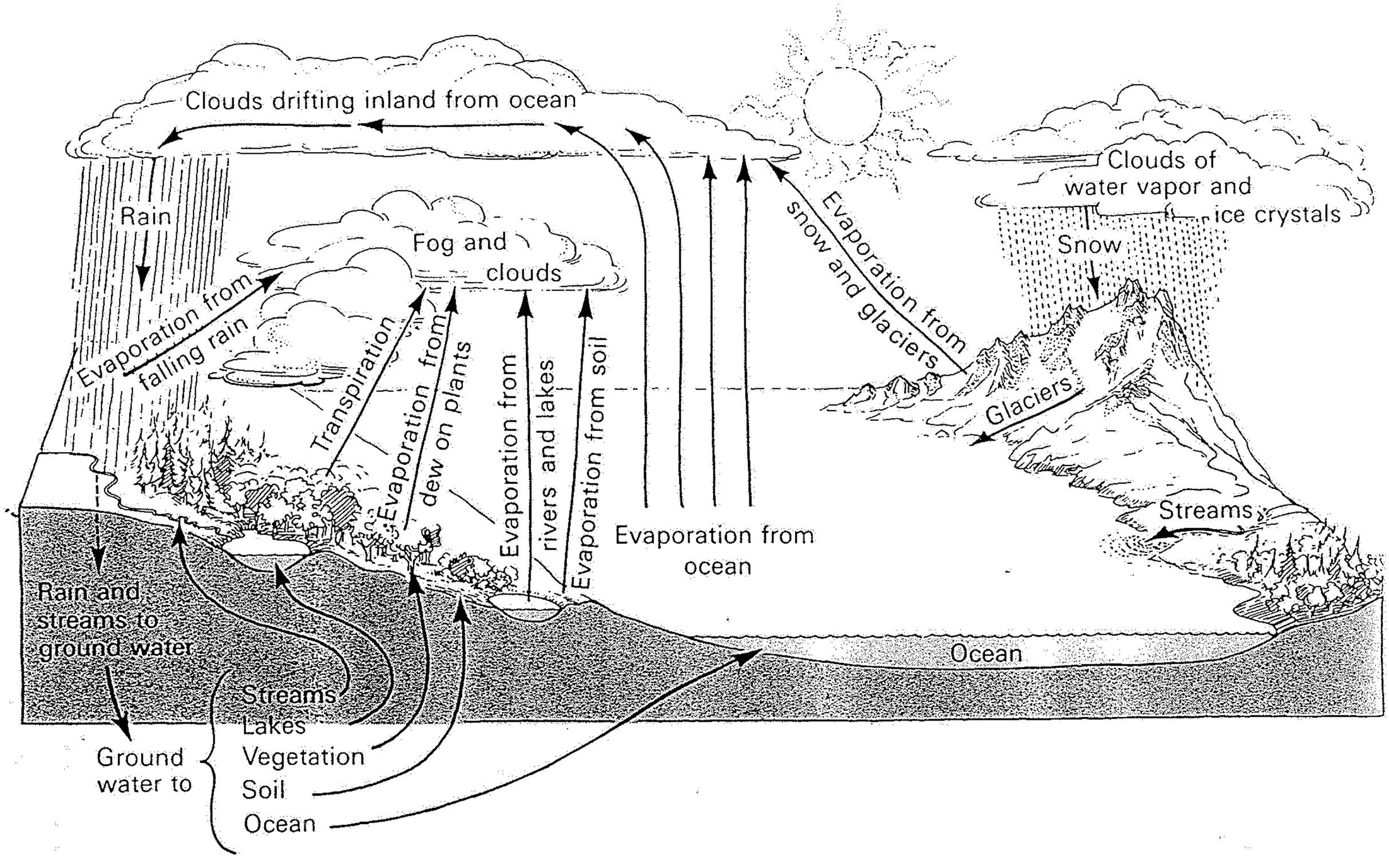

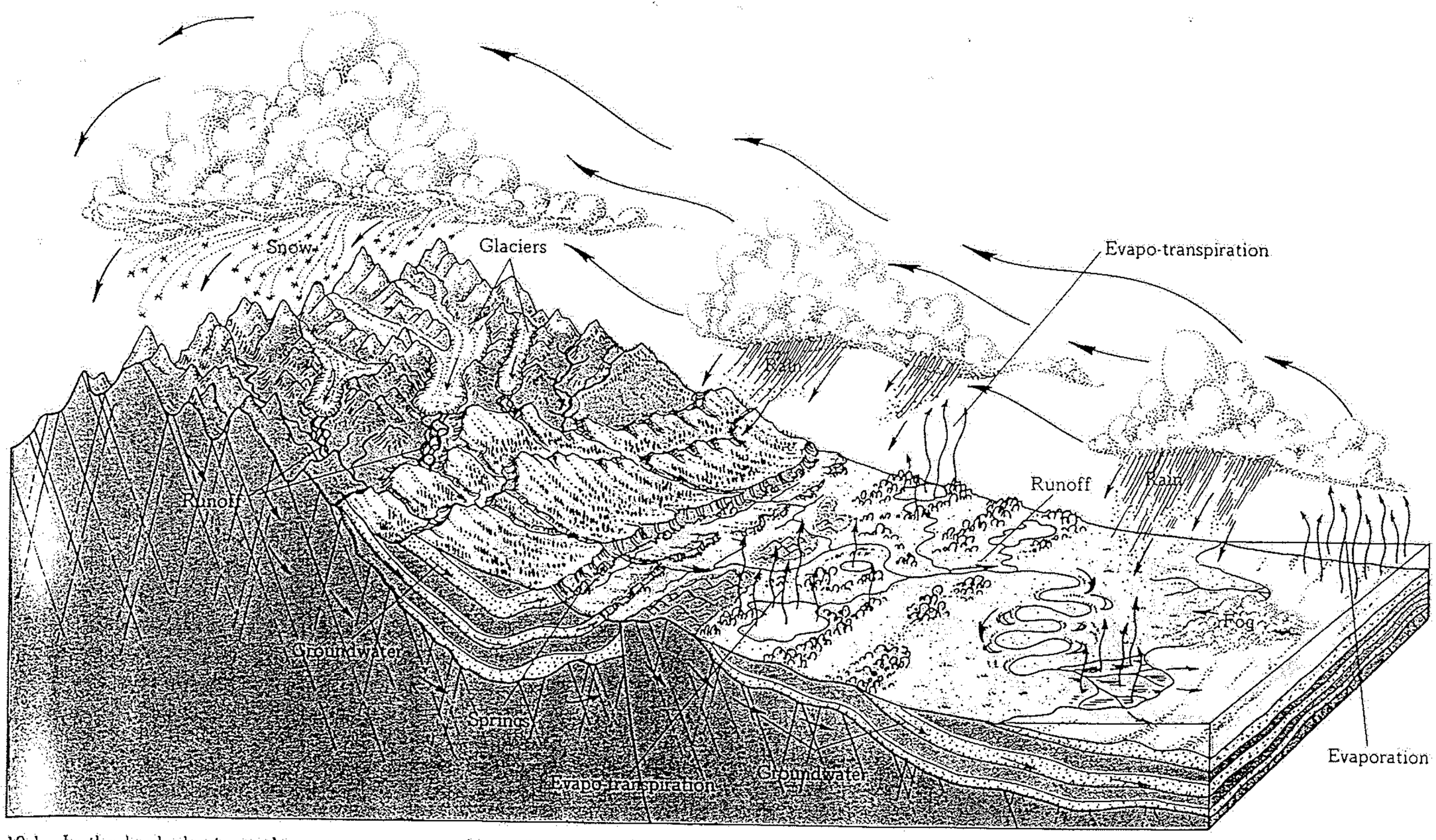

13.1 In the hydrologic cycle water evaporated into the atmosphere reaches the land as rain or snow. Here it may be temporarily stored in glaciers, lakes, or the underground before returning by the rivers to the sea. Or some may be transpired or evaporated directly back into the atmosphere before reaching the sea.

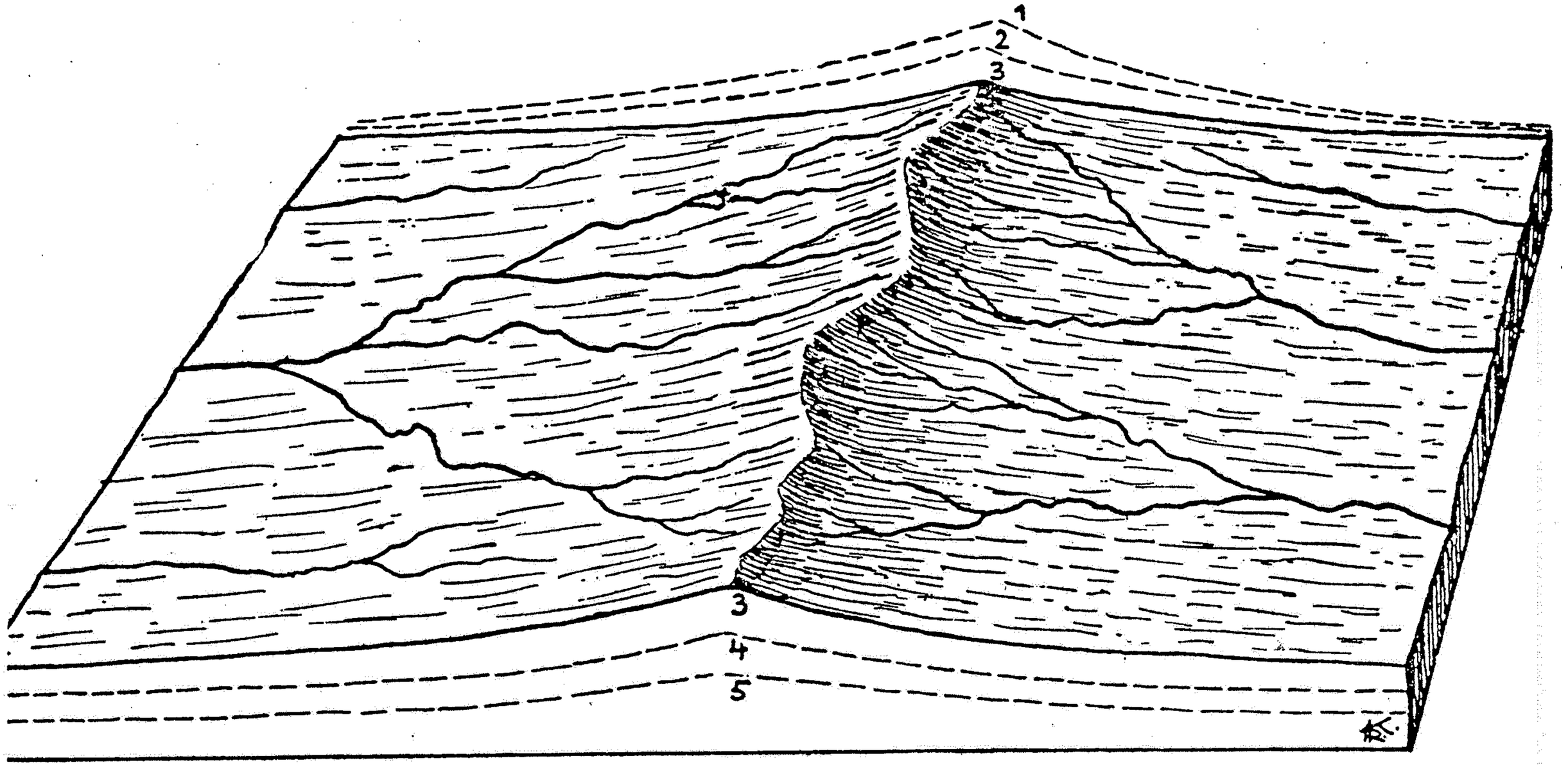

Obr. 50. *Blokdiagram, znázorňující rozvodí a postupné snižování hřbetu účinkem erose. Čáry* 1. *a* 2. *značí dřívější profily rozvodím, čáry* 4. *a* 5. *značí budoucí profily rozvodím.*
(Podle R. E. Flinta.)

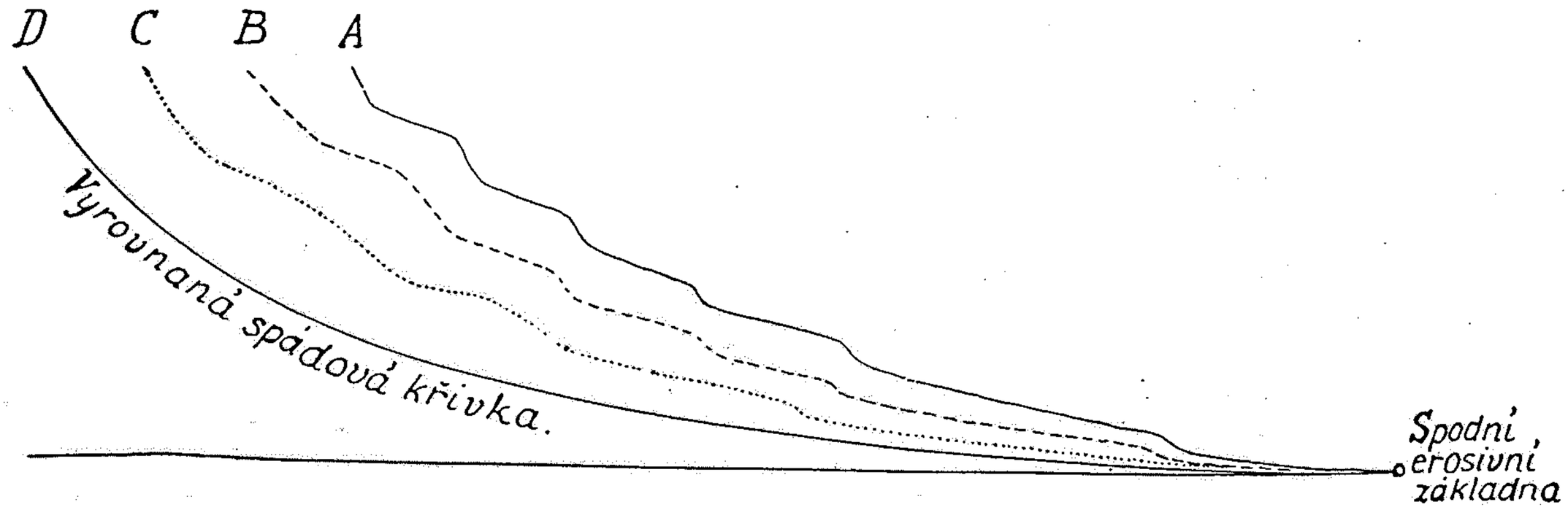

Obr. 48. *Přeměna nevyrovnané spádové křivky údolí ve křivku vyrovnanou působením hloubkové a zpětné erose.*

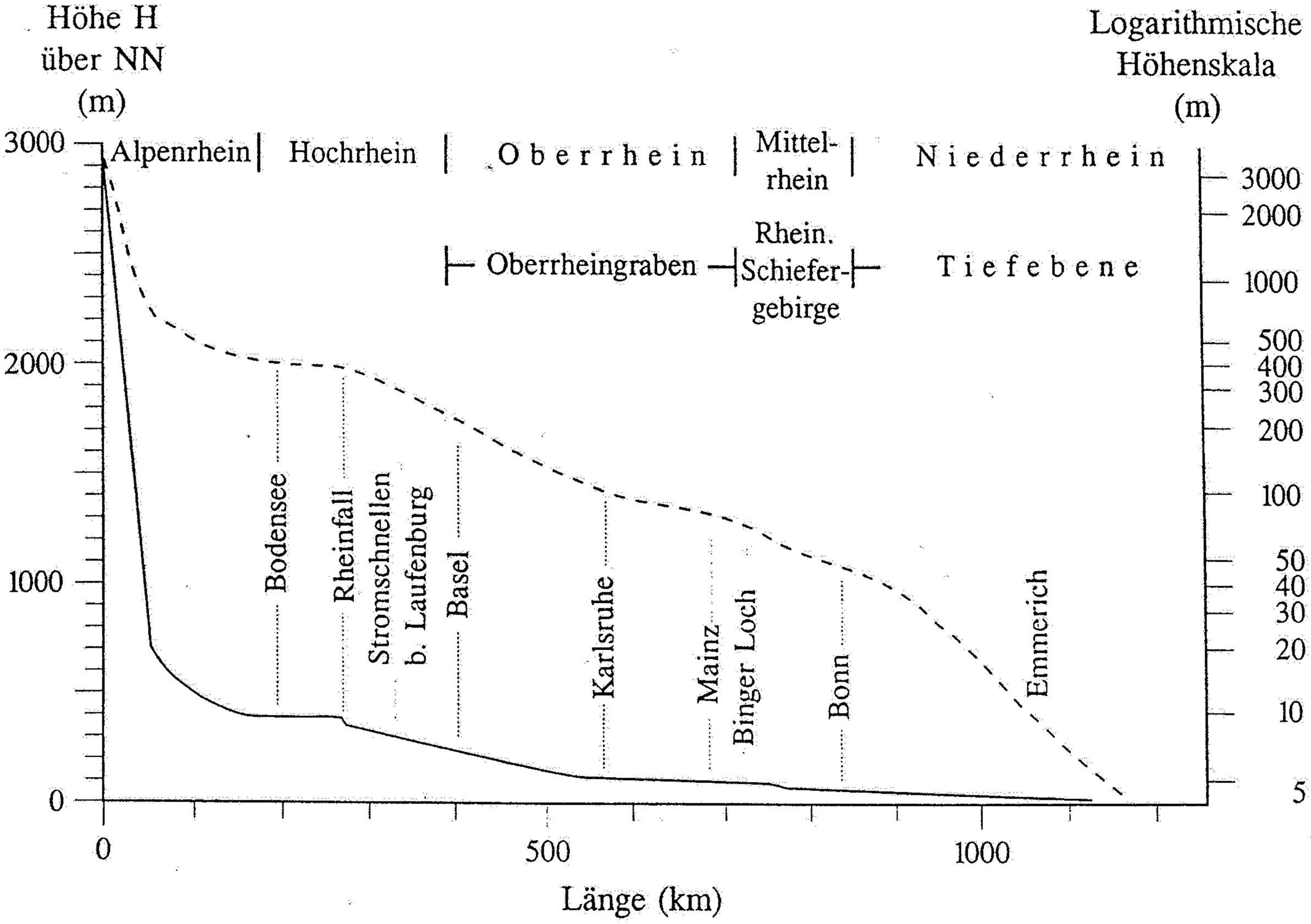

250fach überhöhtes Längsprofil des Rheins mit **(a)** linearer Höhenskala, **(b)** mit logarithmischer Höhenskala. Kurve a zeigt, daß der Rhein das Ausgleichsgefälle noch nicht erreicht hat. Sowohl der Bodensee als auch das Rheintal oberhalb von Bingen stellen regionale Erosionsbasen dar. Die logarithmische Skalierung betont insbesondere die geringen Gefälleunterschiede im Unterlauf des Rheins (nach AHNERT, 1996).

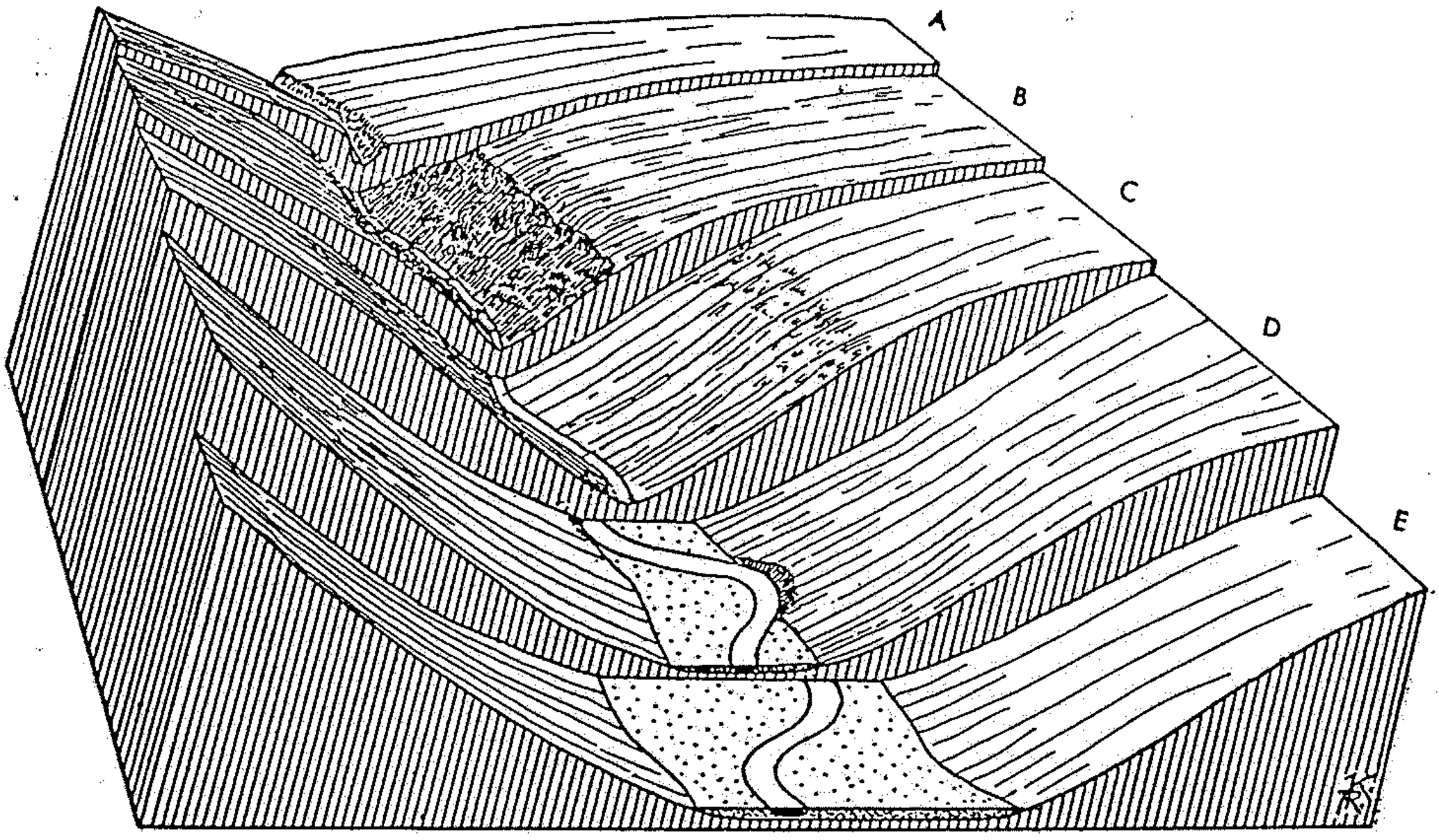

Obr. 55. *Postupné prohlubování a rozšiřování údolí po proudu řeky a vznik údolní nivy.* (Podle W. M. Davise.)

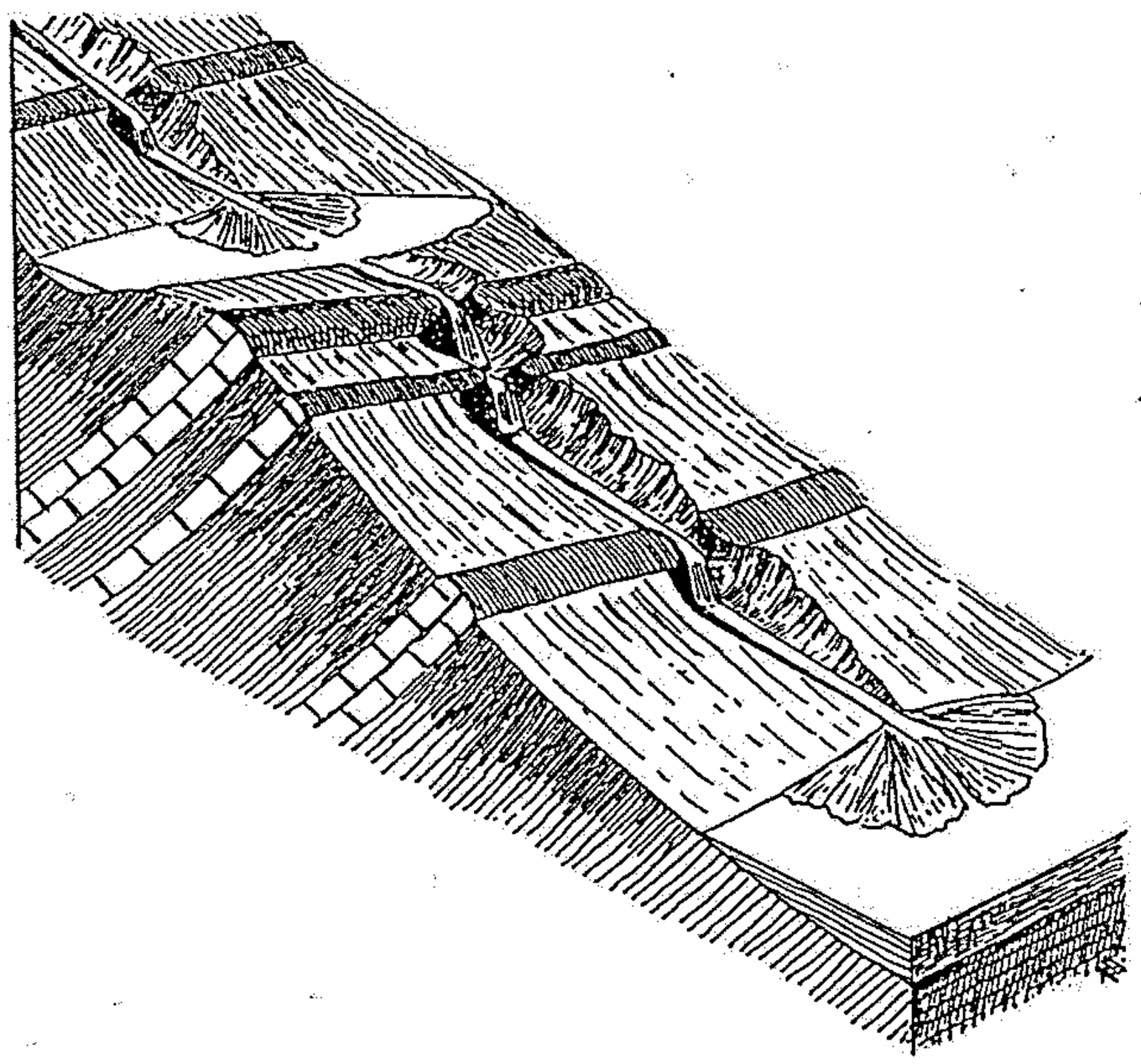

Obr. 65. *Vznik vodopádů na tvrdých lavicích a vyrovnávání spádu koryta mezi jednotlivými tvrdými lavicemi; usazování naplavených kuželů.* (Upraveno podle W. M. Davise.)

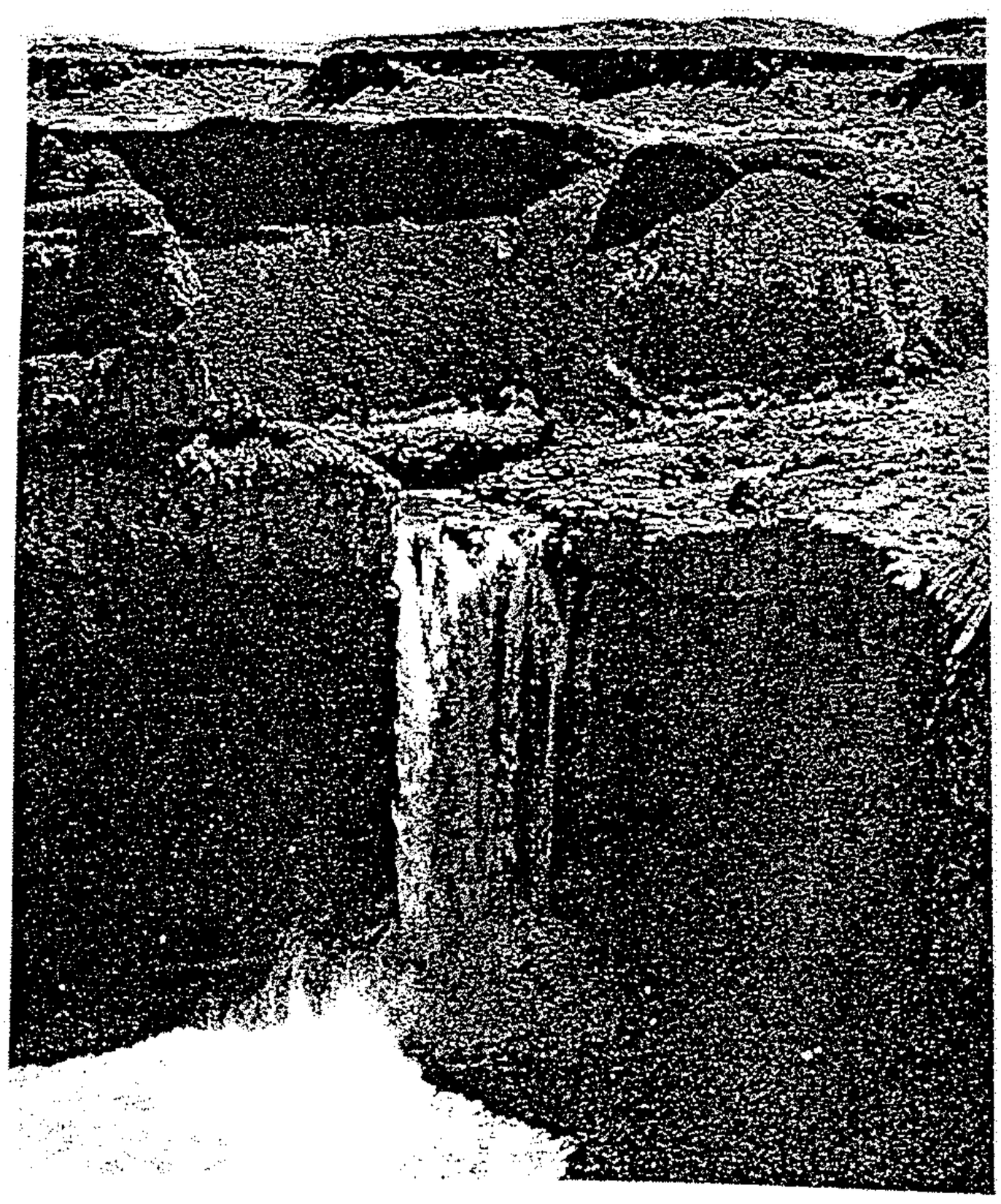

The Palouse Falls on the Palouse River, Washington, are held up by a resistant layer of basalt. (Photograph by F. O. Jones, U.S. Geological Survey)

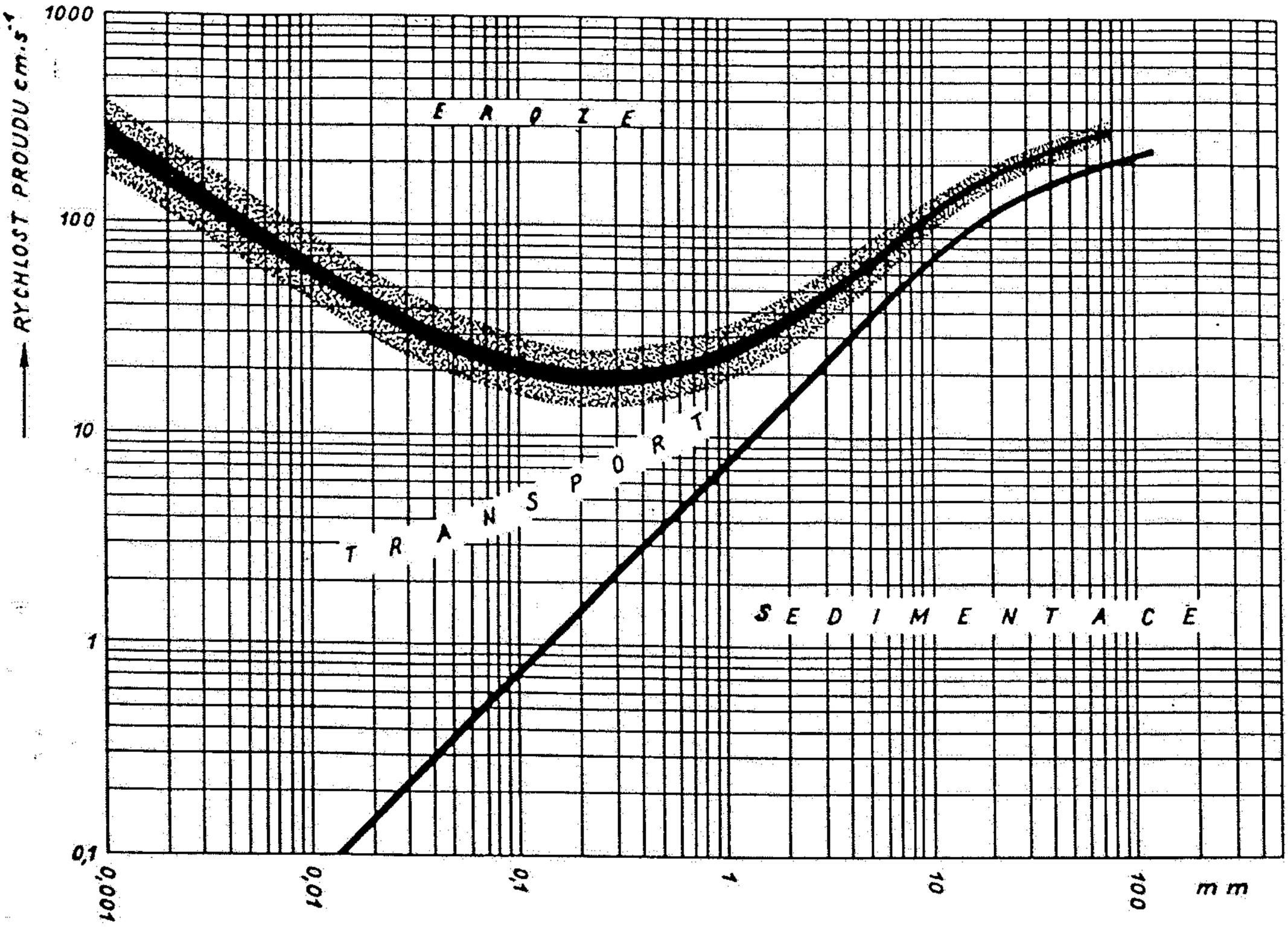

Hjulströmův diagram, ukazující vztah rychlosti proudu k velikosti erodovaných, transportovaných a sedimentovaných částic. Vyjádřeno v logaritmické síti.

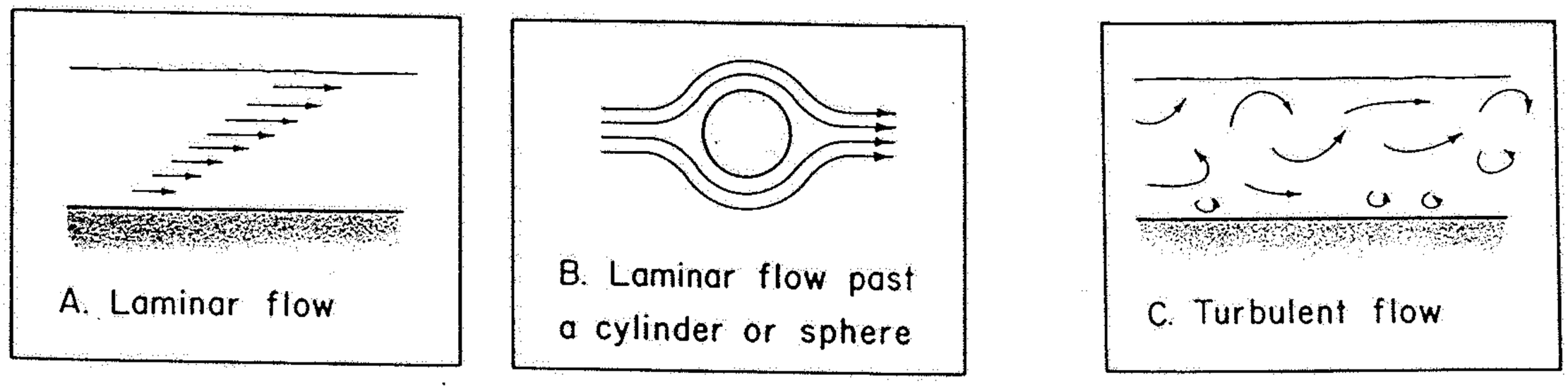

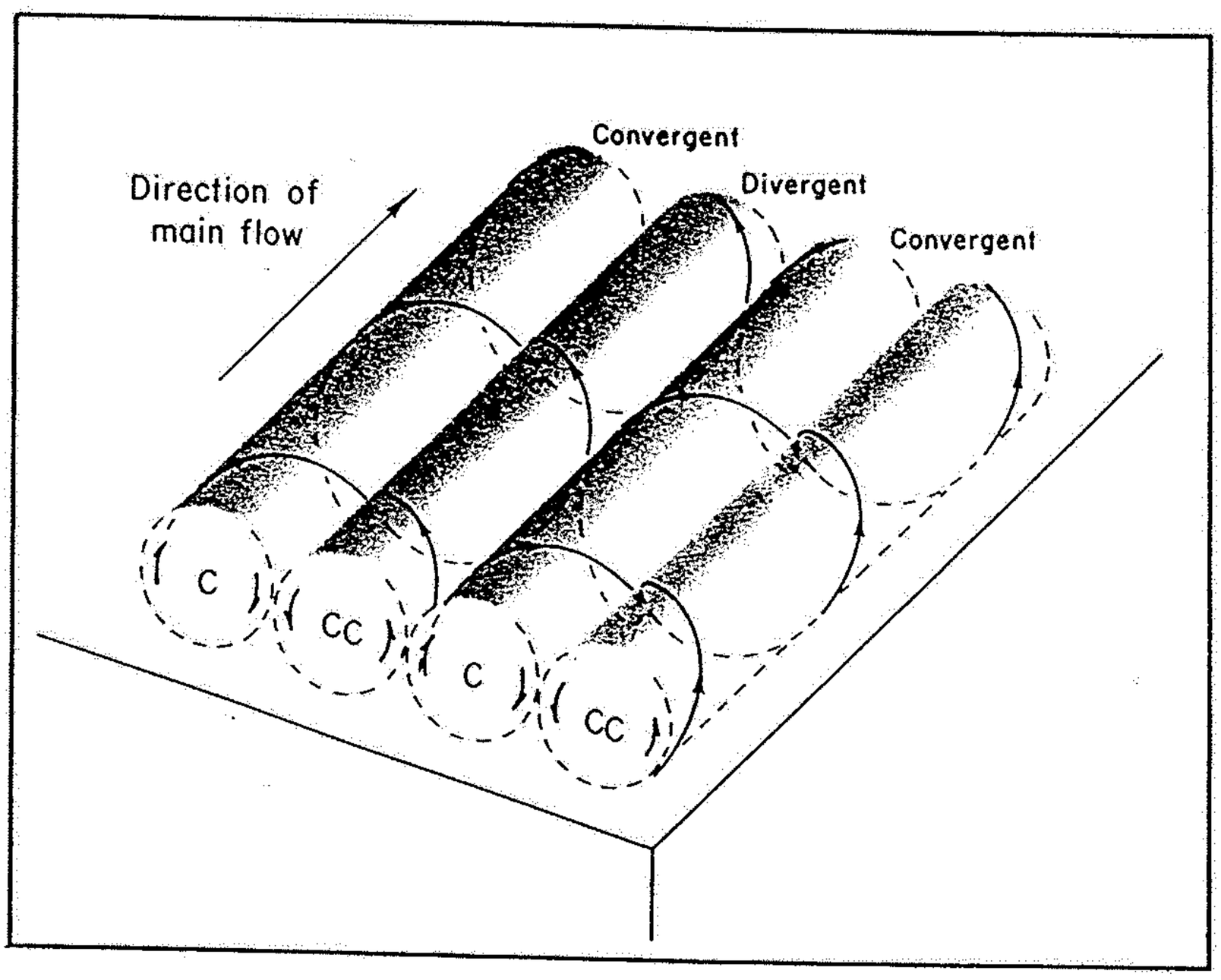

Figure 4-15 *Schematic block diagram through base of body of fluid undergoing turbulent flow in which boundary layer has developed a secondary flow pattern including helicoidal lines of flow (arrows). Small curved arrows at "ends" of "cylinders" show sense of rotation in each "cylinder." Further explanation in text. (Modified from S. Dzulynski, 1965, Fig. 3, p. 197.)*

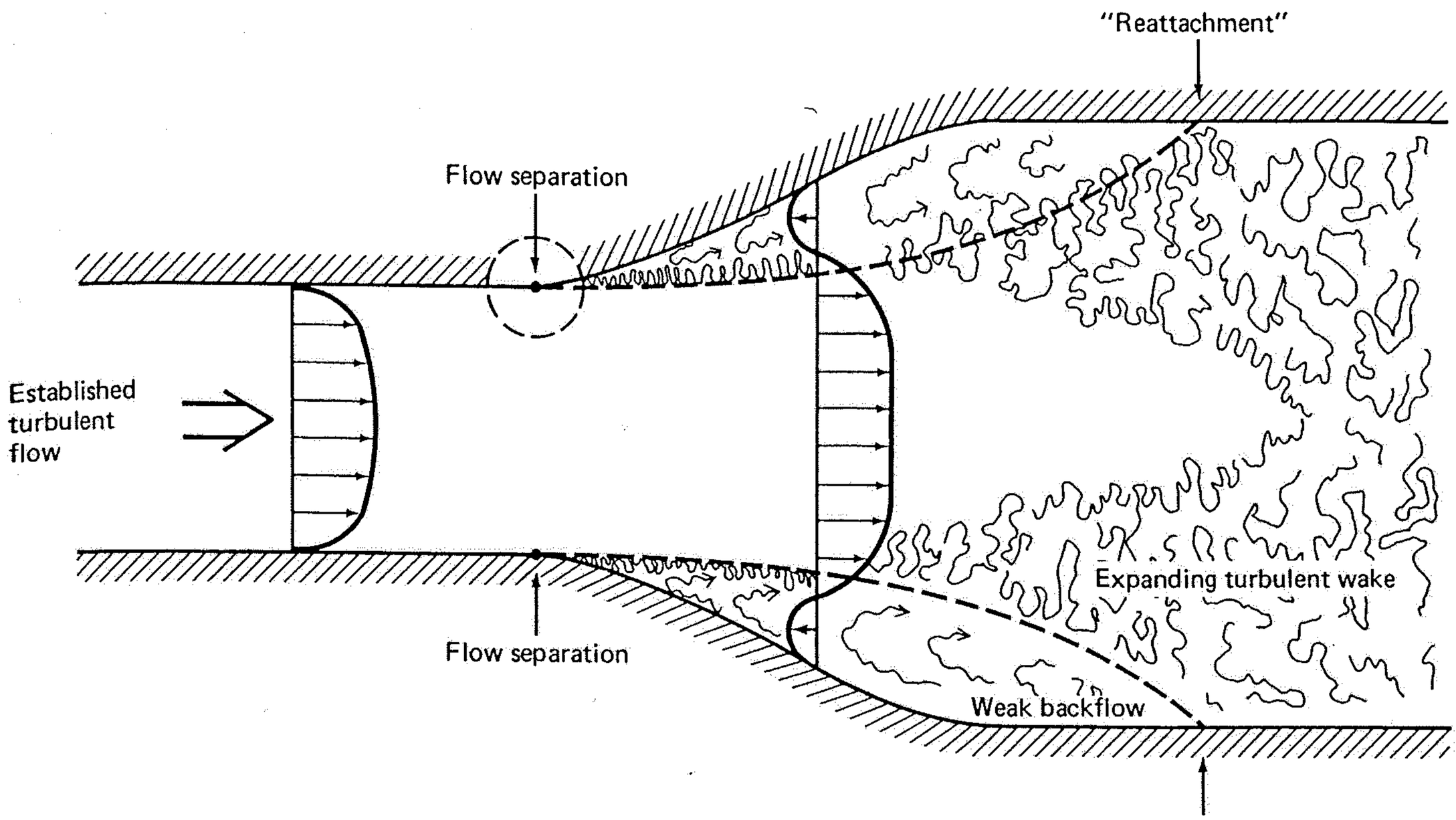

Figure 2-6 Flow separation as it occurs in flow through a pipe with a change in diameter. (From Middleton and Southard, 1977, p. 3.24.)

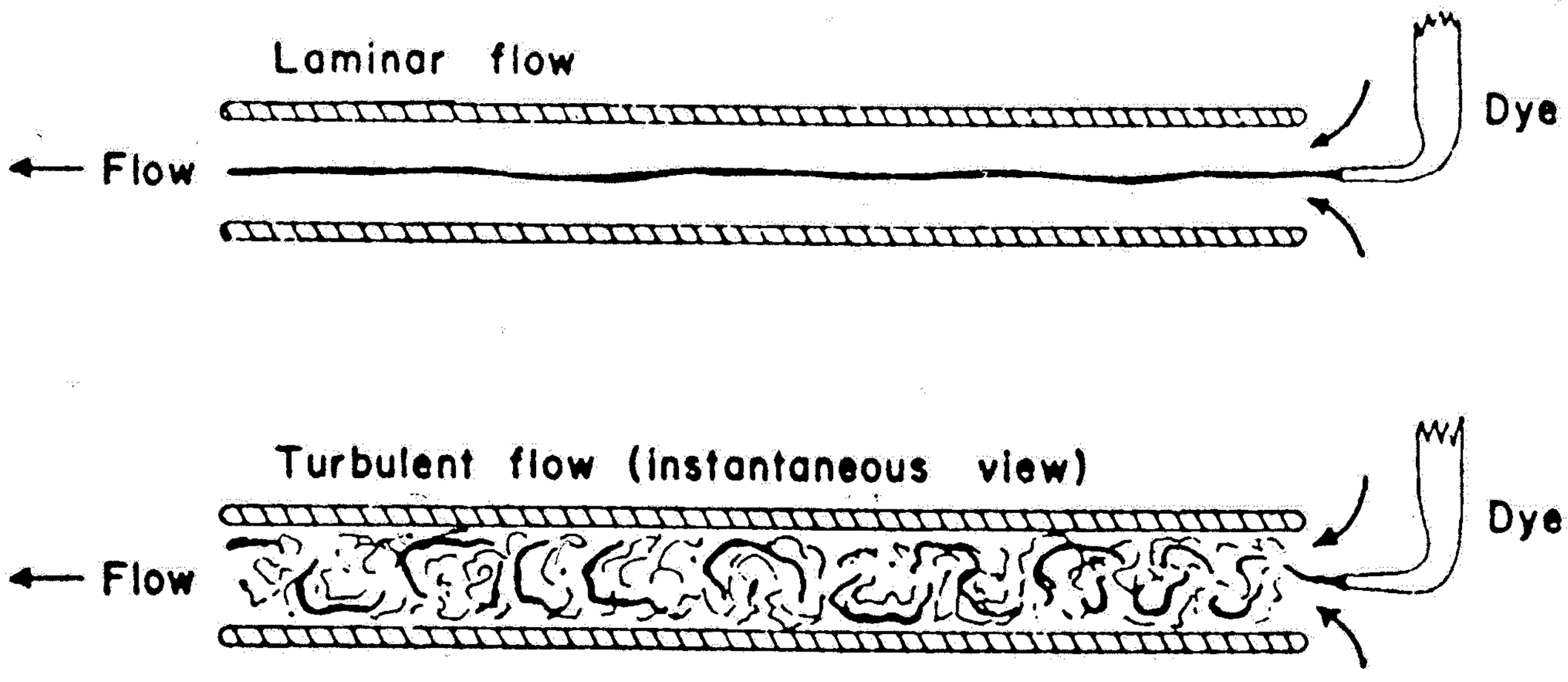

Figure 2-4 Reynold's experiment showing laminar and turbulent flow as dye is passed through a tube. (From Allen, 1970a, p. 33.)

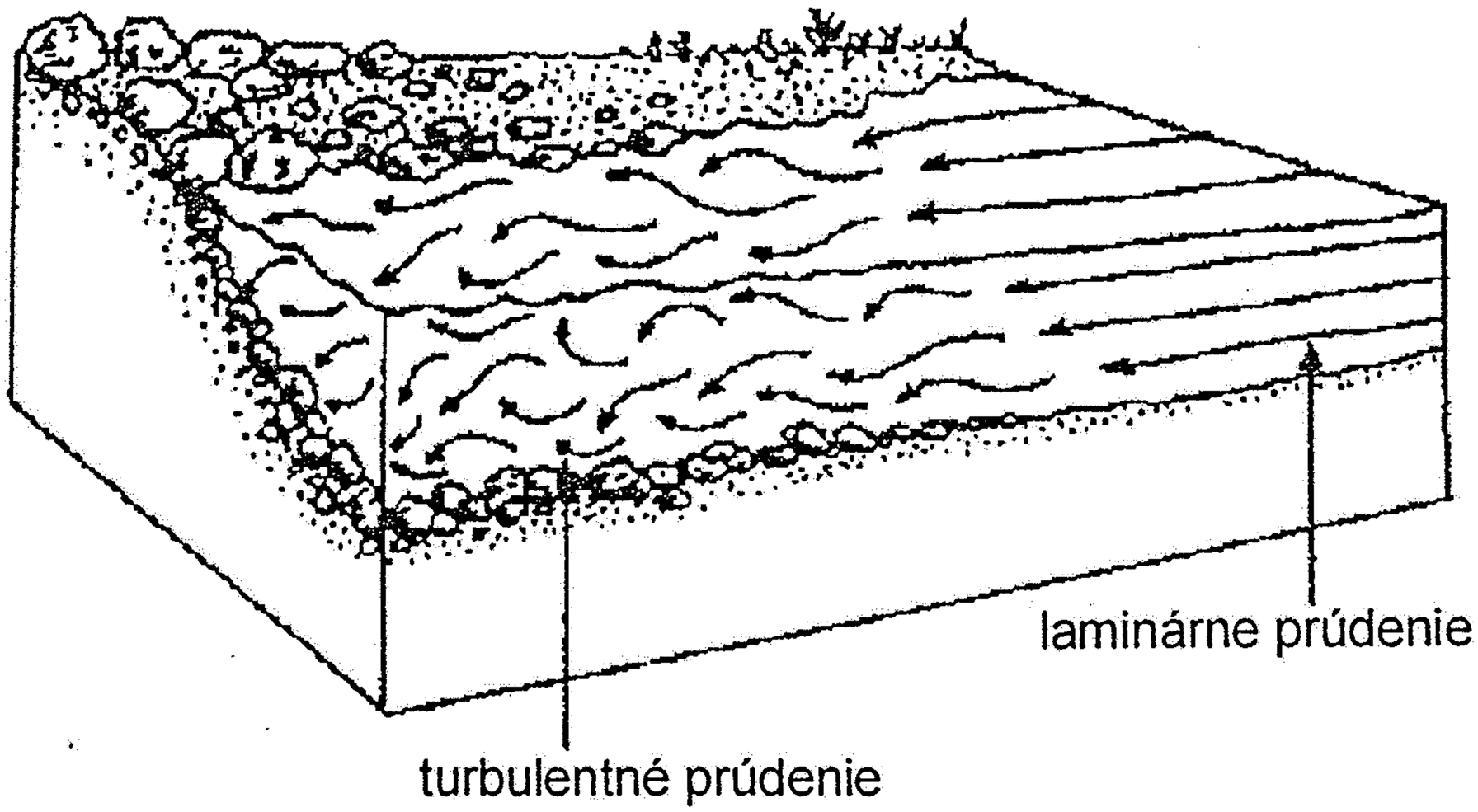

Obr. 16.2. Laminárne a turbulentné prúdenie v koryte rieky. (prevzaté z Prokešovej 1998)

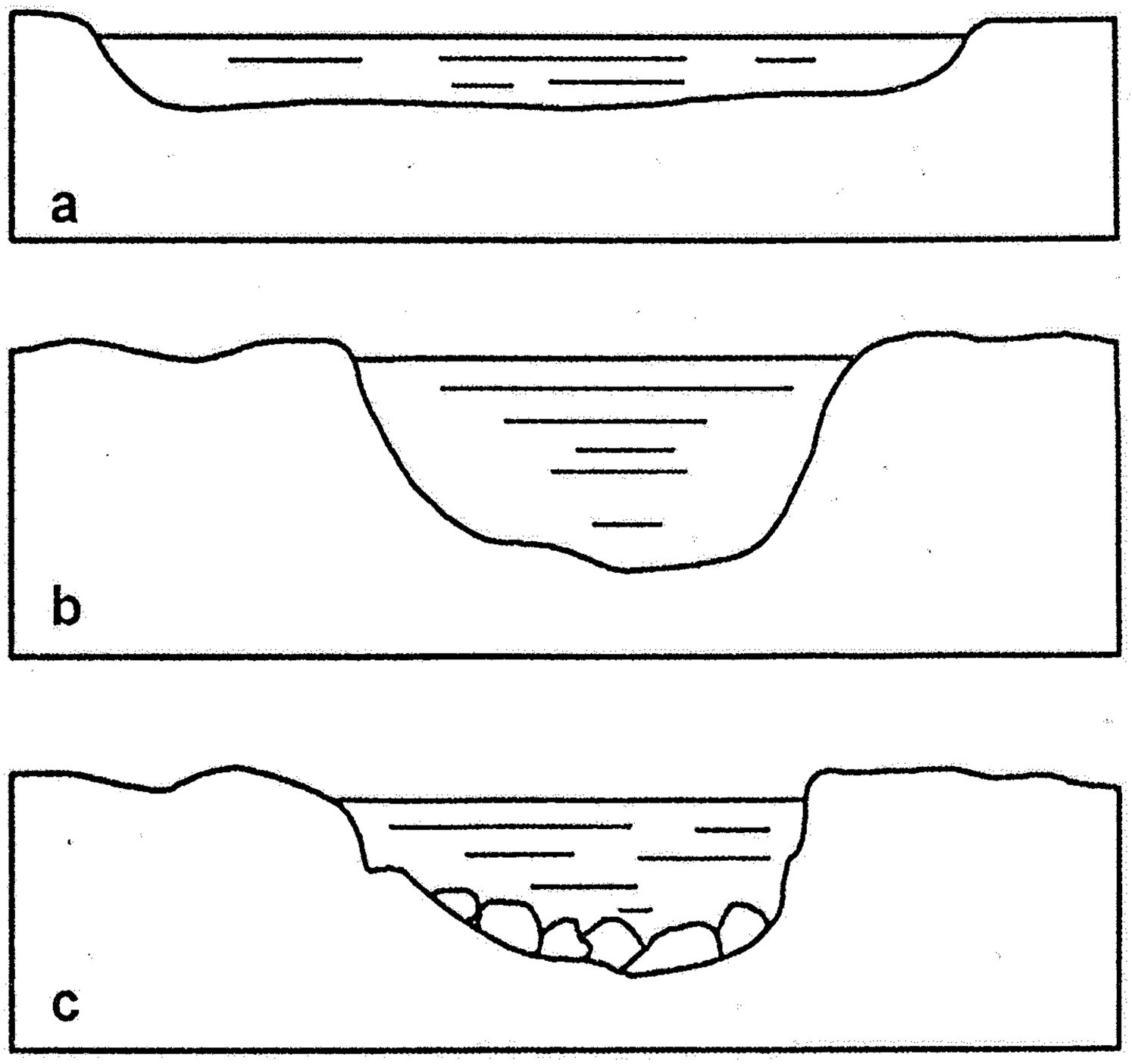

Obr. 16.3. Najvyššiu rýchlosť tok dosiahne v hladkom, poloblúkovitom koryte (b). Rýchlosť spomaľuje zväčšená dĺžka omočeného profilu (a) a drsnosť brehov a dna (c). (podľa Plummera – McGearyho 1996)

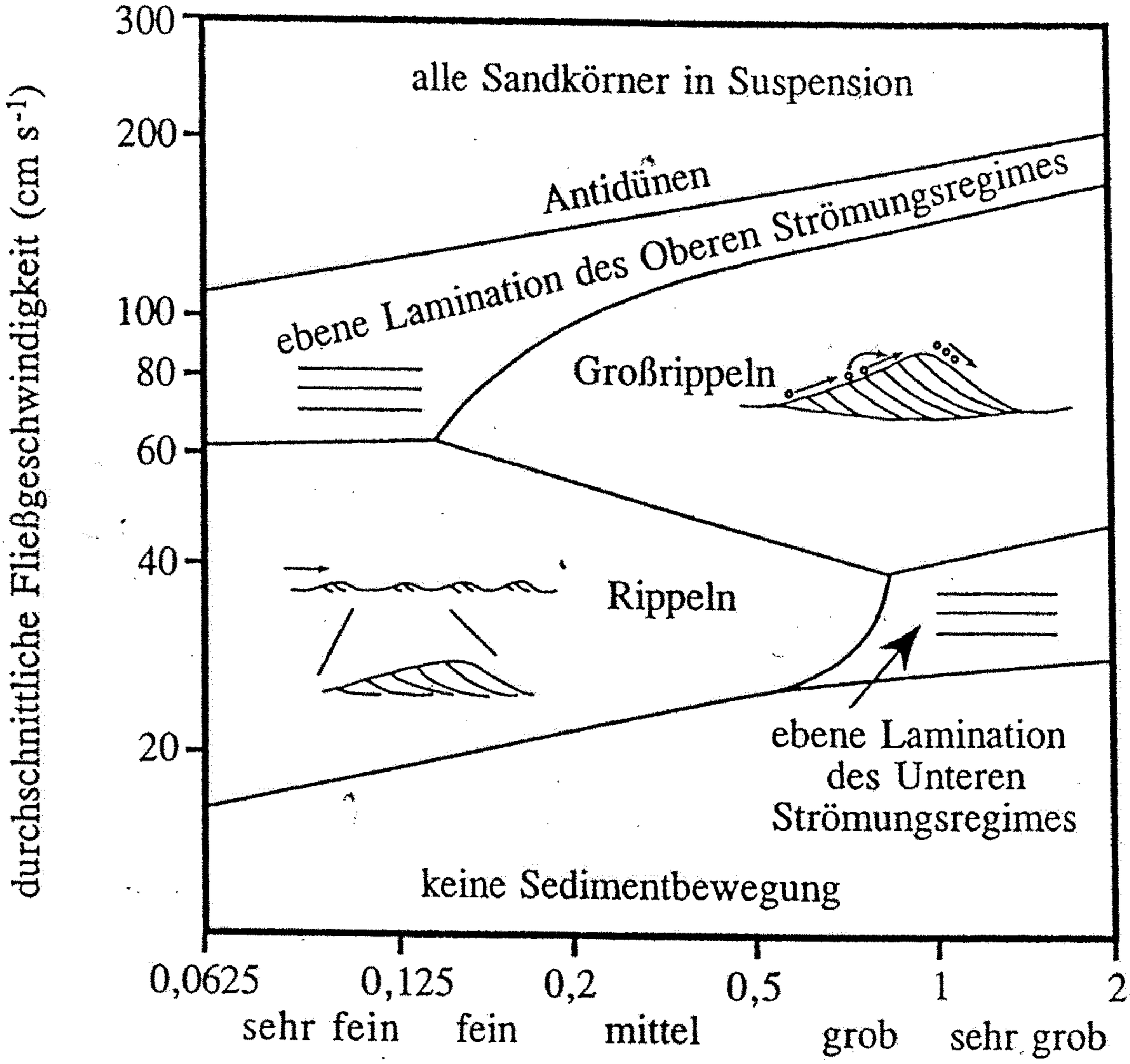

Abb. 5.22
Bei Strömungsgeschwindigkeiten zwischen ca. 20 und 60 cm s^{-1} und Korngrößen bis ca. 0,8 mm entwickeln sich die Rippeln. Im Bereich sehr groben Sandes bildet sich bei gleichen Strömungsgeschwindigkeiten die horizontale Lamination langsam strömenden Wassers (Unteres Strömungsregime). Bei zunehmender Korngröße und Geschwindigkeit bilden sich Megarippeln (Abb. 5.24) und schließlich die horizontale Lamination des schießenden Wassers (Oberes Strömungsregime) heraus. Rippeln und Megarippeln bewegen sich mit der Strömung. In beiden Rippelstabilitätsfeldern gehen die Rippeln mit steigender Strömungsgeschwindigkeit vom 2-D-Typ in den 3-D-Typ über. Der Sonderfall der selten erhaltungsfähigen Antidünen (Abb. 12.44c) bildet sich schließlich bei schießendem Wasser durch Anlagerung von Sediment auf der Luv-Seite und Erosion an der Lee-Seite (verändert nach WALKER, 1992).

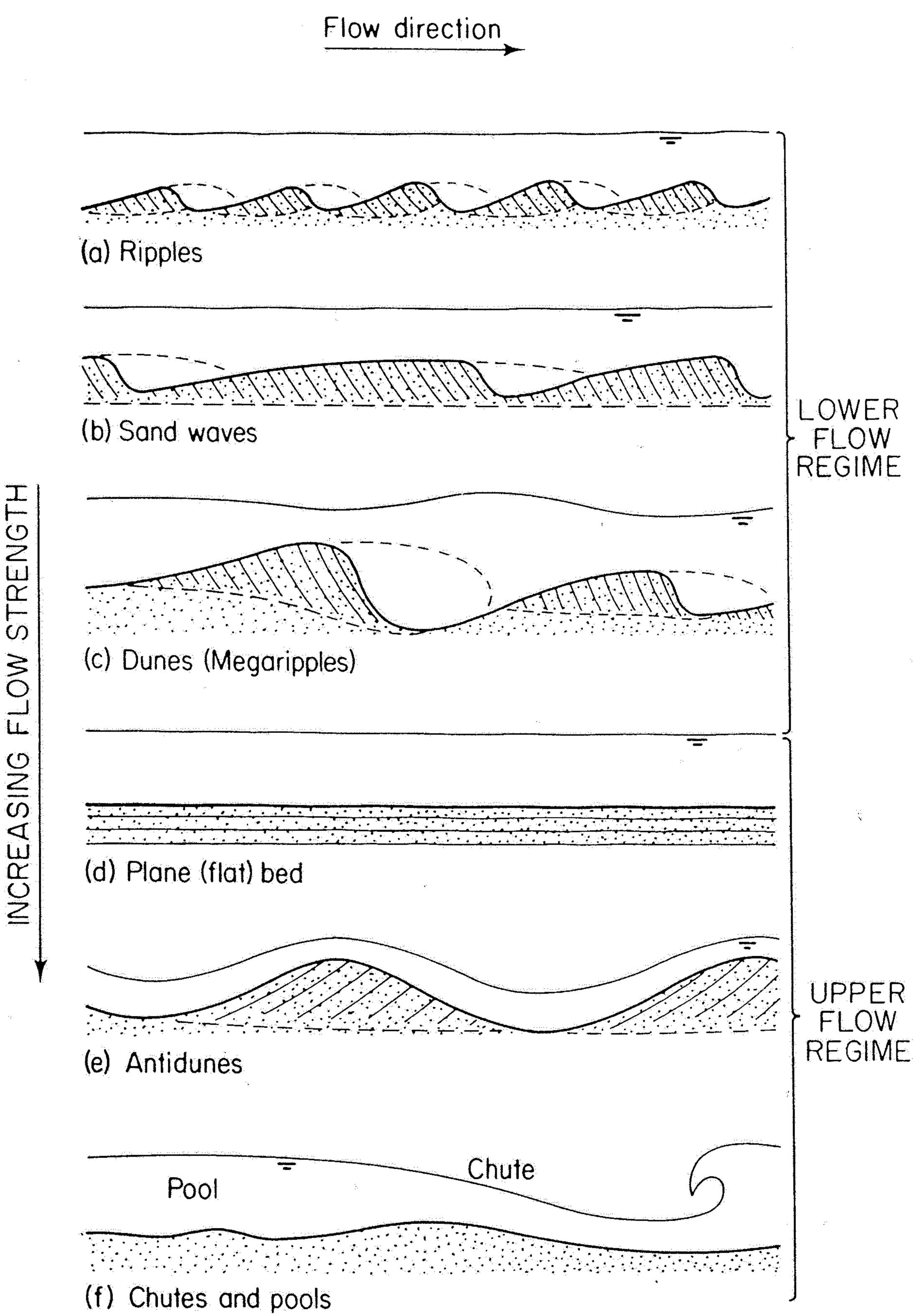

Figure 2–10 Flow-regime sequence of bedforms. (From Simons et al., 1965, p. 36.)

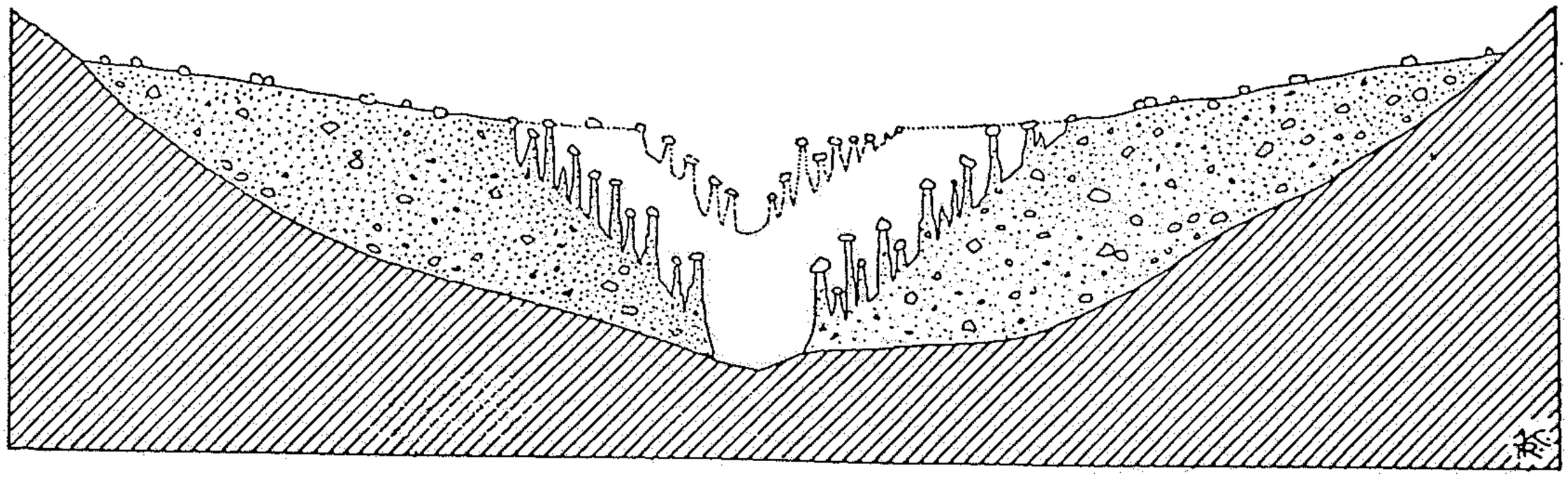

Obr. 45. *Vznik zemních pyramid v sypkých uloženinách (morénách, ssuti a pod.) působením stékající vody za dešťových přívalů.* (Podle G. WAGNERA.)

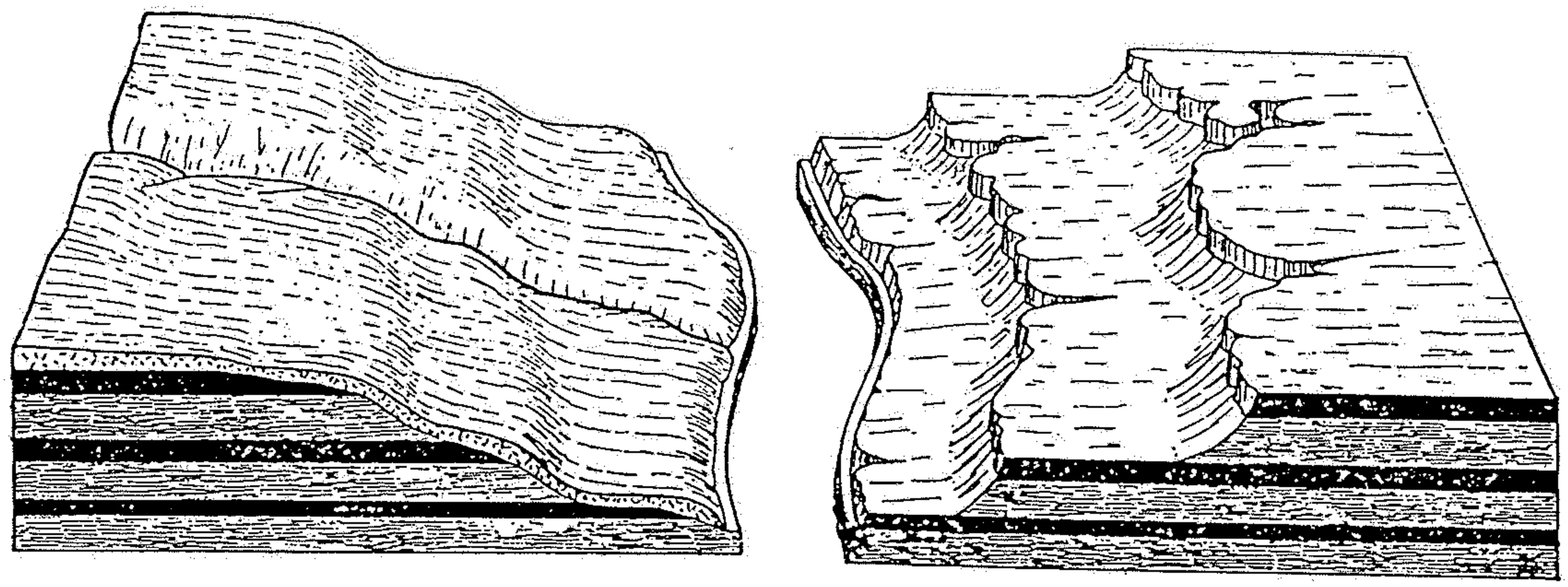

Obr. 43. *Rozdíl v utváření povrchu zemského v oblastech vlhkých (humidních) a oblastech suchých (aridních). Vlevo — stupně tvořené odolnými vrstvami (černě) jsou na povrchu maskovány pláštěm zvětralin, splavených po svahu dešťovým ronem. Vpravo — stupně tvořené odolnými horninami jsou následkem nedostatku srážek a dešťového ronu v tvářnosti krajiny zachovány v podobě širokých planin a příkrých srázů.* (Podle R. J. FLINTA.)

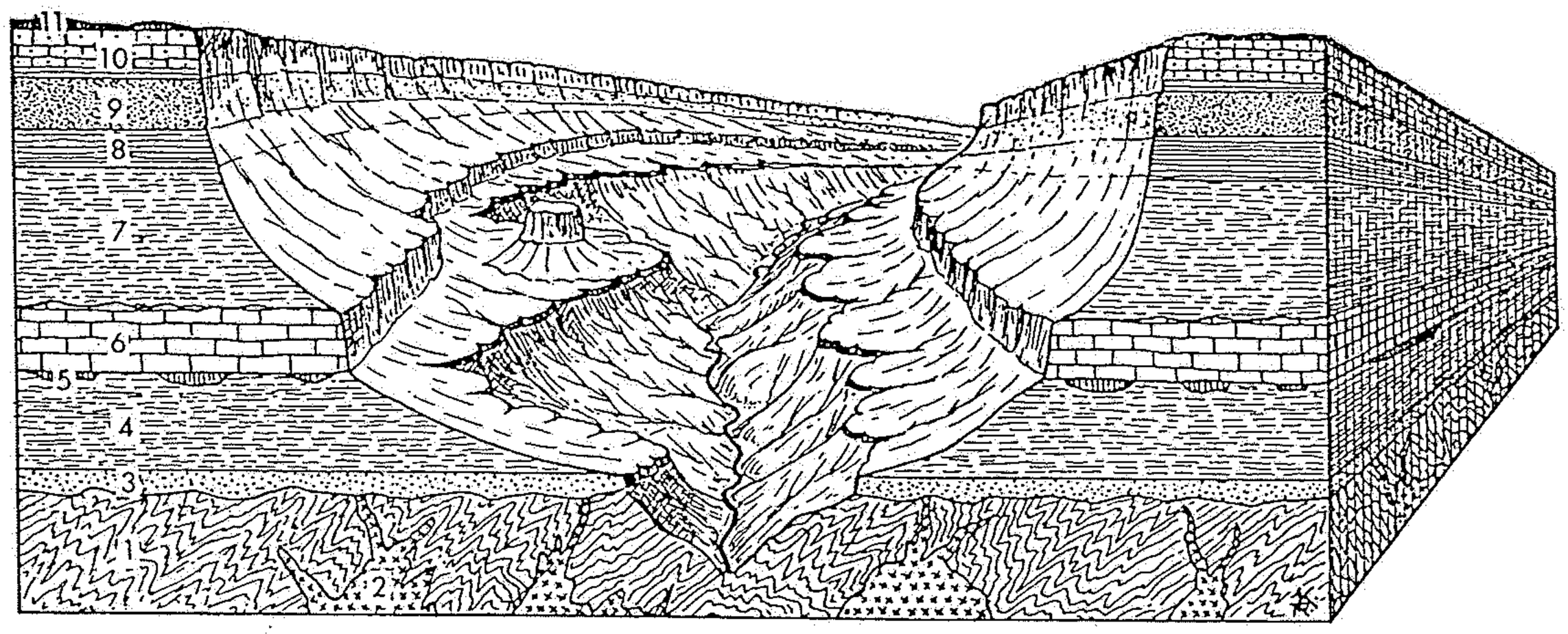

Obr. 44. *Zidealisované znázornění Velkého kaňonu řeky Colorado v Arizoně (USA). Kaňon vzniklý v aridním (suchém) podnebí: tvrdá a odolná souvrství vytvářejí nápadné stupně a příkré srázy. Pohled po proudu řeky. Vysvětlivky čísel:* 1. *Prahorní ruly formace zvané Vishnu;* 2. *žulové pně a apofysy vnikající do rul Vishnu;* 3. *basální kambrický pískovec (Tapeats sandstone);* 4. *kambrické břidlice (Bright Angel shale);* 5. *zbytky devonských vápenců (Temple Buttle limestone);* 6. *spodní karbon — — Mississippian — vápence (Red Wall limestone);* 7. *spodní perm — pískovce a břidlice coconinské;* 10. *permský vápenec kaibabský;* 11. *spodní trias — červené pískovce moenkopské.* (S použitím blokdiagramu LOBECKOVA sestavil autor.)

„Pinacles" – zem. pyramidy
aglomerátové tufy u kráter. jezero Oregon

FIGURE 12–10 *Potholes in the bed of Susquehanna River, Conewago Falls, exposed during the drought of 1947.* (*Photo by* Lancaster Intelligence Journal; *courtesy of H. H. Beck, Franklin and Marshall College.*)

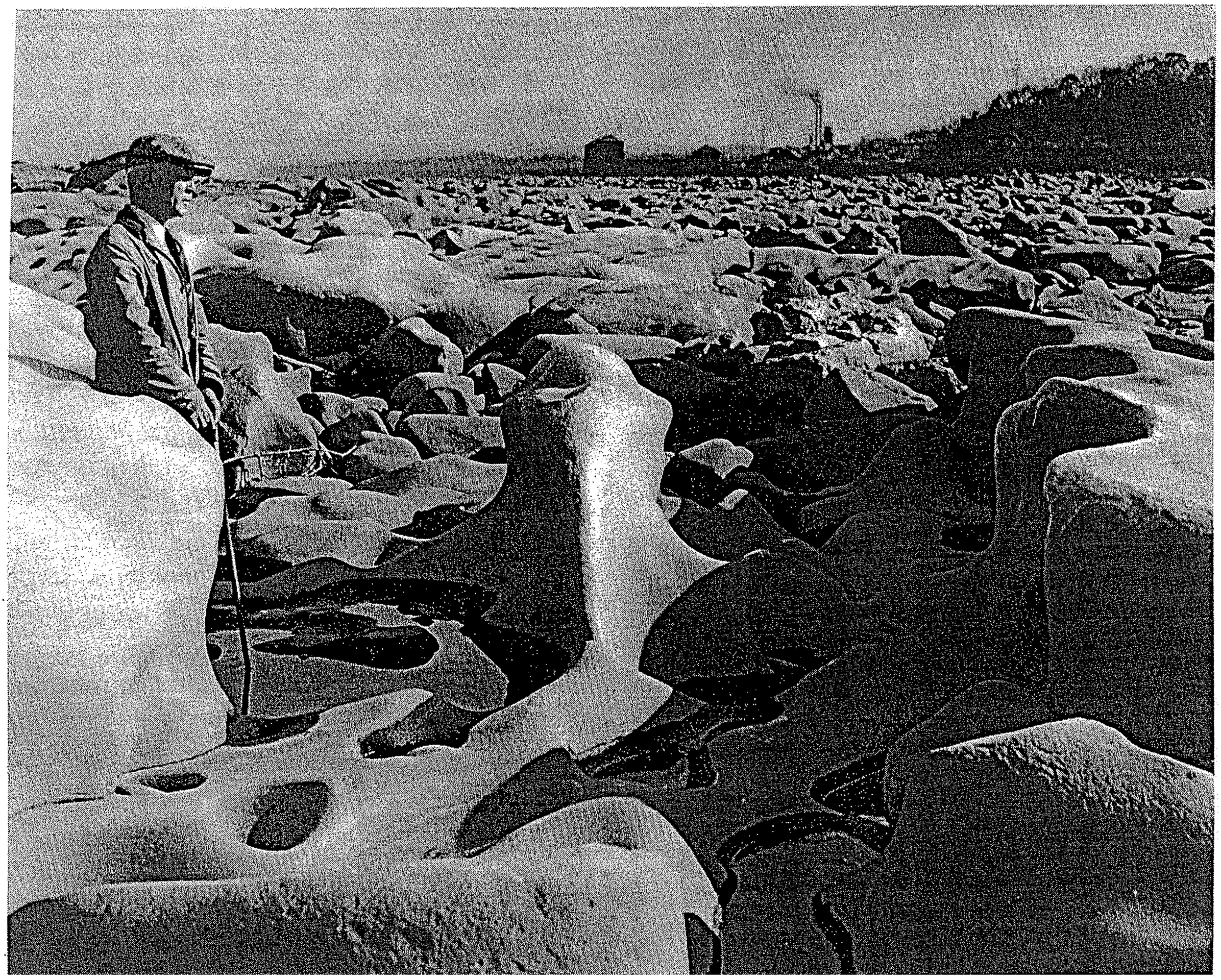

FIGURE 12–18 *Entrenched meanders of the San Juan River, Utah. (Photo by Tad Nichols, Tucson, Arizona.)*

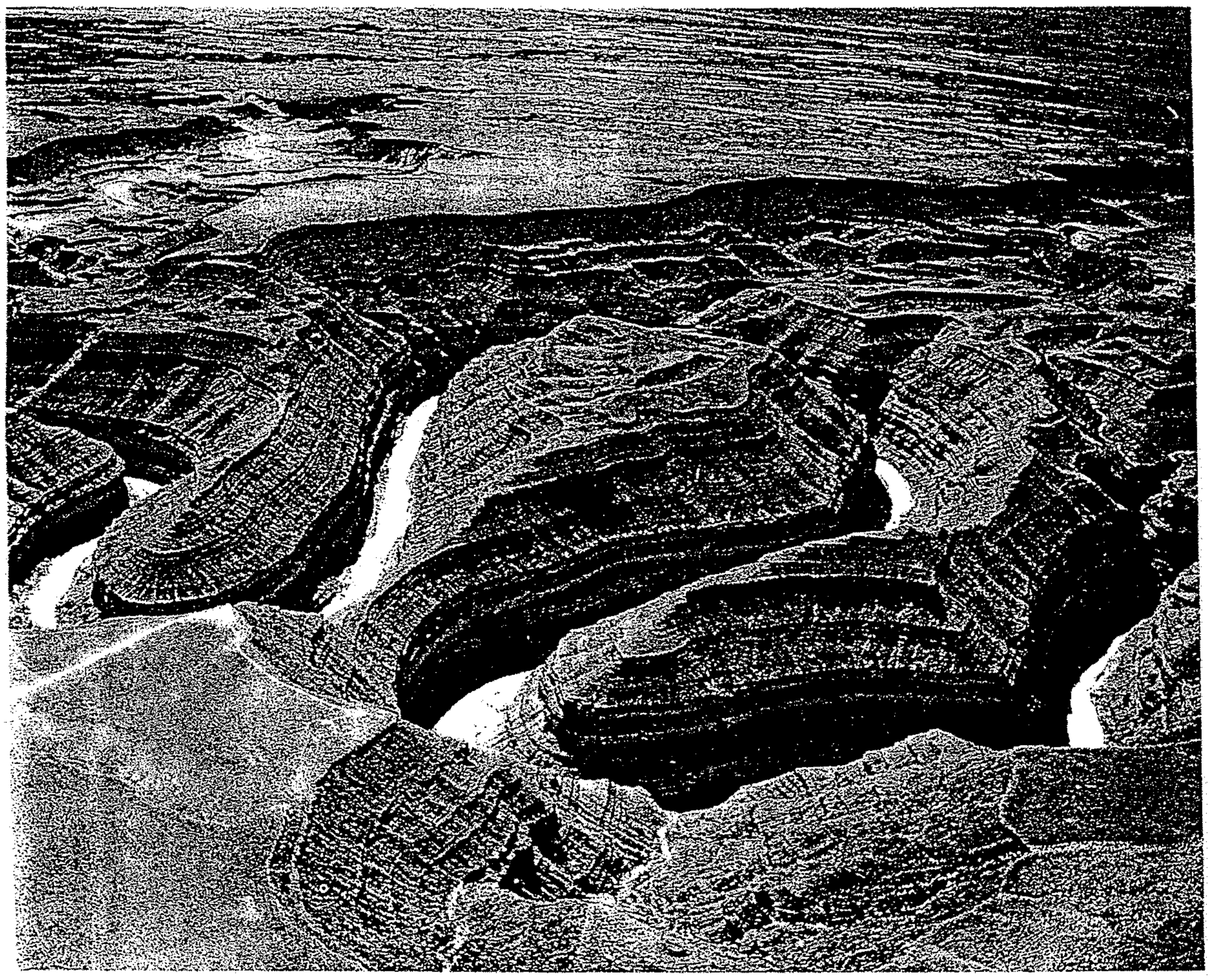

Faulted and entrenched fans at the mouth of Tuber Canyon, Panamint Range, California. Note the new fans growing on the downdropped block, and their relation to the newly entrenched channels on the upthrown block. (Photo by John S. Shelton, Claremont, California.)

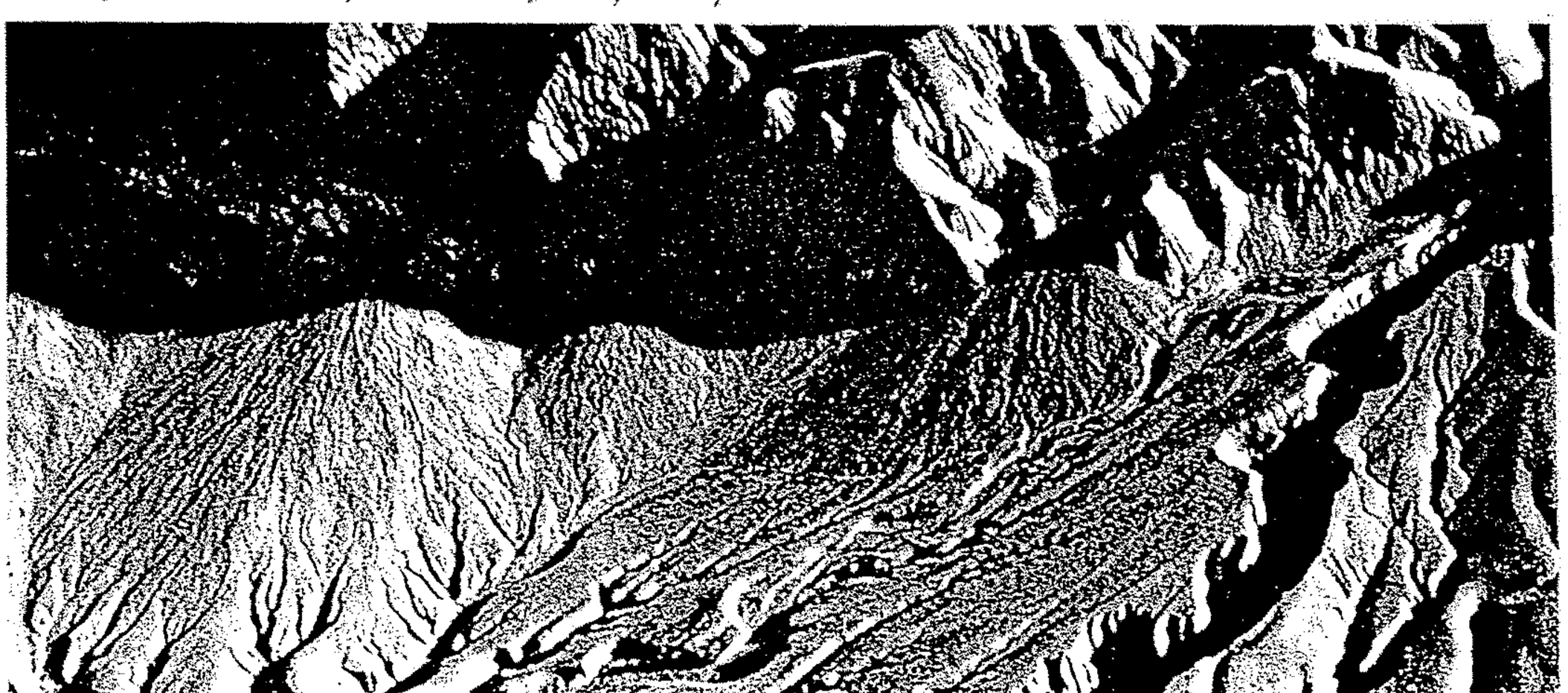

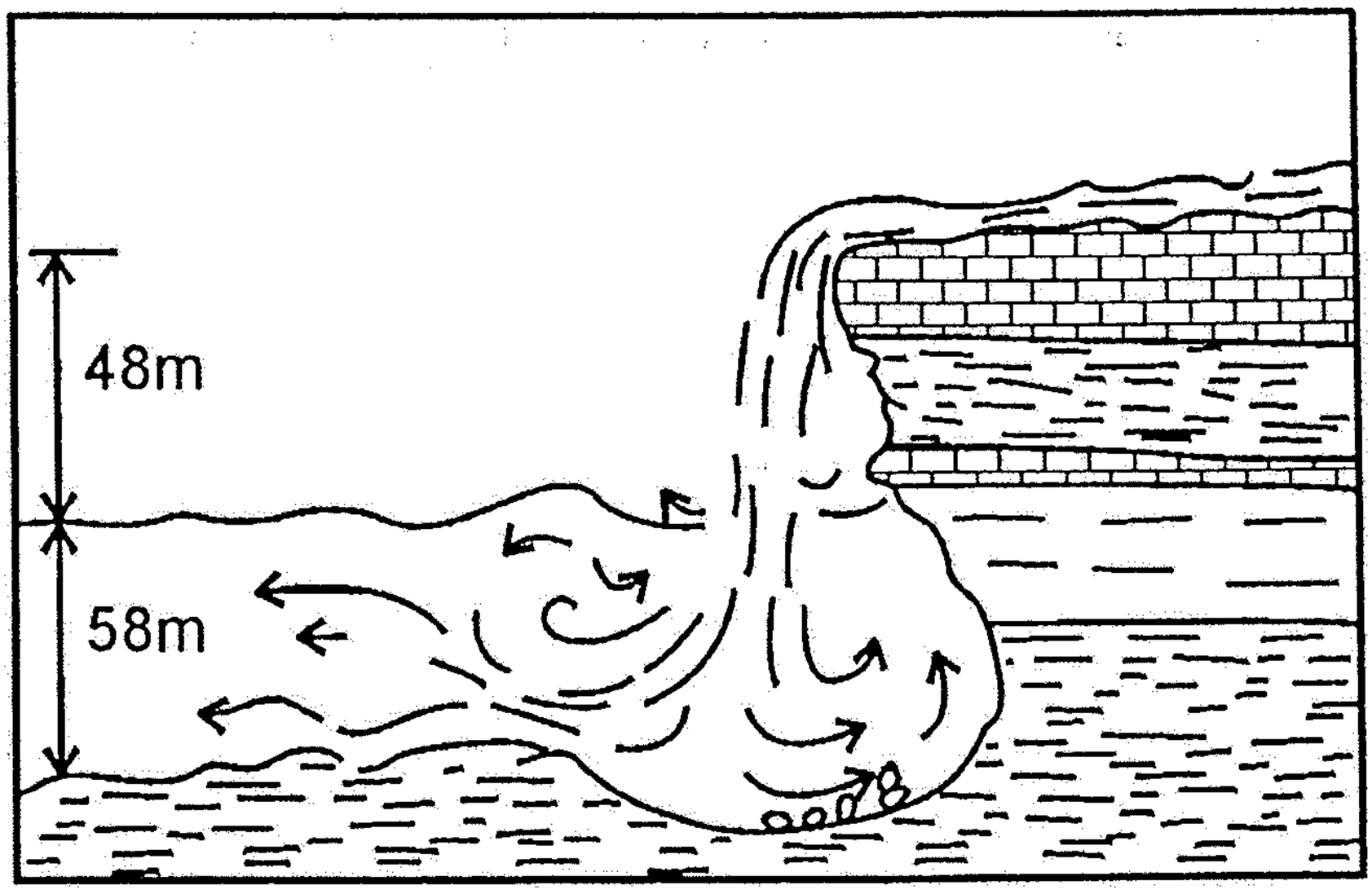

Obr. 16.8. Ústup Niagarských vodopádov sa deje pádom ich podkopanej hrany do vývariska. Vďaka vodorovnemu uloženiu vrstiev si zachovávajú aj pri ústupe stálu výšku. (upravené podľa Gilberta ex Kettnera 1954)

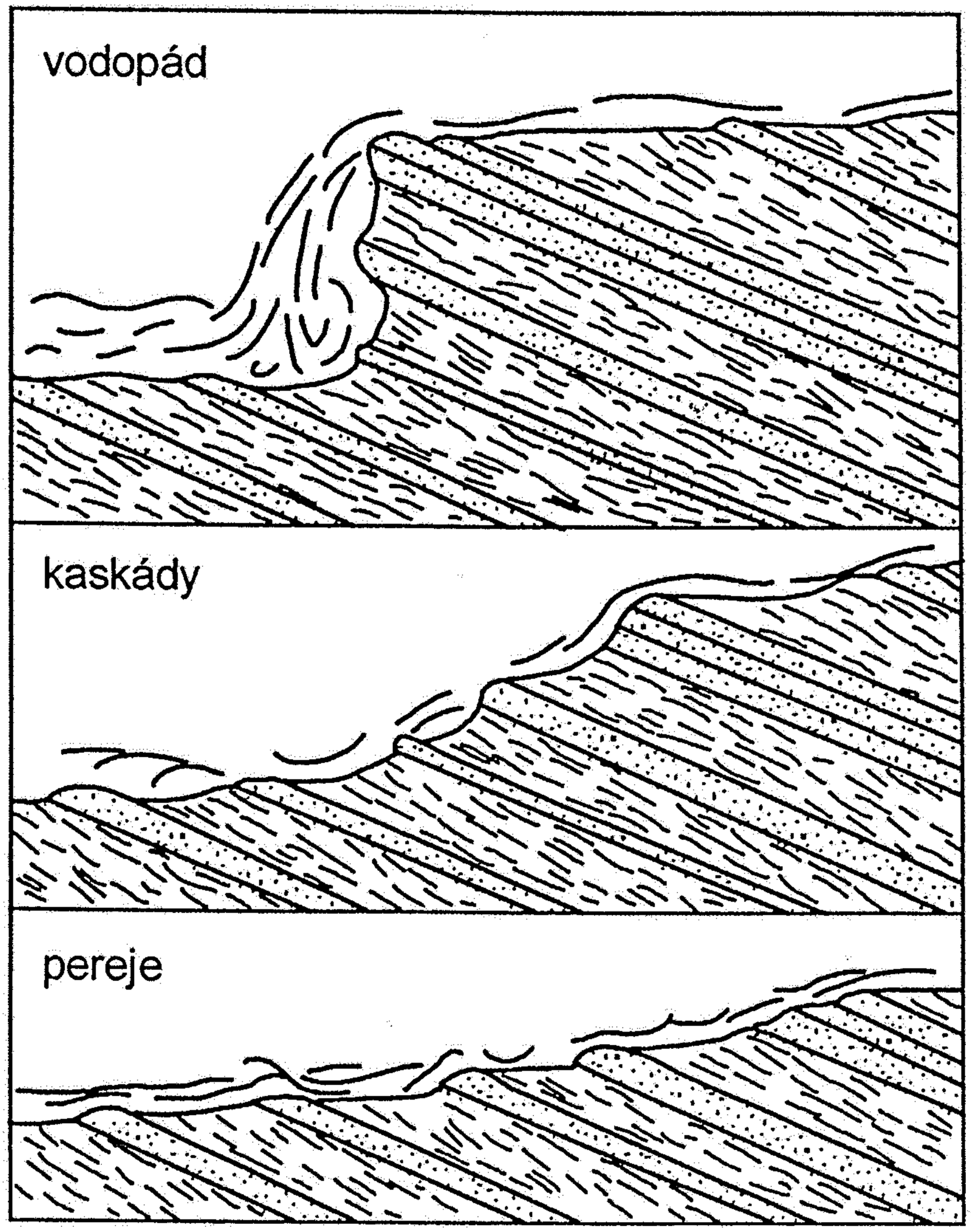

***Obr. 16.9.** Na protismerne uklonených vrstvách vodopád zaniká transformáciou na kaskády a pereje*

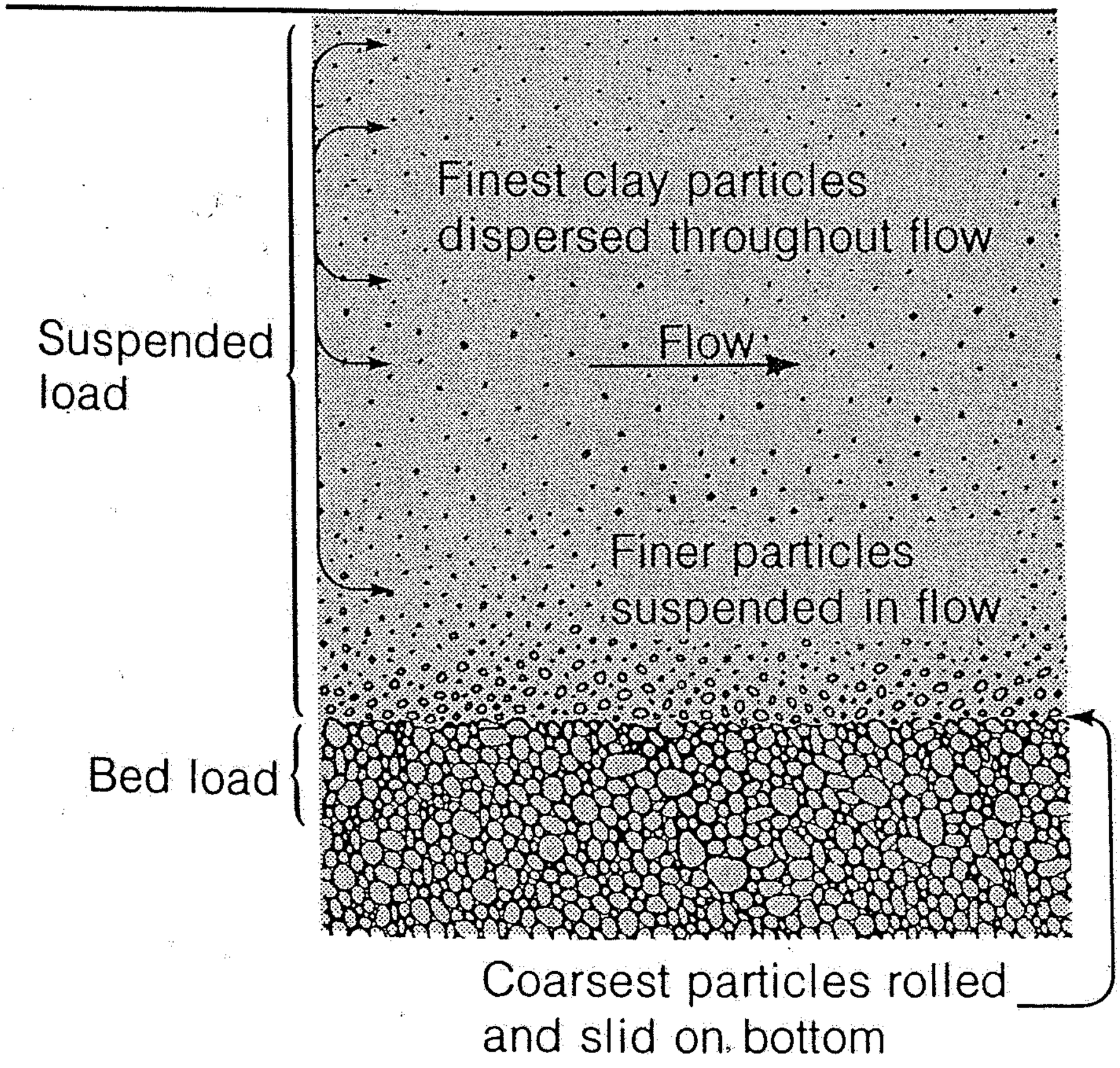

Figure 8-4

A current flowing over a bed of sand, silt, and clay particles transports particles in two ways: (1) as bed load, which moves by sliding and rolling along the bottom; and (2) as suspended load, which moves by being temporarily or permanently suspended in the flow itself. The finest clay particles remain permanently suspended in all but extremely sluggish flows.

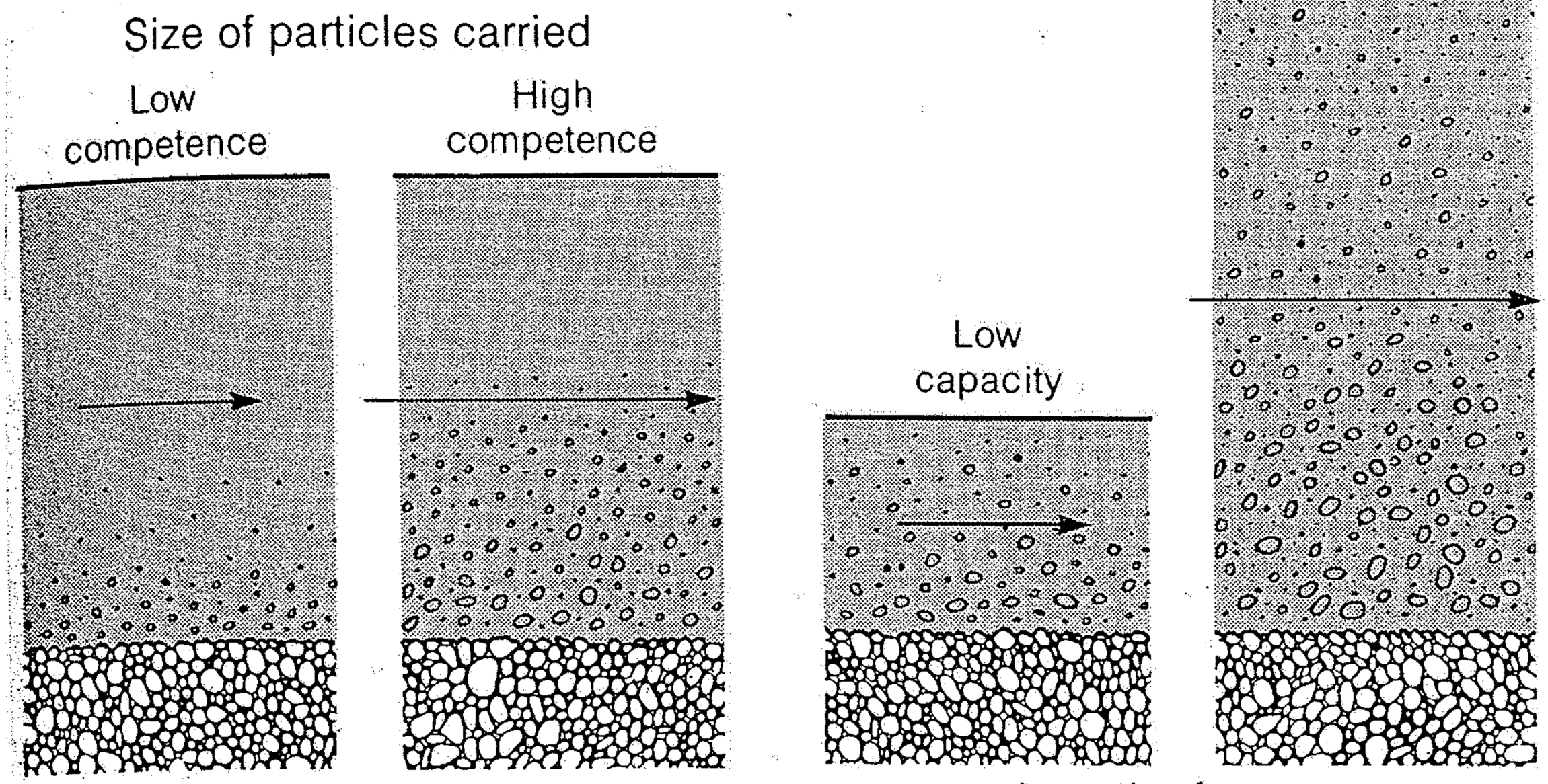

Figure 8-5

The competence of a current to carry particles is a measure of the largest-size particles it can carry. The capacity of a current is a measure of the number of particles it can carry. Although both depend on velocity to some extent, competence depends much more directly on velocity, and capacity depends largely on discharge, the volume of water flowing past a point in a given time.

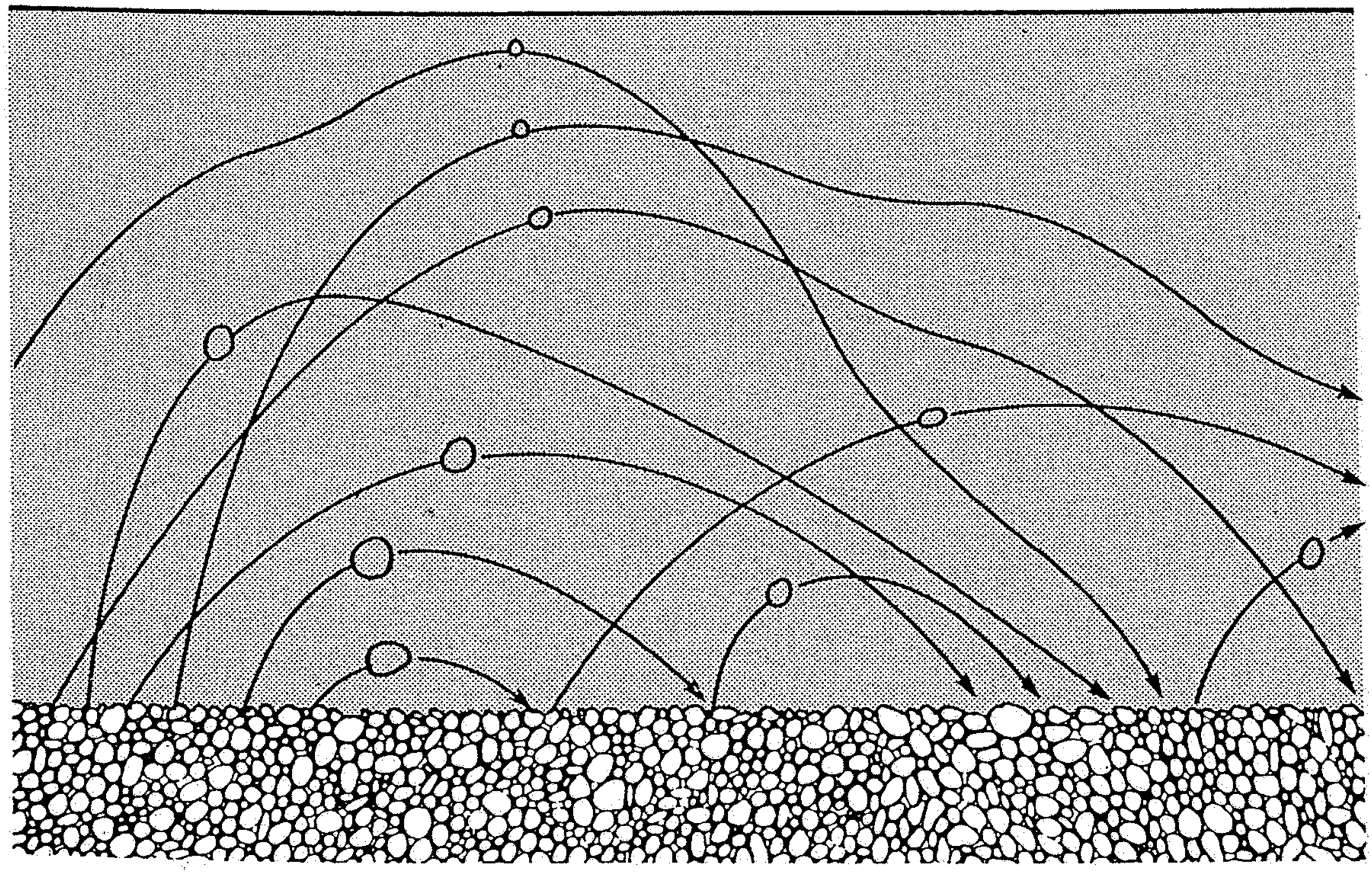

Figure 8-6

Saltation is an intermittent "jumping" motion of grains. Turbulent eddies pull grains up into the flow, where they travel with the flow for a distance before falling back to the bed. In general, the smaller the particle, the higher it will jump and the farther it will travel. Turbulence keeps some very small particles suspended throughout a long travel path before they fall back to the bed.

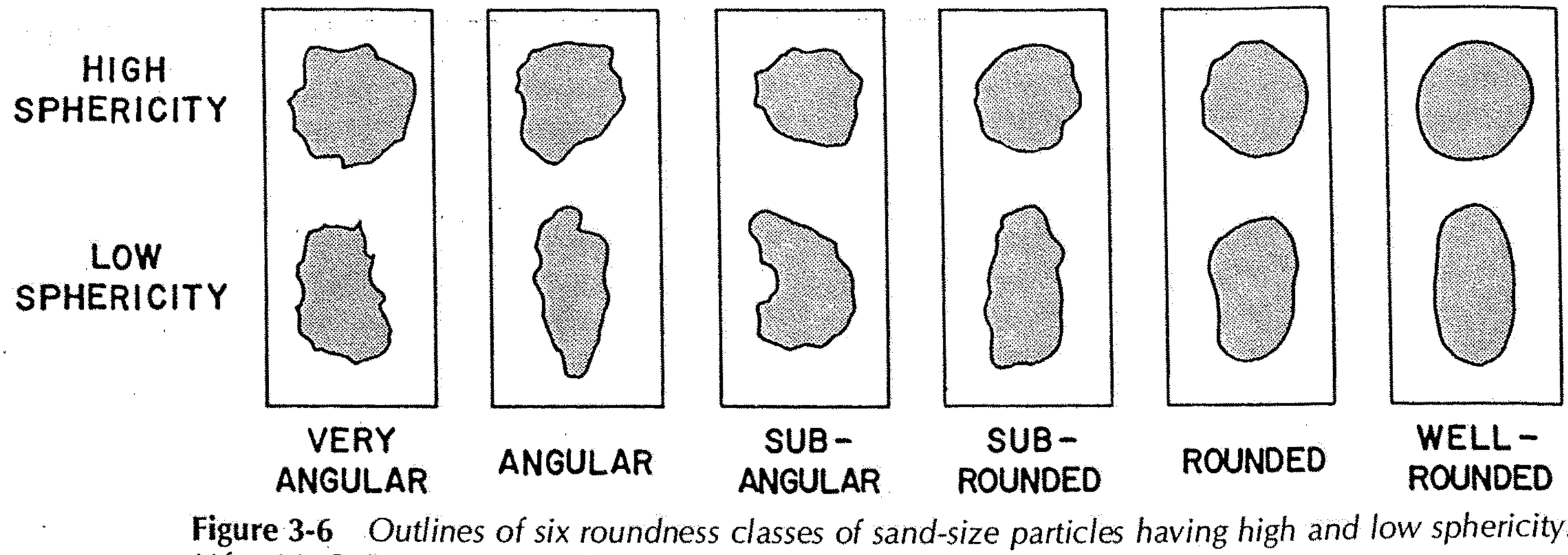

Figure 3-6 *Outlines of six roundness classes of sand-size particles having high and low sphericity. (After M. C. Powers, 1953, Fig. 1, p. 118.)*

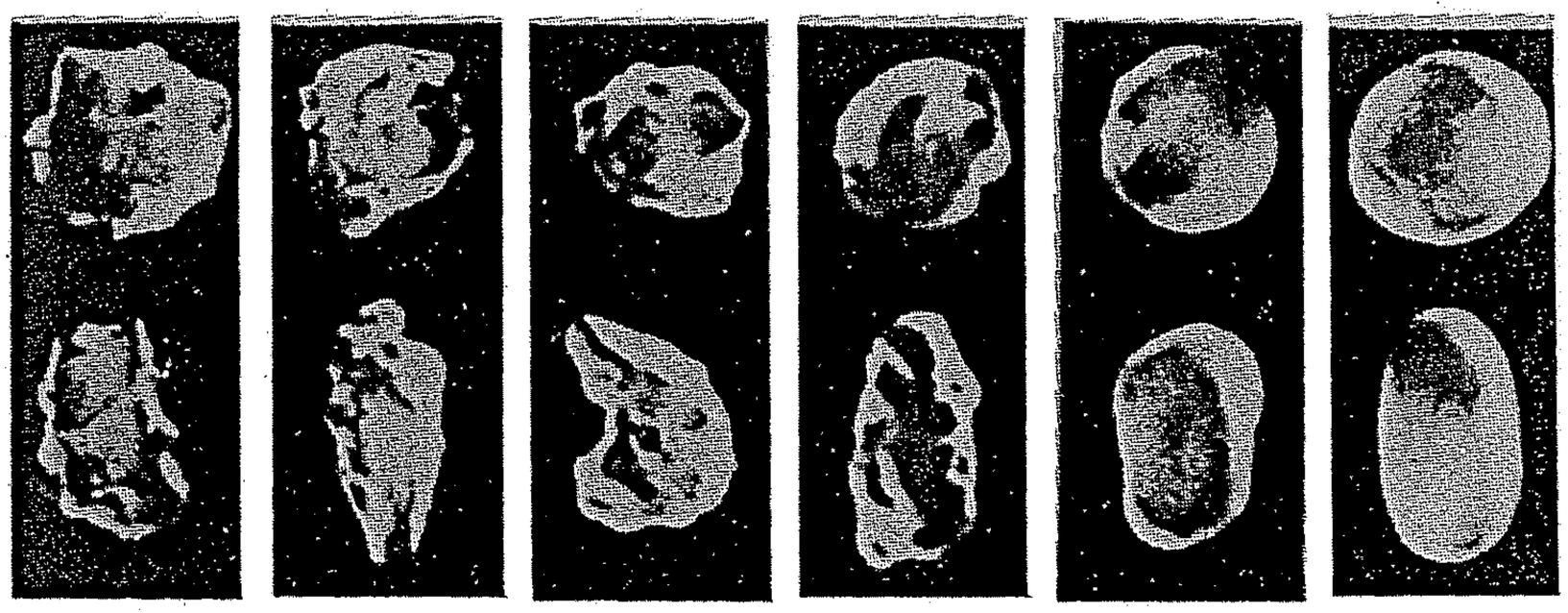

Fig. 3-19 Images of grains for the determination of roundness. (From Powers, 1953.)

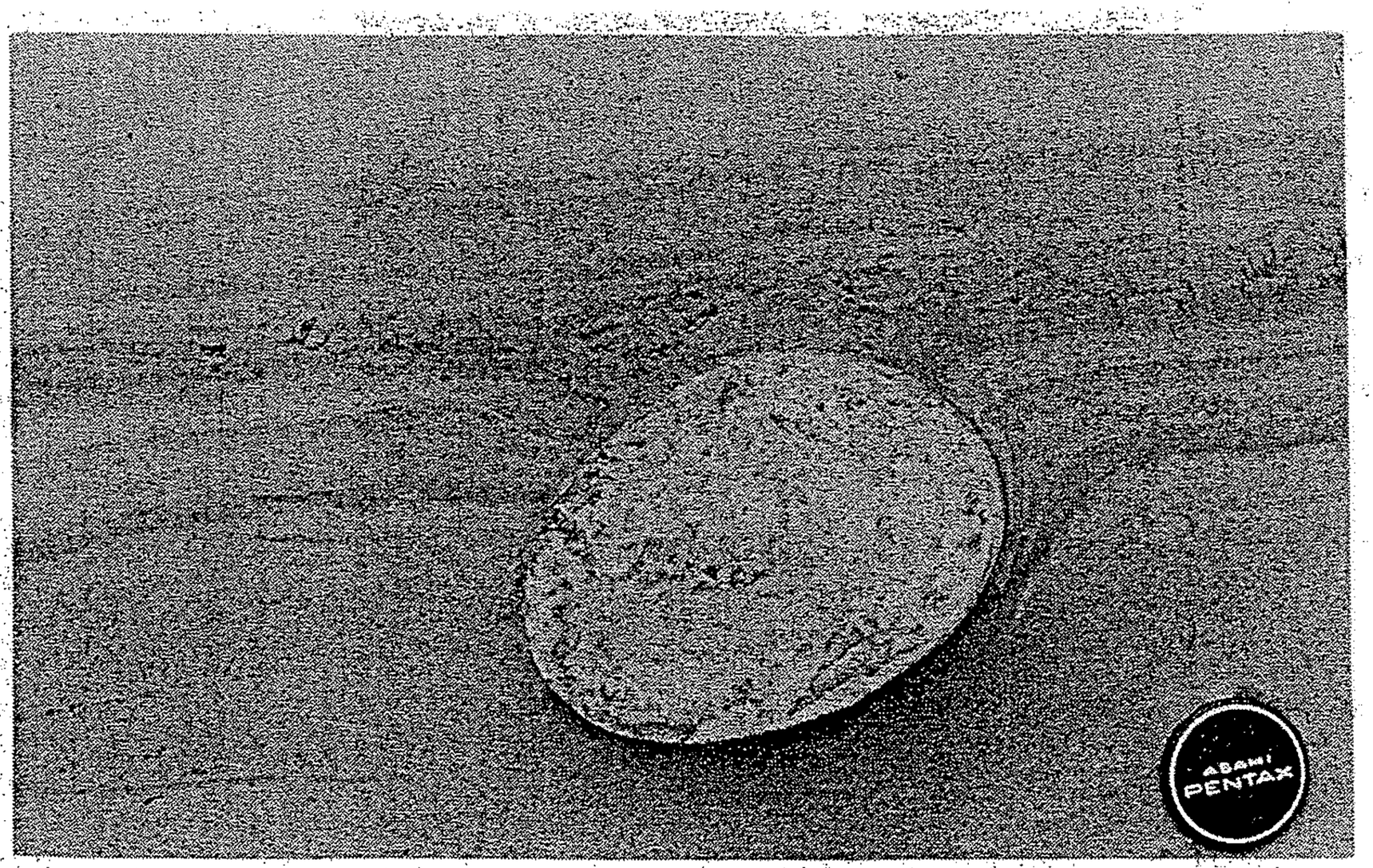

Figure 9-9 *Well-rounded dropstone, long diameter approximately 20 cm, enclosed within laminated sediment of proglacial Malaspina Lake, Alaska, exposed as a result of a lowering of the lake level. (T. C. Gustavson, courtesy Harlequin Productions, M. O. Hayes, J. H. Hartshorn.)*

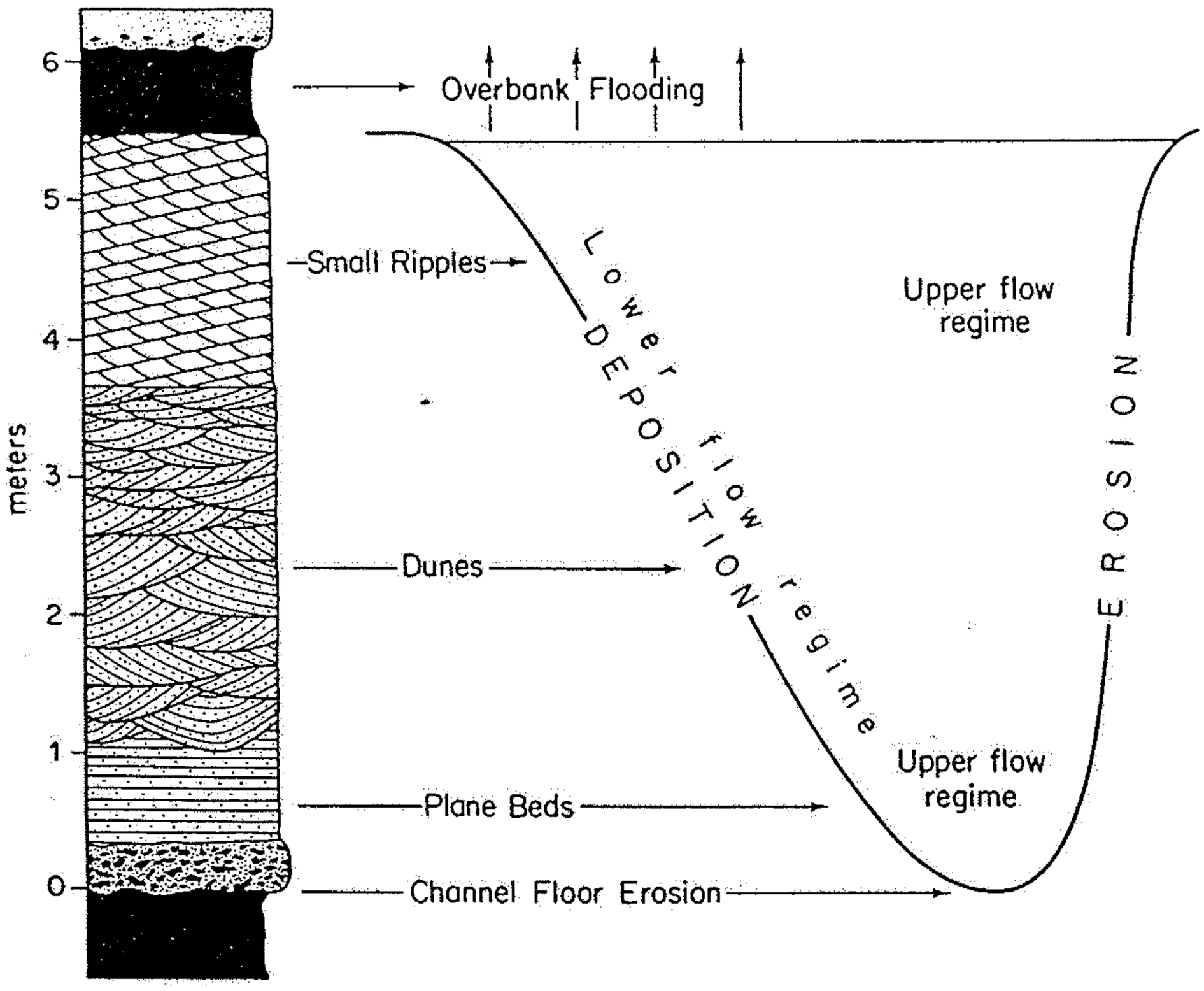

Fig. 5-6 Interpretation by Allen (1963) of a British Old Red Sandstone cyclothem in terms of flow regimes in a meandering channel model. Highest upper flow regime is represented by the erosional lower contact and basal lag conglomerate. Because of lateral migration of the channel, successively higher deposits correspond to sediments deposited successively higher on the point bar, under progressively lower flow regime conditions.

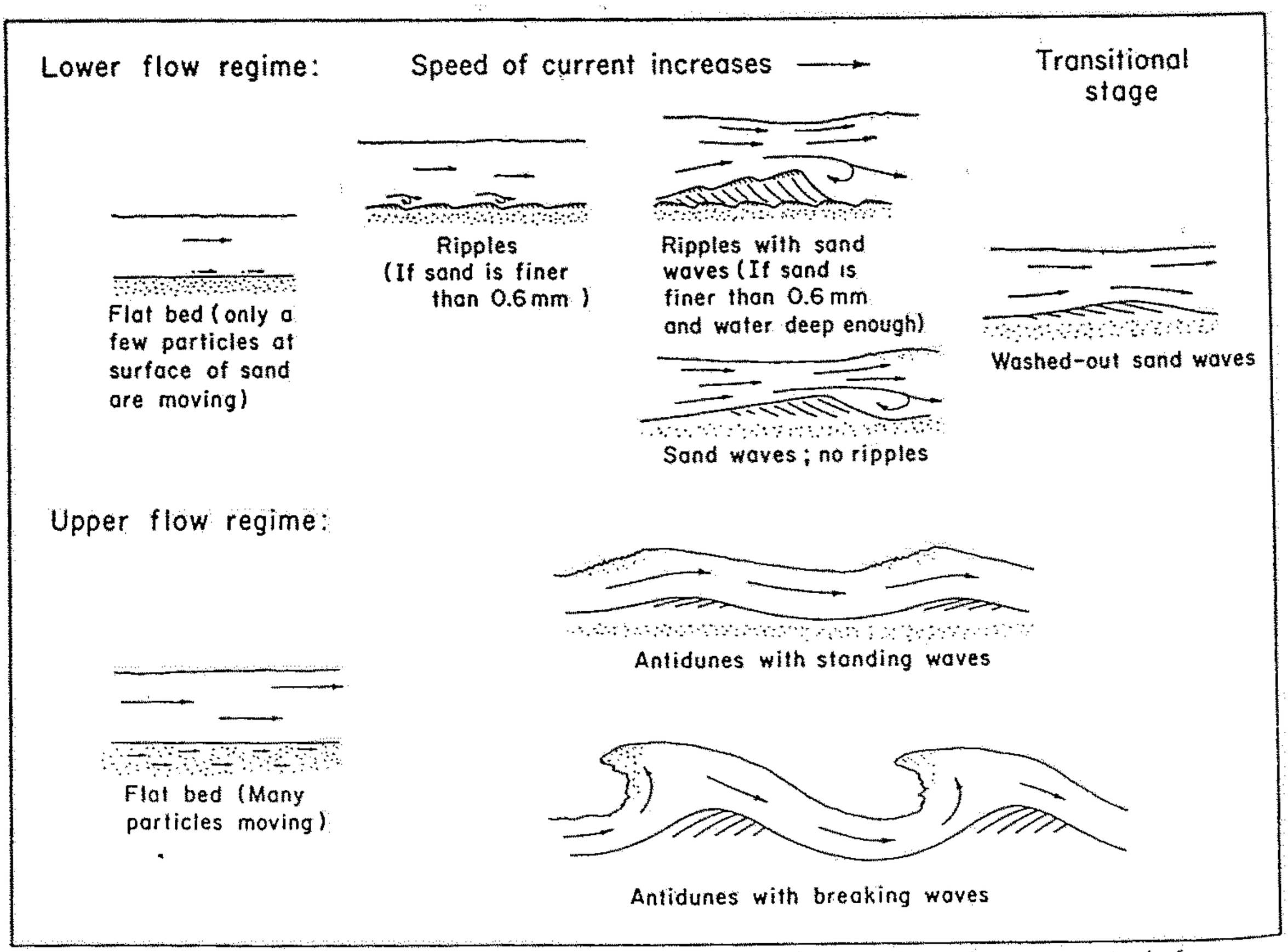

Figure 4-33 *Schematic profiles of water and sediment showing features formed at progressively faster currents. Further explanation in text. (Based on D. R. Simons, E. V. Richardson, and C. F. Nordin, Jr., 1965, and J. C. Harms and R. K. Fahnestock, 1965.)*

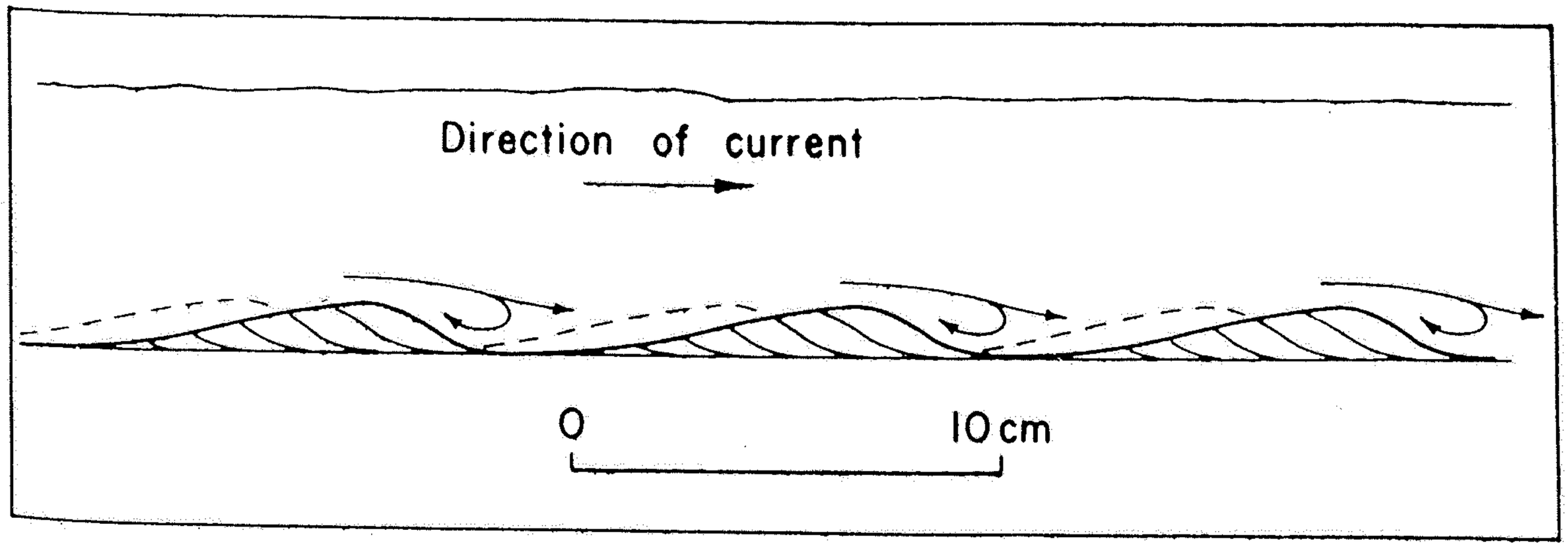

Figure 4-28 *Small-scale ripples in fine sand migrate downcurrent because sand, eroded from gently dipping upcurrent sides, accumulates in inclined layers on steeply dipping downcurrent sides. As ripples migrate, these inclined layers become cross strata. Dashed lines indicate a set of former upstream positions of eroded ripples. Curved arrows in water are flow lines in boundary layer near separation eddies that form downcurrent from each ripple crest. (Based on various sources.)*

Fig. 161. Showing generation of cross-bedding by migrating small ripples. Each migrating ripple produces a bed with foreset laminae. The following ripple erodes the top layer and deposits a new bed with foreset laminae. The surface morphology of ripples is preserved. The flow is from right to left. Laboratory experiment. (After Reineck 1961)

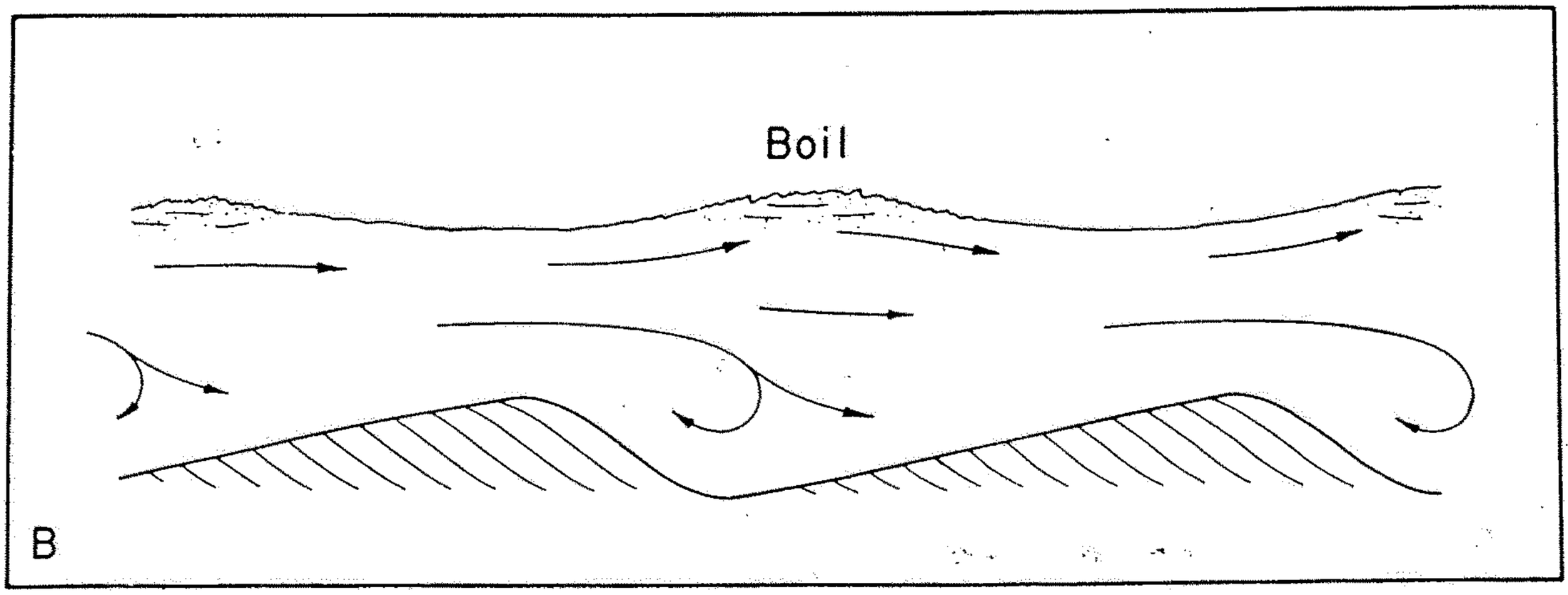

Figure 4-30 *Schematic profiles in vertical plane parallel to current, of water flowing over fine sand shaped into sand waves.*

A. Ripples on upcurrent side of sand wave advance to crest and are destroyed when sand avalanches down steep downcurrent slope. Ripples in trough downcurrent of avalanche face migrate in a direction opposite to that of main current. These backflow ripples are preserved beneath the sand wave as sand from avalanche face, which shifts downcurrent, buries them. The combination of small-scale cross strata of backflow ripples with large-scale cross strata of sand waves is unique to fine sand transported by flowing water; it results from the flow separation created by the sand wave. (Modified from J. R. Boersma, 1967, Fig. 12, p. 231.)

B. Schematic profile of water and sediment in vertical plane parallel to direction of current of water flowing over coarse sand shaped into sand waves. Over crests of sand waves, the surface of the water is depressed; over troughs between sand waves, the surface of the water is heaped up into boils. Small-scale ripples, as in Figure 4-30A, do not form in coarse sand. (Modified from D. R. Simons, E. V. Richardson, and C. F. Nordin, Jr., 1965, Fig. 3, p. 36.)

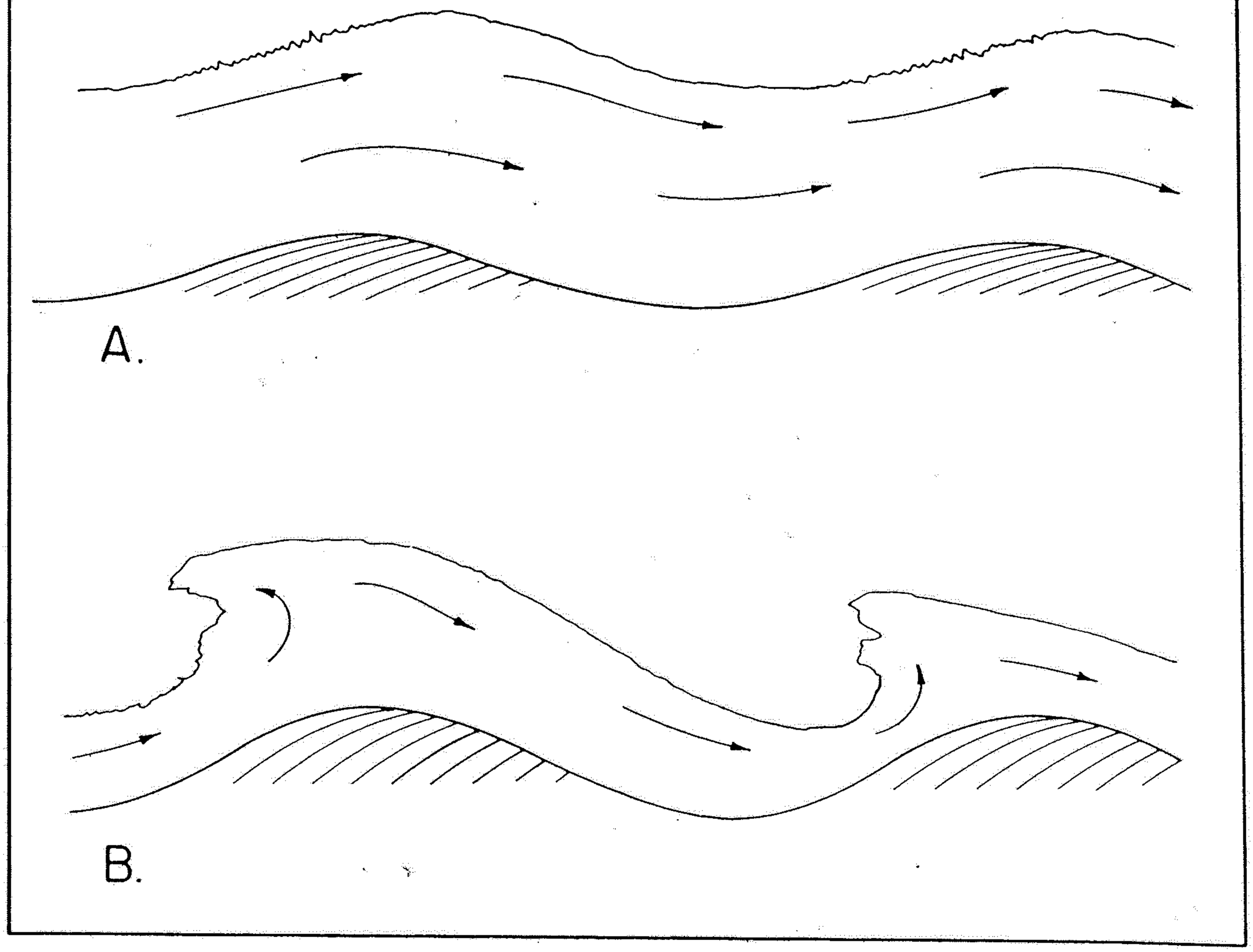

Figure 4-32 *Schematic profile, in vertical plane parallel to direction of current, through water and sediment shaped into antidunes.*

A. When water over troughs is always deeper than heights of crests of antidunes, standing-wave antidunes form. The surface of the water above the upstream sides of the antidunes is billowy, but no breaking occurs.

B. When water in troughs becomes shallower than heights of antidunes, water waves break, and crash over in an upcurrent direction. Great turbulence is created when water waves over antidunes break. (Based on D. R. Simons, E. V. Richardson, and C. F. Nordin, Jr., 1965, and J. C. Harms and R. K. Fahnestock, 1965.)

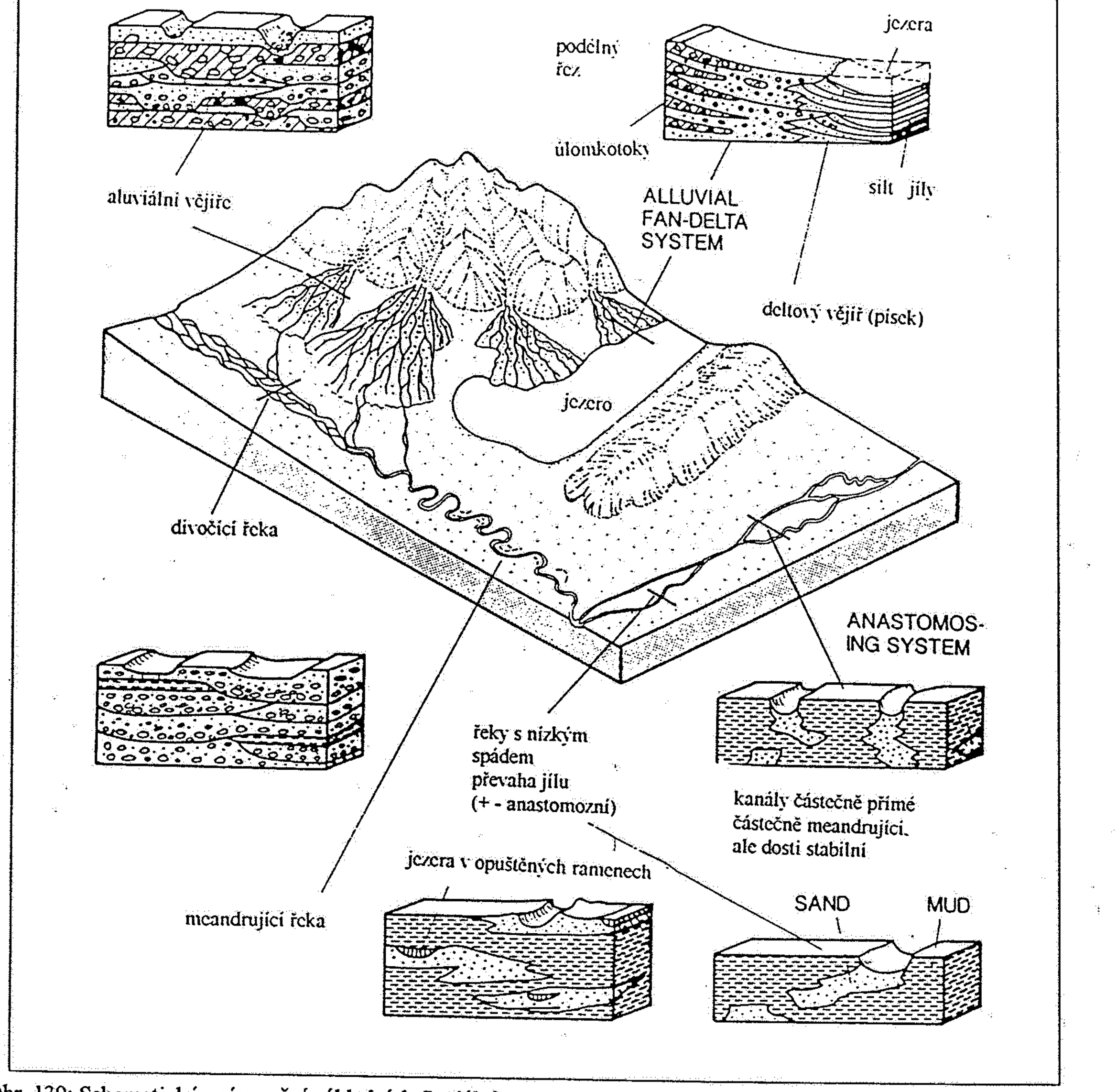

Obr. 139: Schematické znázornění základních fluviálních systémů a jejich základní charakteristika (podle Einselle 1992)

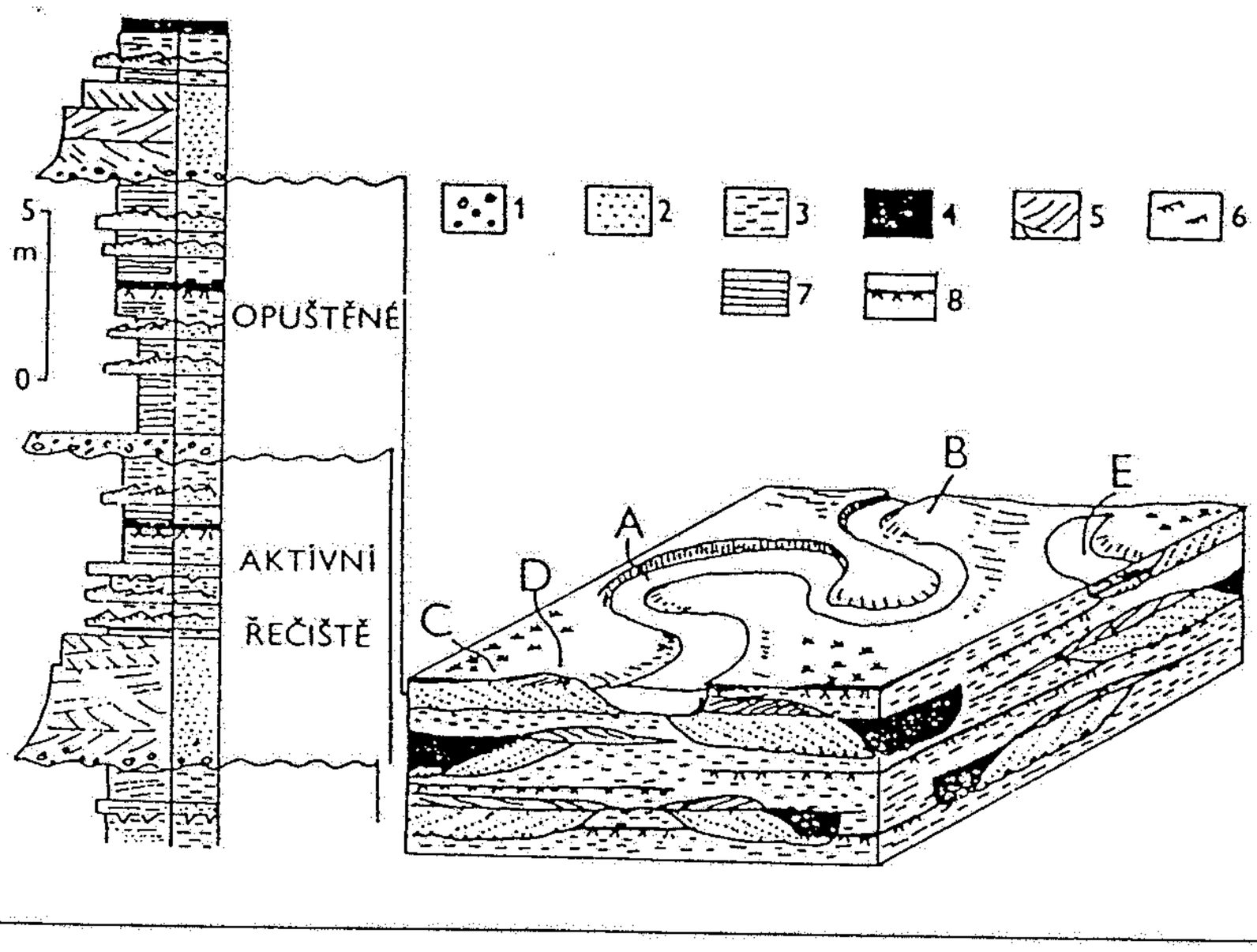

Obr. 138: Schematický blokdiagram znázorňující meandrující říční tok a nivu. Vedle výsledný modelový vertikální sled sedimentů. A - řečiště, B - agradační val, C - niva s močálem, D - jesepní val, E - opuštěný meandr, 1. slepence, 2. pískovce, 3. prachovce, 4. jílovce, 5. šikmé zvrstvení, 6. jemně čečinovité zvrstvení, 7. horizontální zvrstvení, 8. stopy kořenů rostlin (podle Selley 1976 in Kukal 1986)

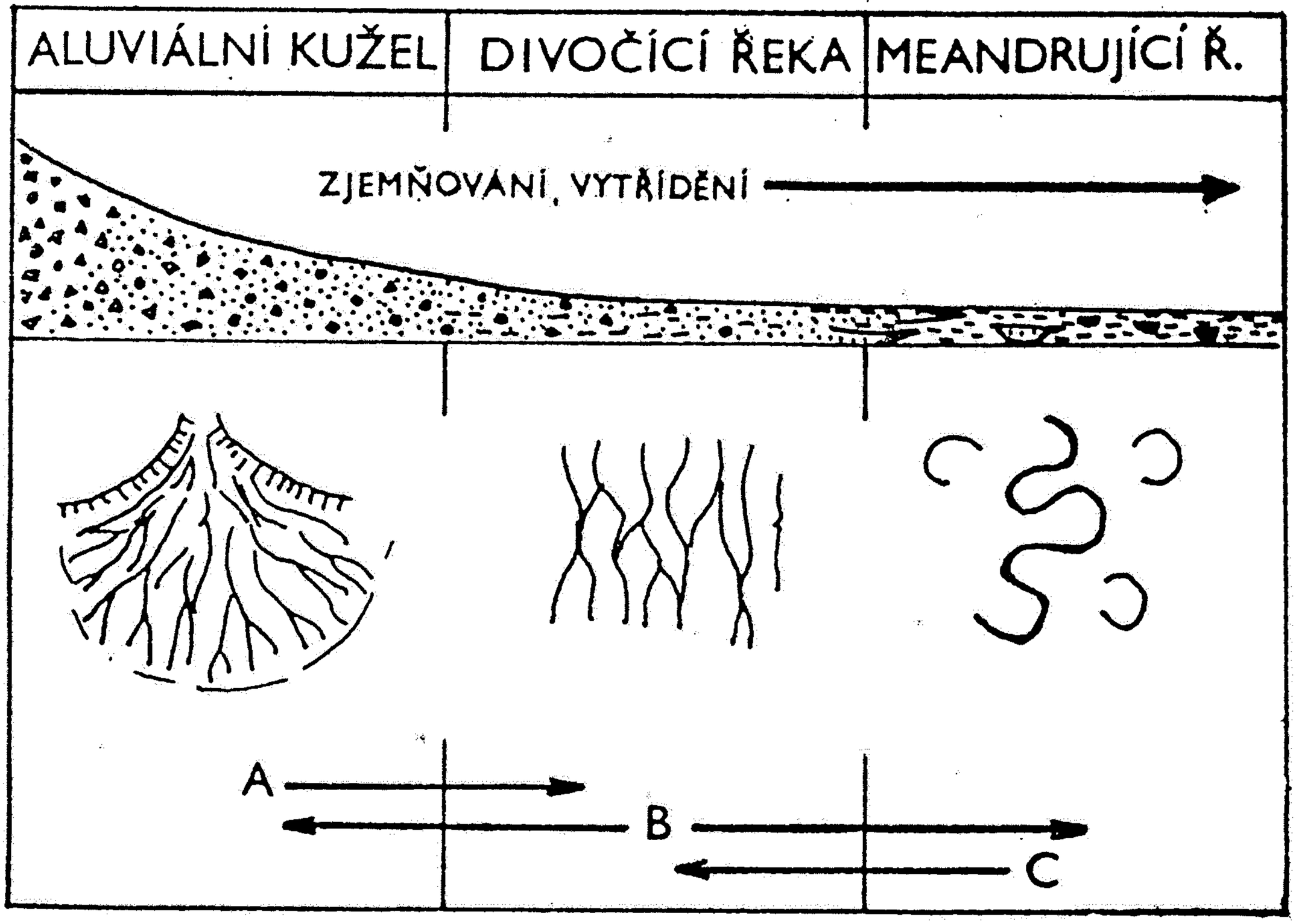

88. Přechody mezi aluviálními kužely, divočícími řekami a meandrujícími řekami. Nahoře v řezu je vyznačeno zjemňování sedimentů, uprostřed systém řečišť, dole mechanismus sedimentace: A — nasycené toky a plošné splachy, B — řečištní transport po dně, C — sedimentace ze suspenze.

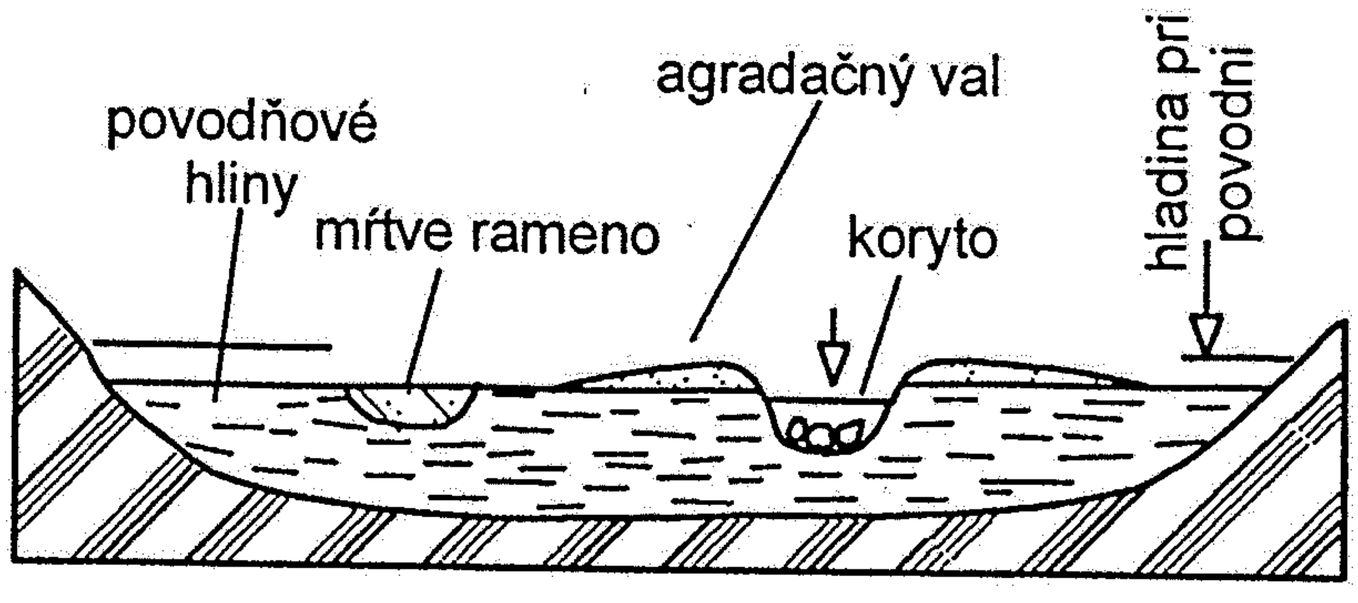

Obr. 16.14. Prierez aluviálnou nivou. (podľa Plummera – McGearyho 1996)

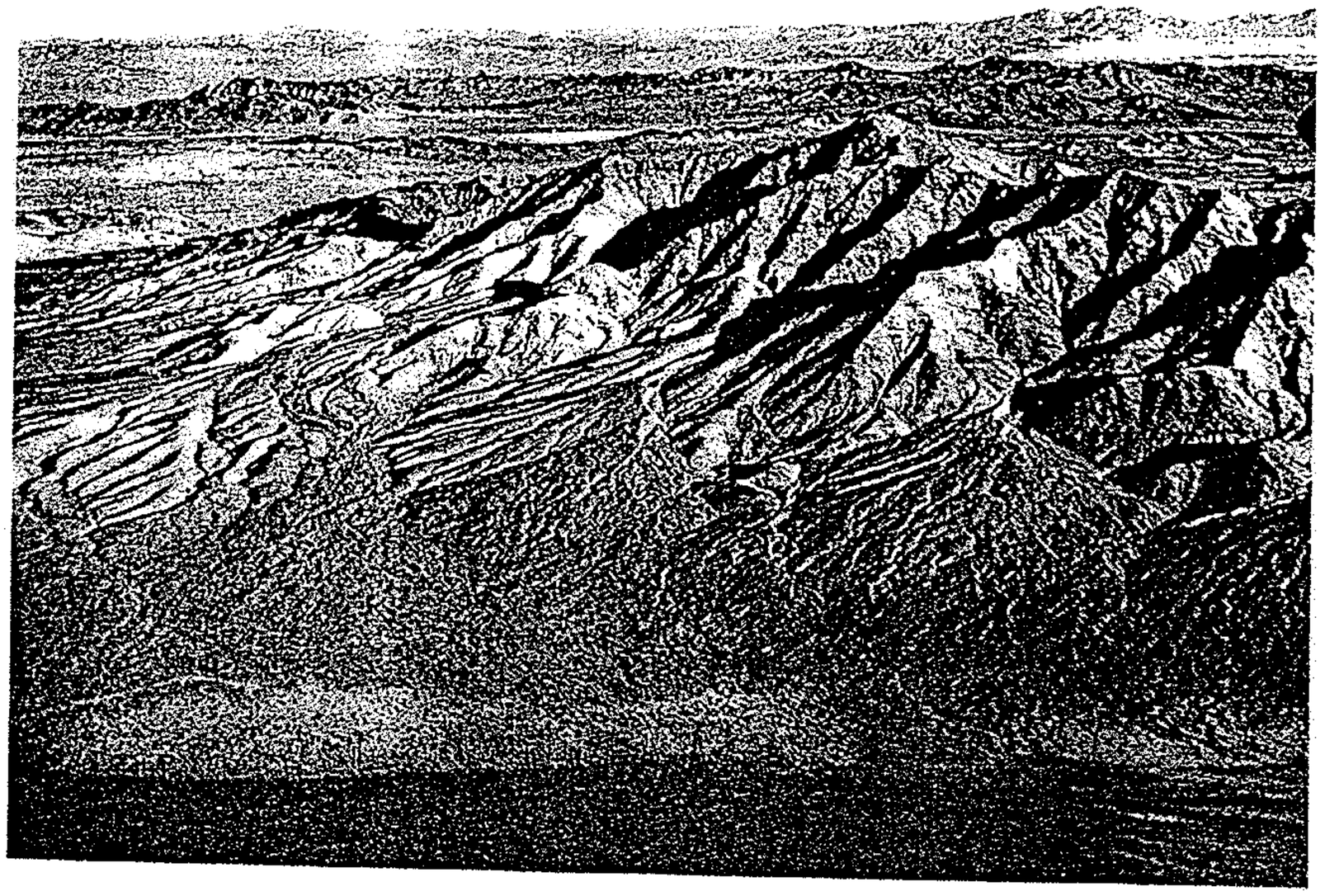

Figure 8-18
Alluvial fans in the Mohave Desert, California. Each cone-shaped fan has been deposited where the channel changes abruptly at the base of the mountains from a narrow, confined valley upstream to a broad, unconfined plain. The fans have grown together at their feet, completely obscuring the original mountain slopes. [Photo by J. R. Balsley, U.S. Geological Survey.]

13.42 Alluvial fans in Death Valley, California. The varying sizes of fans relate to the varying sizes of the drainage basins providing material to the fans. The larger the drainage basin, the larger the fan. The largest fan shown here has a radius of about 2.5 km. [Fairchild Aerial Photograph Collection, Whittier College.]

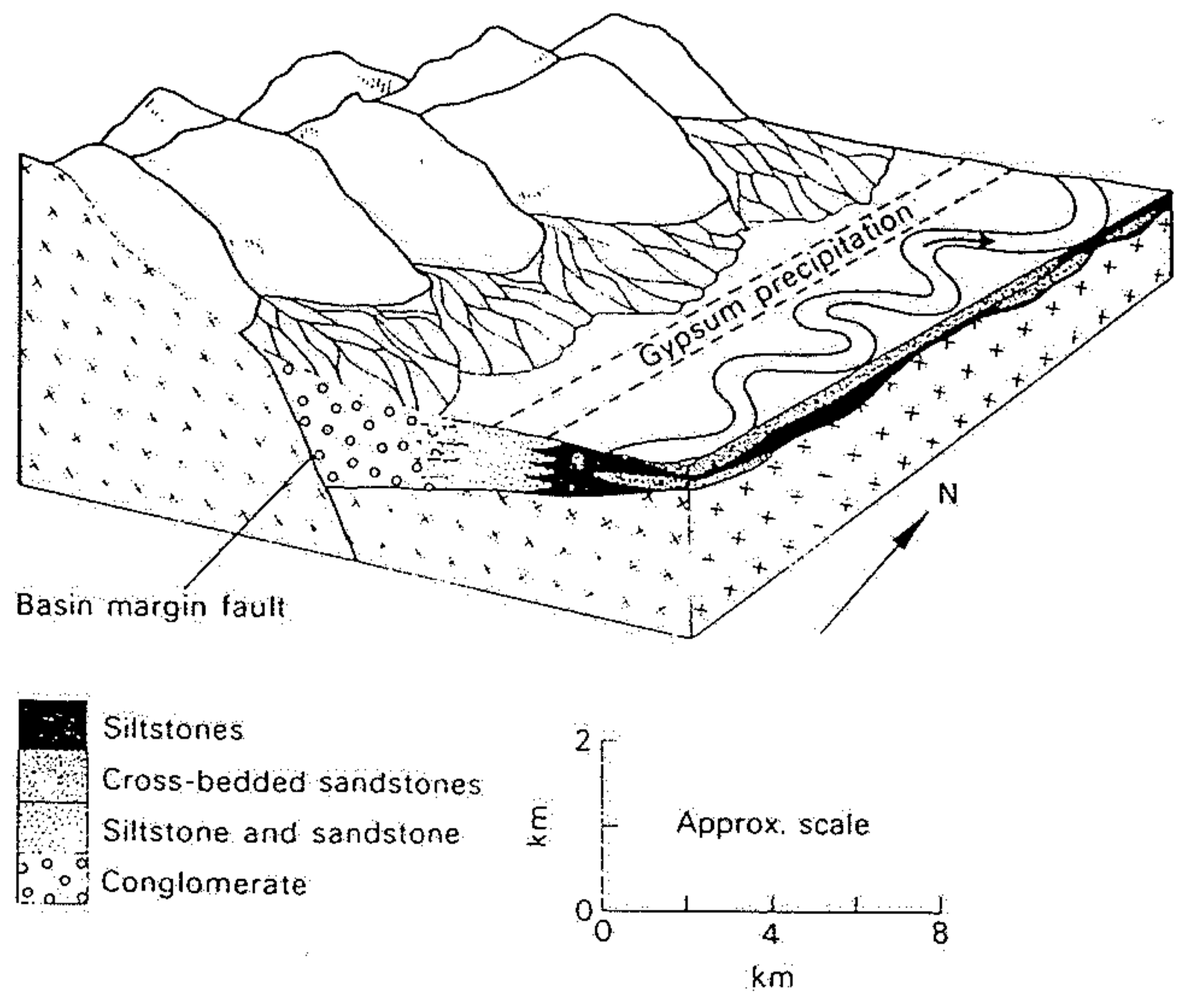

Fig. 3.34. The environment envisaged for deposition of the Røde Ø Conglomerate and associated sediments, Permian, East Greenland (after Collinson, 1972).

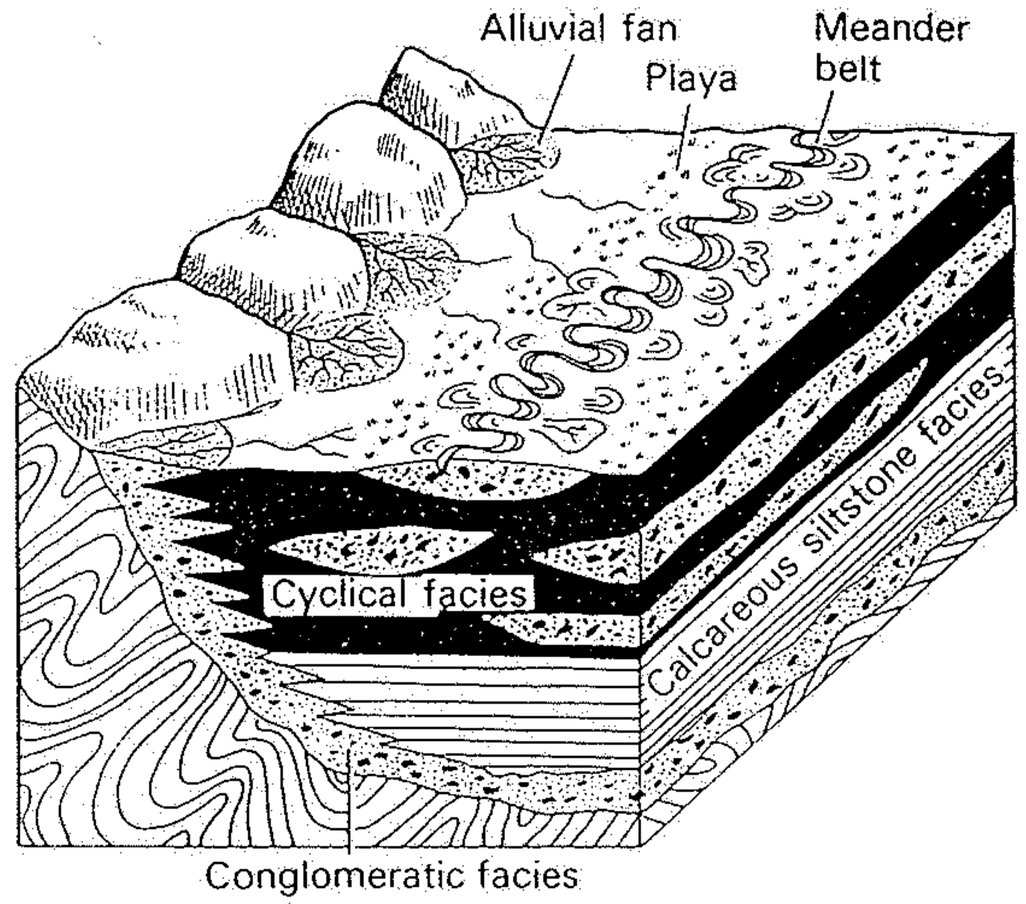

Fig. 3.54. Facies sequence and environmental interpretation of the conglomeratic and cyclical facies in the Old Red Sandstone of Anglesey, Wales (after Allen, 1965b). The calcareous siltstone facies is shown as representing a period of playa deposition prior to the arrival of the meander belt. Alternatively, it may have been deposited between the fans and the meander belt as the source area retreated.

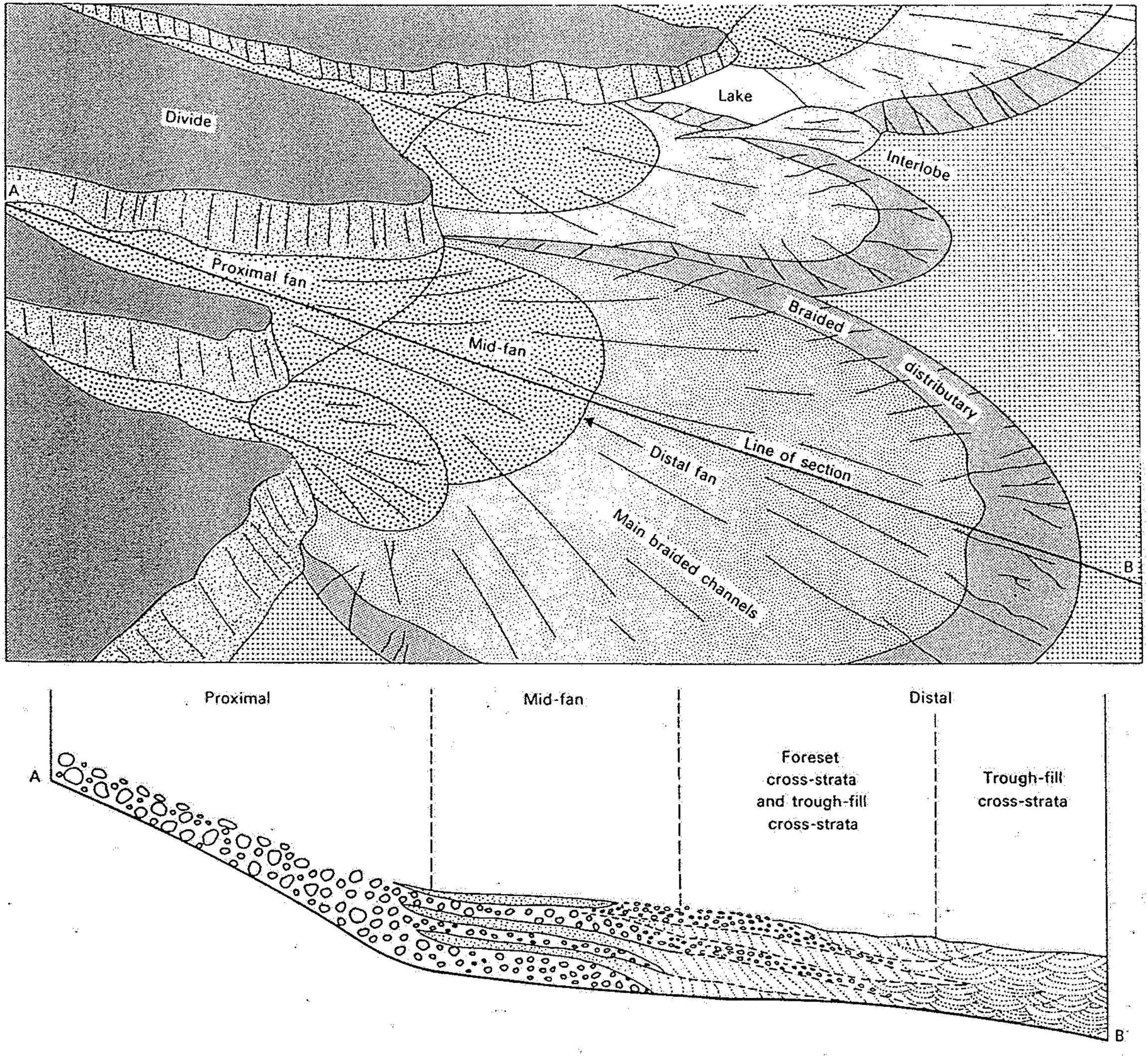

Fig. 3.38. Distribution of facies and environments in the humid deposits of the Van Horn Sandstone, Texas. The environmental and facies changes are all gradational and the diameters of the fans are of the order of 30–40 km (after McGowen and Groat, 1971).

Figure 8-20

Braided stream choked with erosional debris, near the edge of a melting glacier. Muddy River, near junction with McKinley River, Alaska. [Photo by B. Washburn.]

Figure 8-21

Meander bed and floodplain of the Animas River a few miles above Durango, Colorado. The river flows toward the lower left. [From *Geology Illustrated* by J. S. Shelton. W. H. Freeman and Company. Copyright © 1966.]

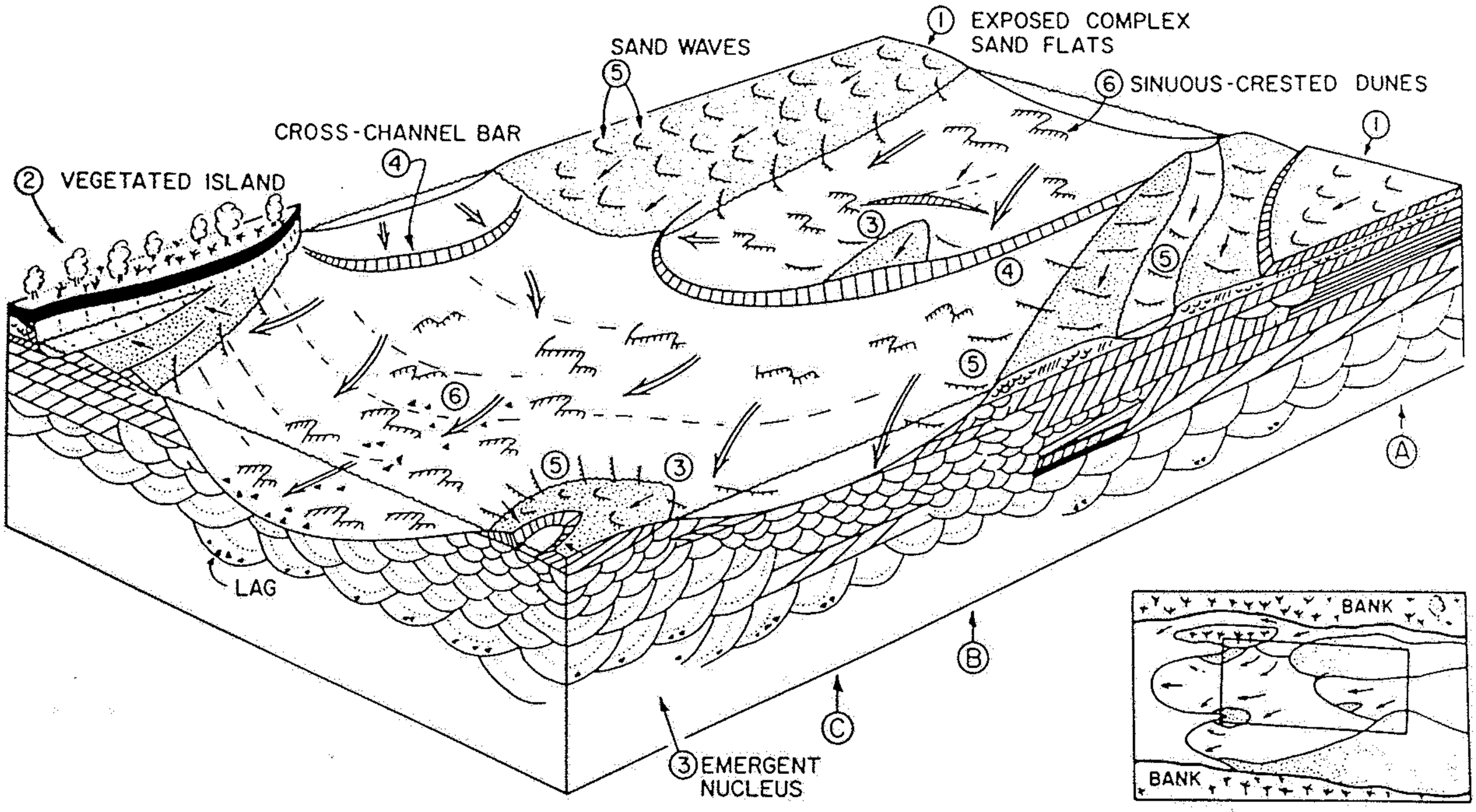

Figure 9

Block diagram showing elements (numbered) of a braided river (based on the South Saskatchewan). Stippled areas exposed, all other features underwater. Bar in left corner is being driven laterally against a vegetated island, and is forming a slough in which mud is being deposited. Large sandflats (e.g., right hand corner) may develop by growth from an emergent nucleus on a major cross-channel bar (see Fig. 10). Vertical fining-upward sequences A, B and C are shown in Figure 12, and include in-channel and bar top deposits. See Figure 2 and text for details.*

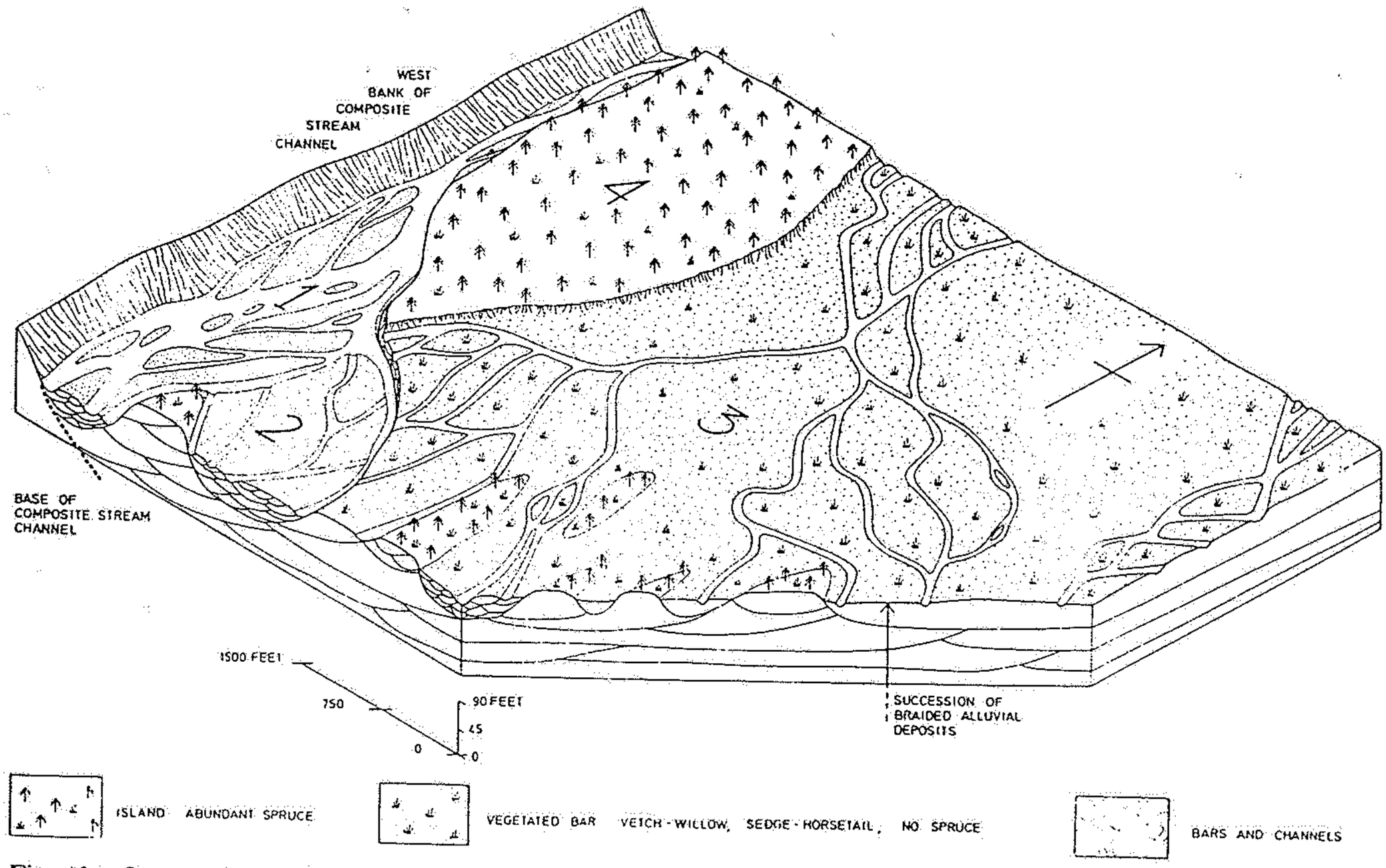

Fig. 404. Composite model of a braided river deposit. (After Williams and Rust 1969)

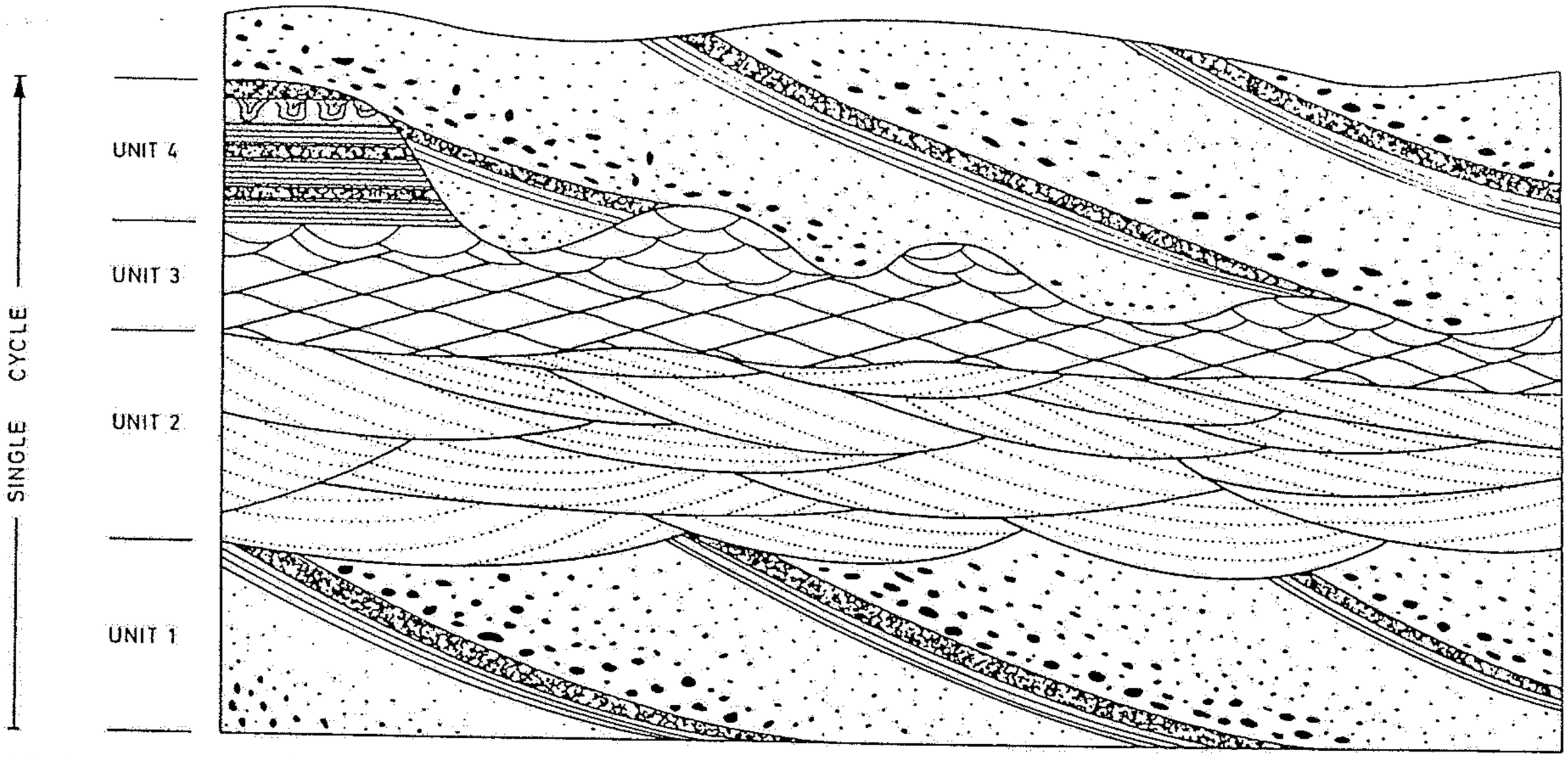

Fig. 401. Schematic vertical sequence of a braided river deposit. Unit 1–large-scale cross-bedding with pebbles; unit 2–megaripple bedding, medium sand; unit 3–small ripple bedding, fine sand; unit 4–fine sand and mud, horizontal bedding, occasional convolute bedding. (Based on data of Doeglas 1962)

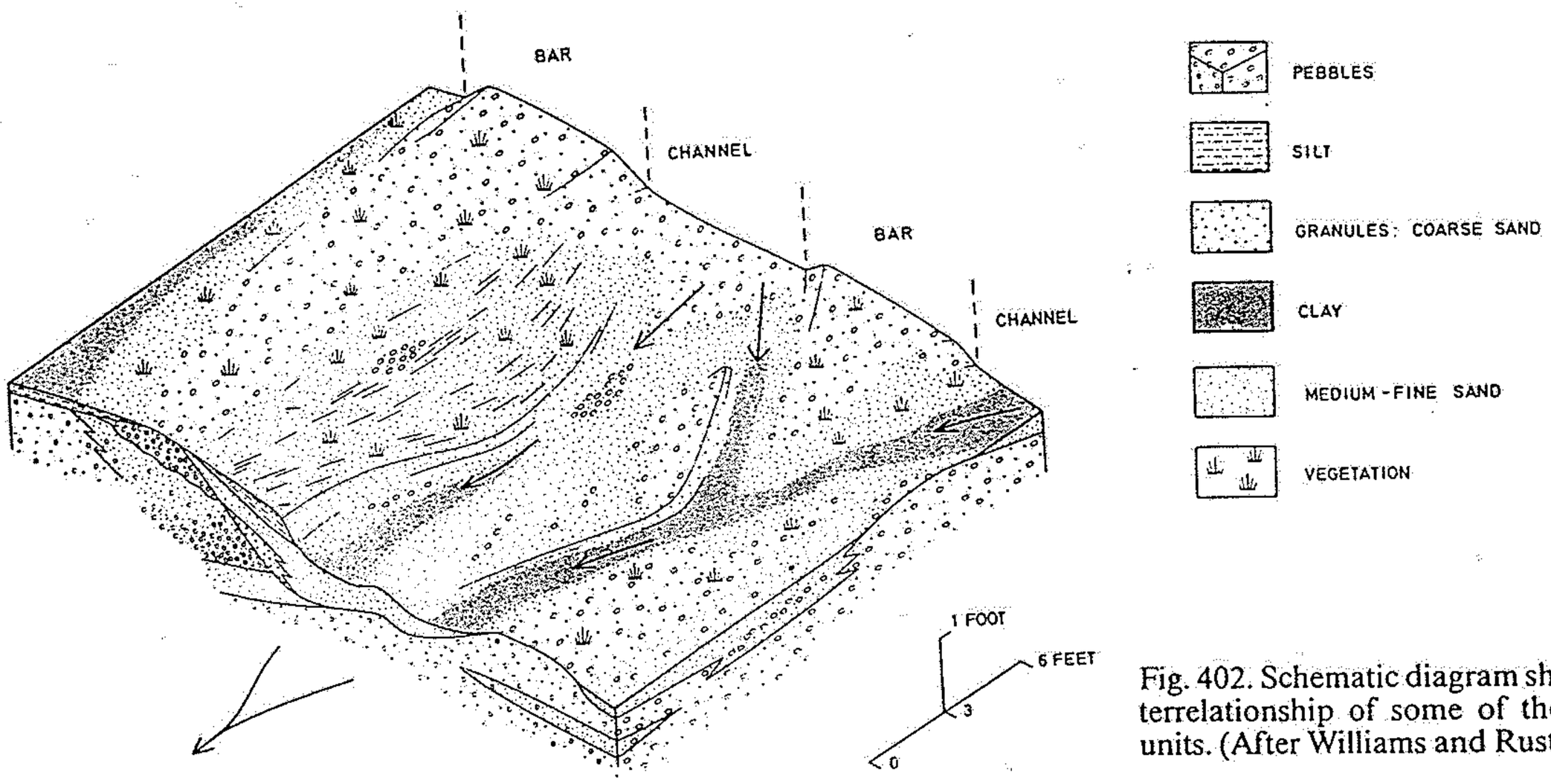

Fig. 402. Schematic diagram showing the interrelationship of some of the lithological units. (After Williams and Rust 1969)

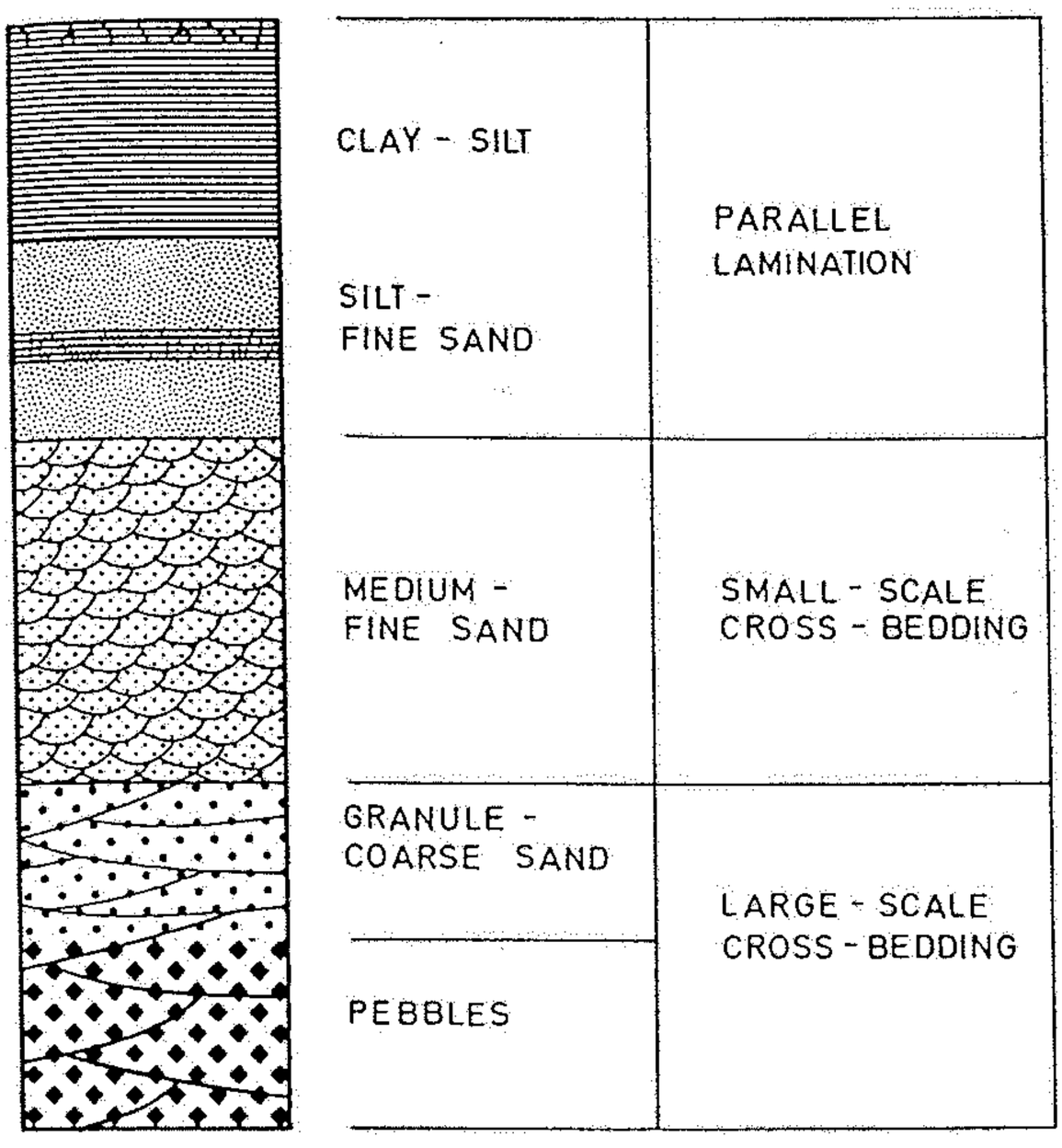

Fig. 403. Fining upward sequence of a channel-fill in a braided river. (Modified after Williams and Rust 1969)

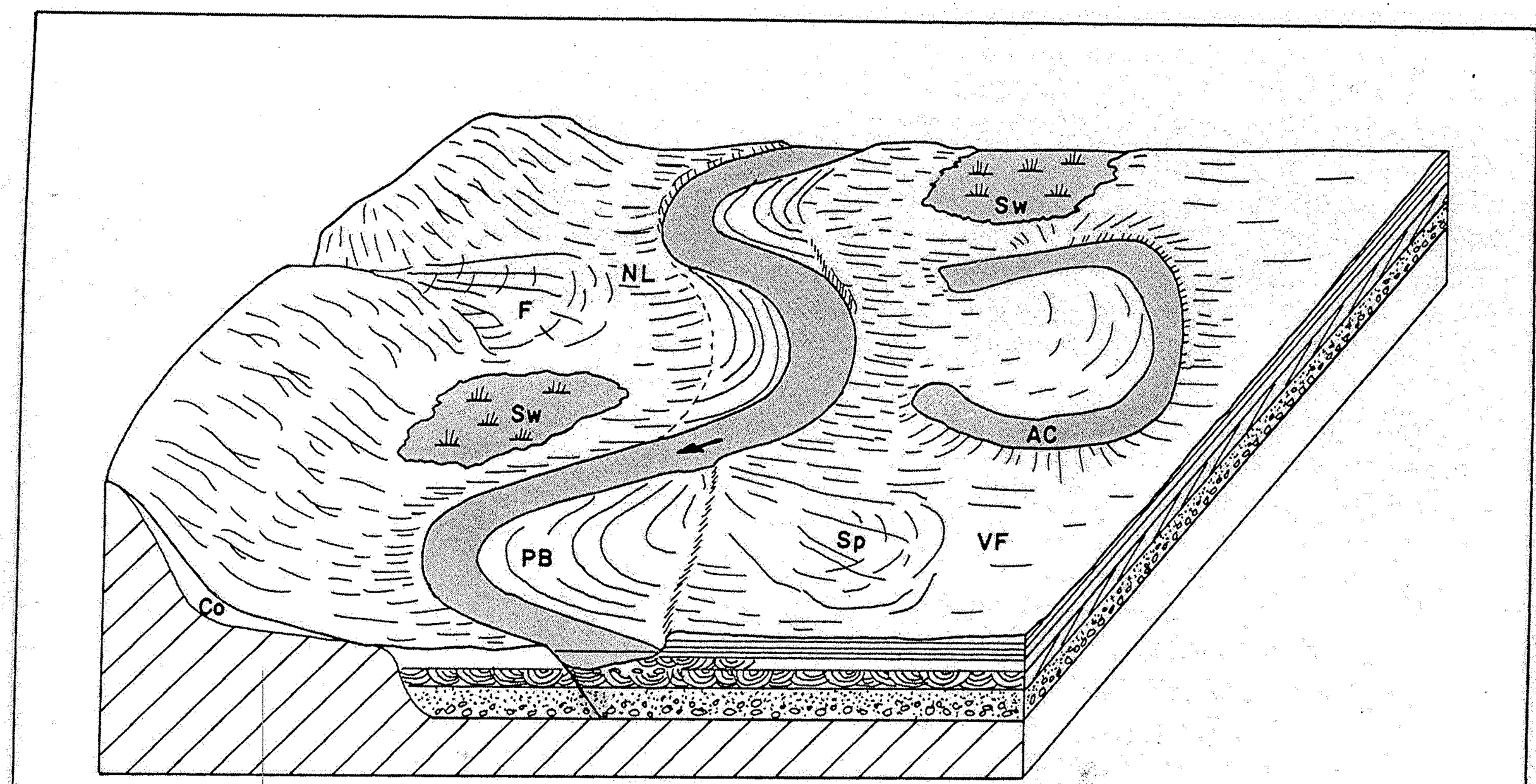

Figure 8-37 *Oblique view from above of schematic block diagram of one edge of an alluvial plain having a master stream with well-developed meanders. Slope wash from valley wall at left contributes colluvium (Co.). Tributary stream at left has built fan (F) onto alluvial plain. NL = natural levee; PB = point bar; Sp = splay deposit; Sw = swamp; AC = abandoned channel (now an ox-bow lake and filling with fine sediments); VF = valley floor. (Suggested by drawings in S. C. Happ, Gordon Rittenhouse, and S. C. Dobson, 1940, Fig. 6, p. 27; J. R. L. Allen, 1964, Fig. 4, p. 168; R. J. LeBlanc, 1972, Fig. 15, p. 151; and G. S. Visher, 1972, Fig. 11, p. 94.)*

13.17

Velocity increases away from a stream's channel walls, and the zone of maximum velocity is thrown to the outside of the bends.

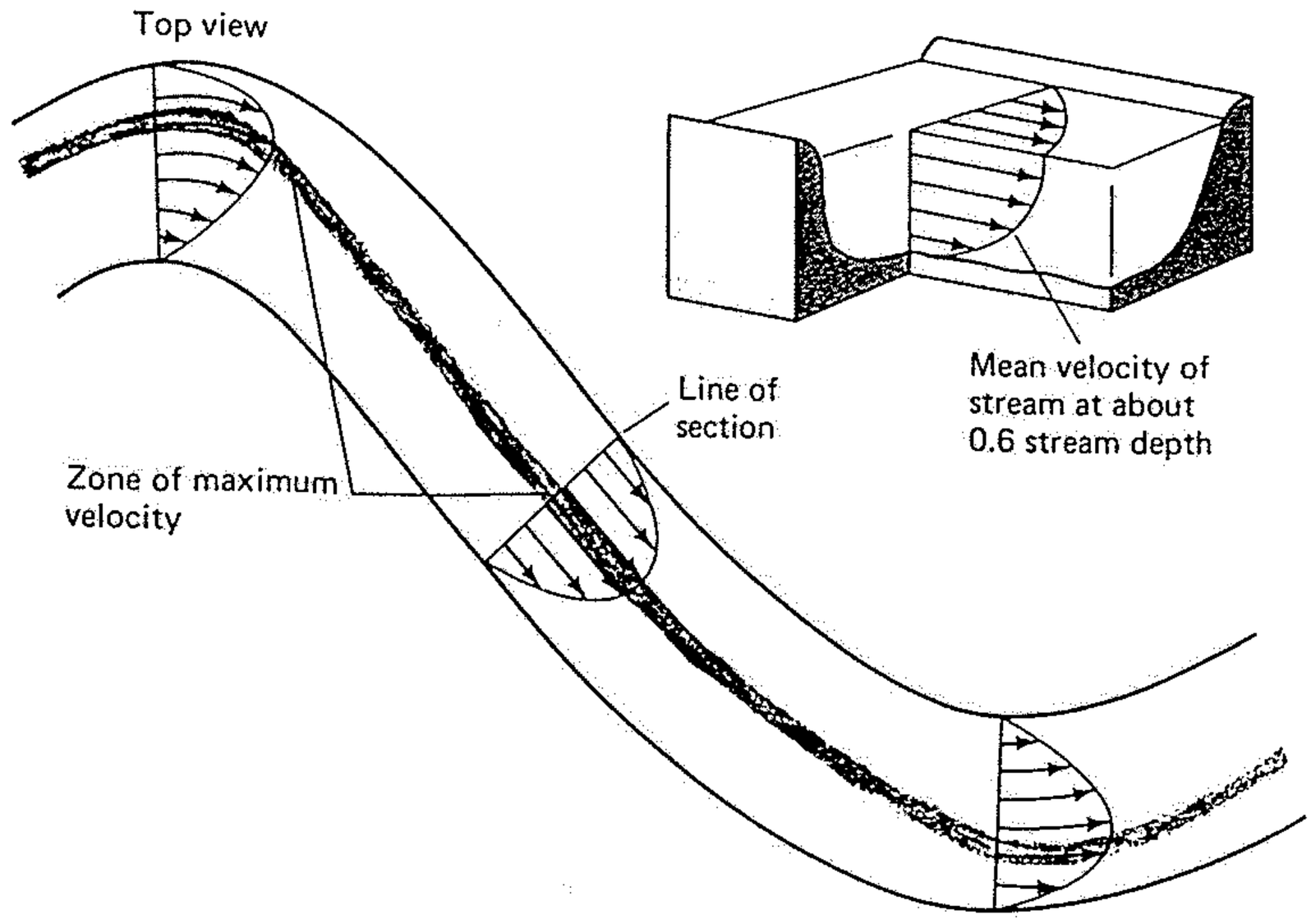

FIGURE 12–20
Localization of erosion and deposition of marked sands in an experimental sinuous stream. (After J. F. Friedkin, U.S. Waterways Experiment Station, 1945.)

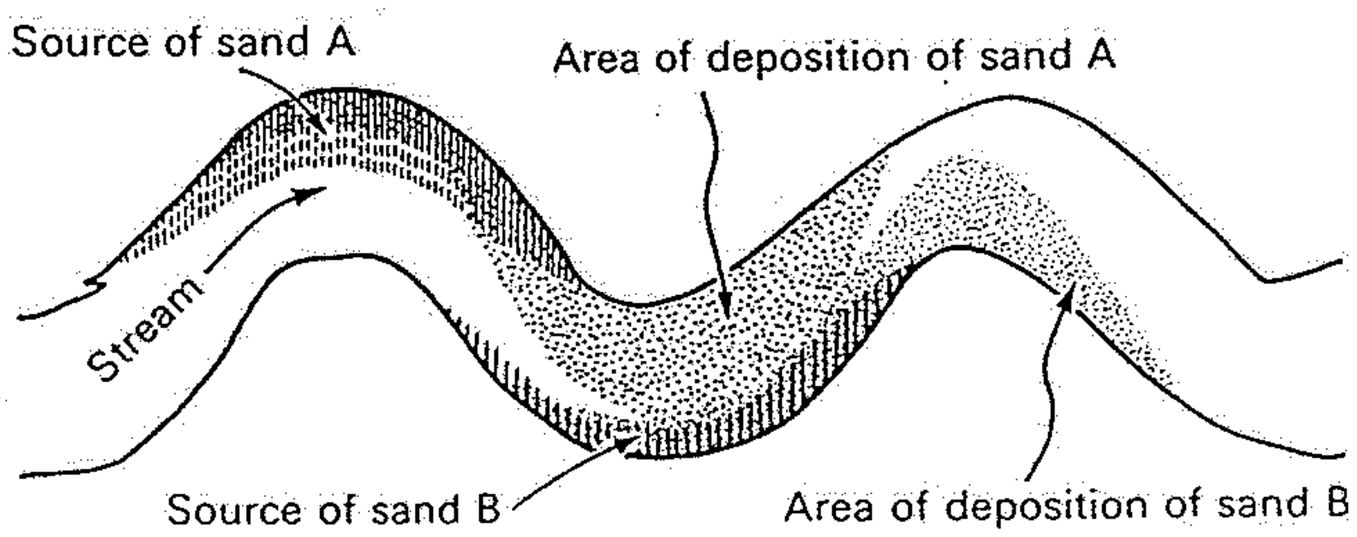

13.18

Along a bend in a river, erosion occurs on the outside and deposition on the inside. This series illustrates the results of this process in a small stream near Washington, D.C., over the years from 1953 through 1959. (Adapted from Luna B. Leopold, M. Gordon Wolman, and John P. Miller, Fluvial Processes in Geomorphology, W. H. Freeman and Company, San Francisco, p. 325, Fig. 7-54-B; copyright 1964)

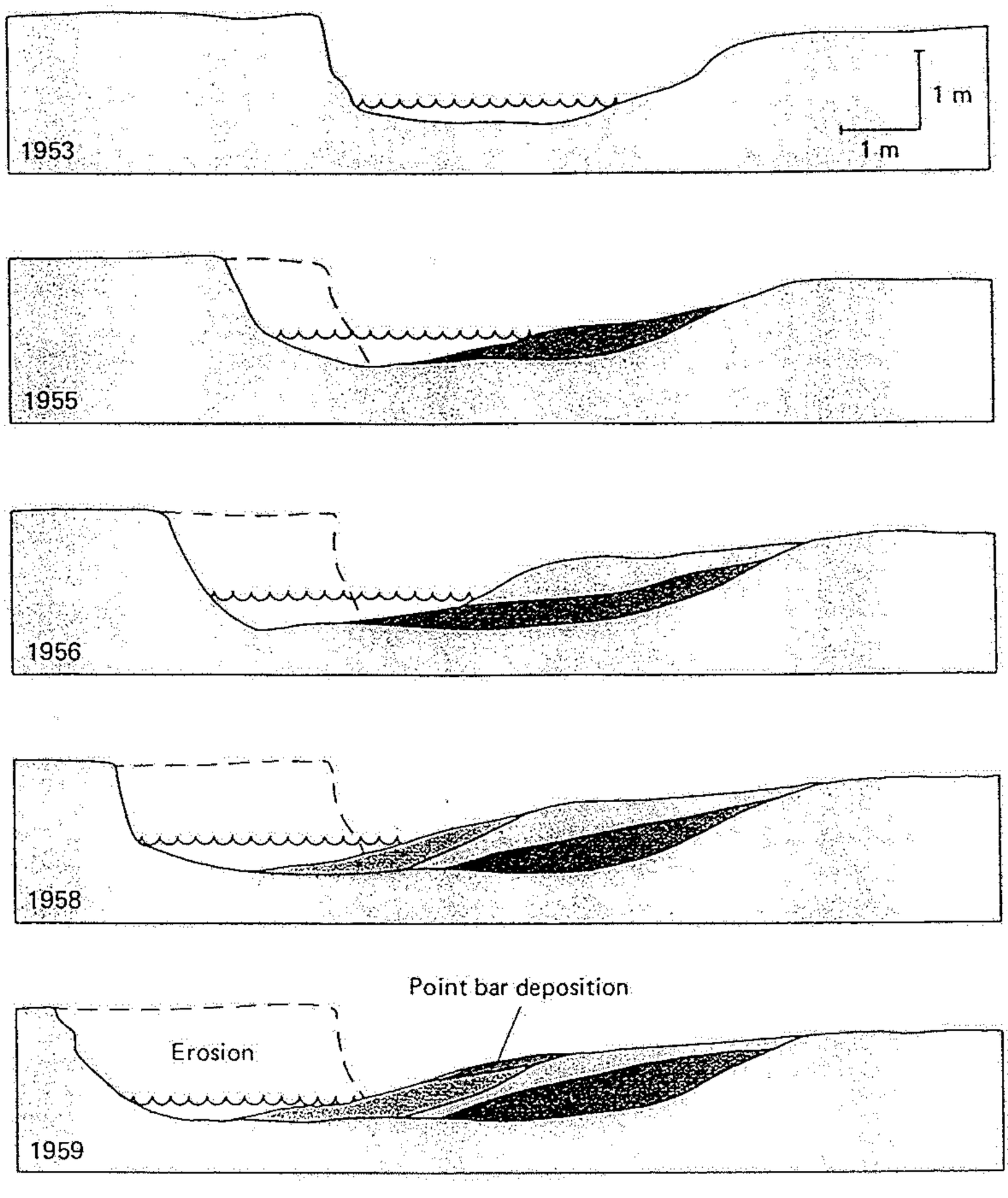

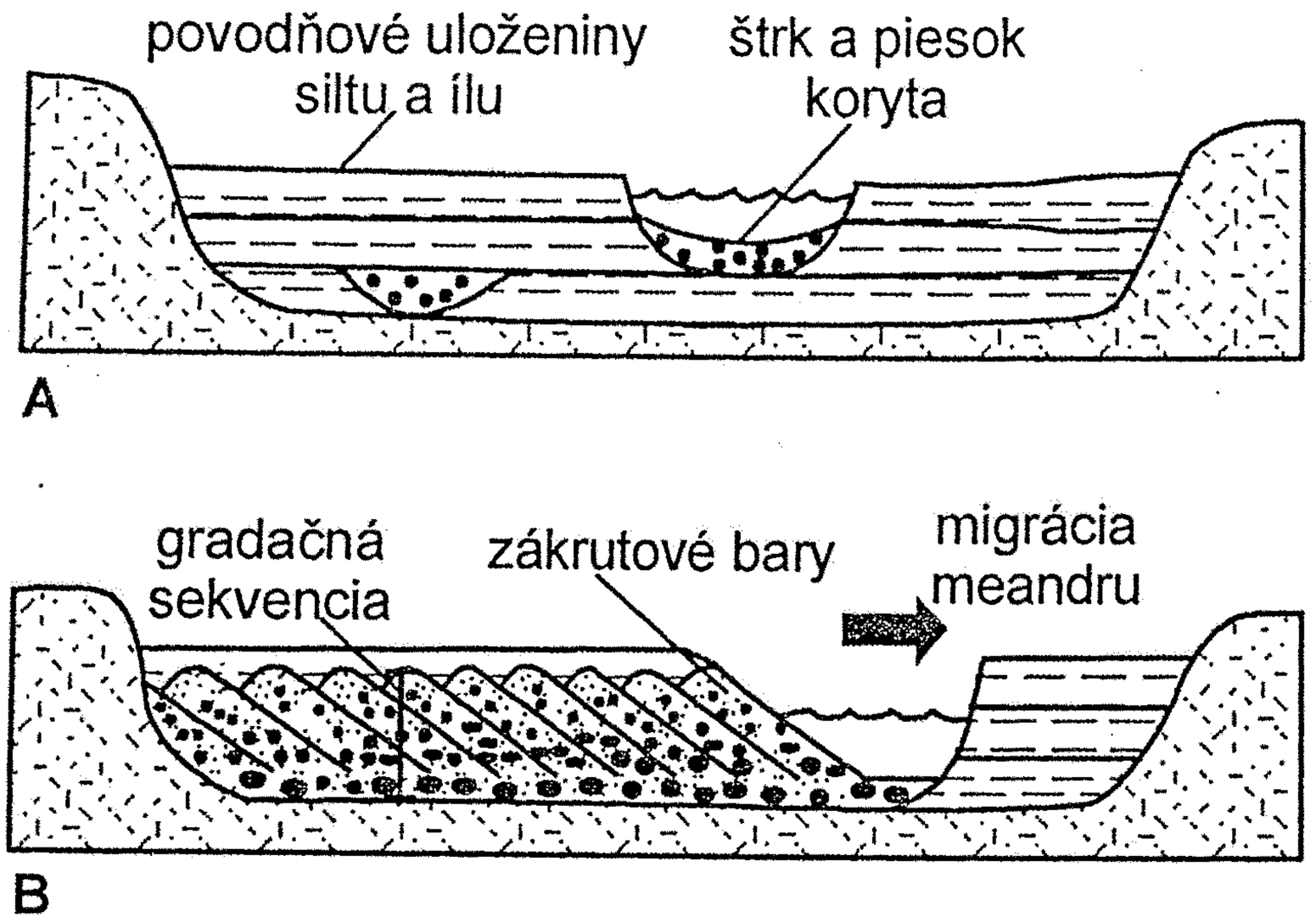

Obr. 16.12. *Tvorba aluviálnej nivy: A – pri záplavách z horizontálne uložených povodňových sedimentov s uzavretými šošovkami štrkov riečneho koryta, B – bočnou eróziou nárazových brehov meandrov a usadzovaním v korytách (štrky), na nánosových brehoch – jemné štrky a piesky zákrutových barov (gradačná sekvencia) prekryté jemnými povodňovými sedimentami. (upravené podľa Plummera – McGearyho 1996)*

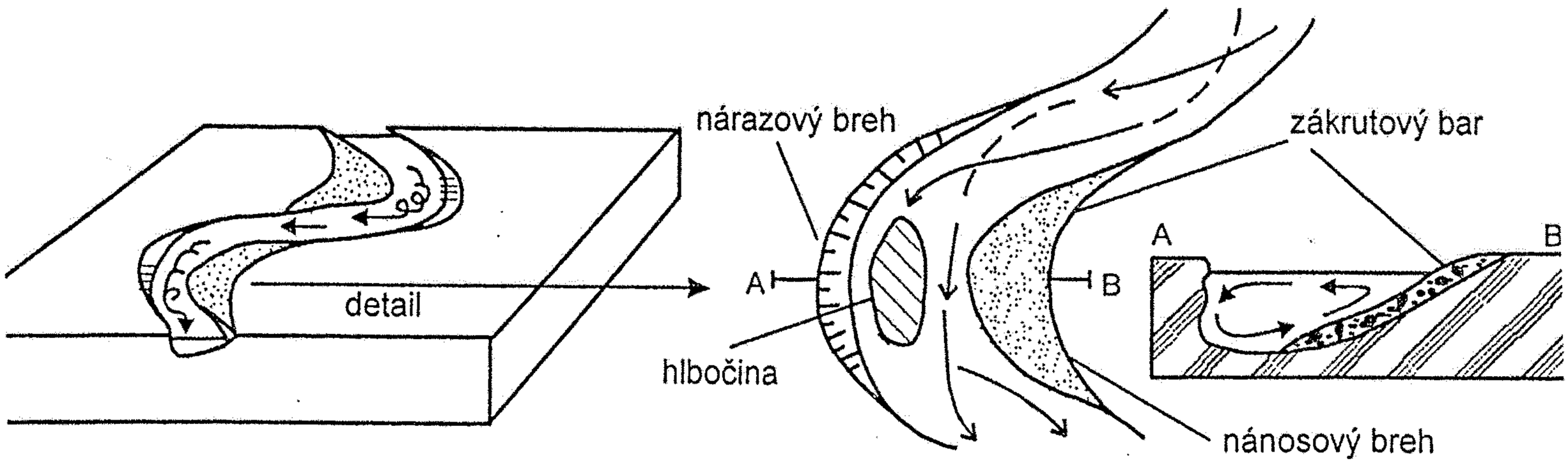

Obr. 16.13. *Skrutkovitý pohyb vody v koryte zákruty rozrušuje nárazový breh a dno (tvorí sa tu priehlbeň – hlbočina) a uvoľnený materiál a ukladá na nánosový breh. Nános – zákrutový bar má v pôdoryse mesiačikovitý tvar. (upravené podľa Plummera – McGearyho 1996)*

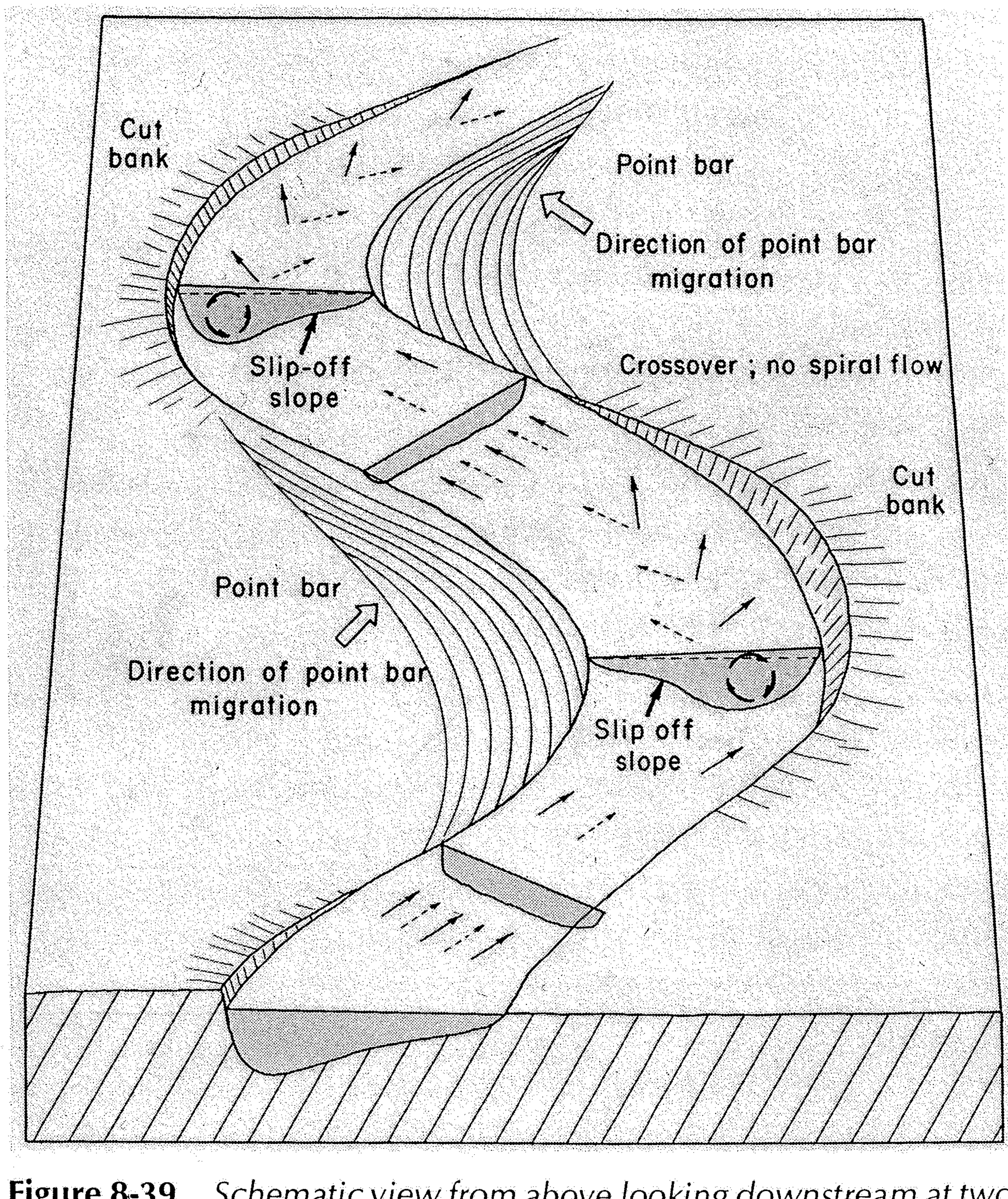

Figure 8-39 *Schematic view from above looking downstream at two meander bends and intervening crossover. Heaping up of water against outside shores of bends creates spiral flow which deepens channel in bends. In between meander bends (crossover reaches), water becomes shallow and lacks spiral flow. Solid arrows indicate directions of current at surface; dashed arrows, directions of current along bottom; circular arrows having only one barb, directions of spiral flow in plane of shaded transverse sections. Further explanation in text. (Based on J. F. Friedkin, 1945.)*

Prostředí	***Litologie***	***Sedimentární struktury***
Říční koryta	*středno až hrubozrnný písek*	*laterální akrece, korytovité šikmé zvrstvení*
Agradační valy	*jemnozrnný (jílovitý) písek až prach*	*čeřinovité a planární zvrstvení*
"Niva"	*písčitý prach až prachovitý jíl*	*deformace sedimentárních struktur; rostlinné zbytky (kořeny, listy), drobné kluzné plochy, konkrece*
Průvalové vějíře	*- jemno až hrubozrnný písek* *- jílovitý jemnozrnný písek až prach*	*- planární a korytovité šikmé zvrstvení* *- čeřinové a mázdřité zvrstvení,horiz. laminace*
Průvalová koryta	*středno až hrubozrnný písek*	*korytovité šikmé zvrstvení*
Mělká jezera na nivě	*prachovitý jíl*	*horizontální laminace; org. detrit na vrst. plochách*

Model fluviálního prostředí meandrující řeky (Miall, 1985).

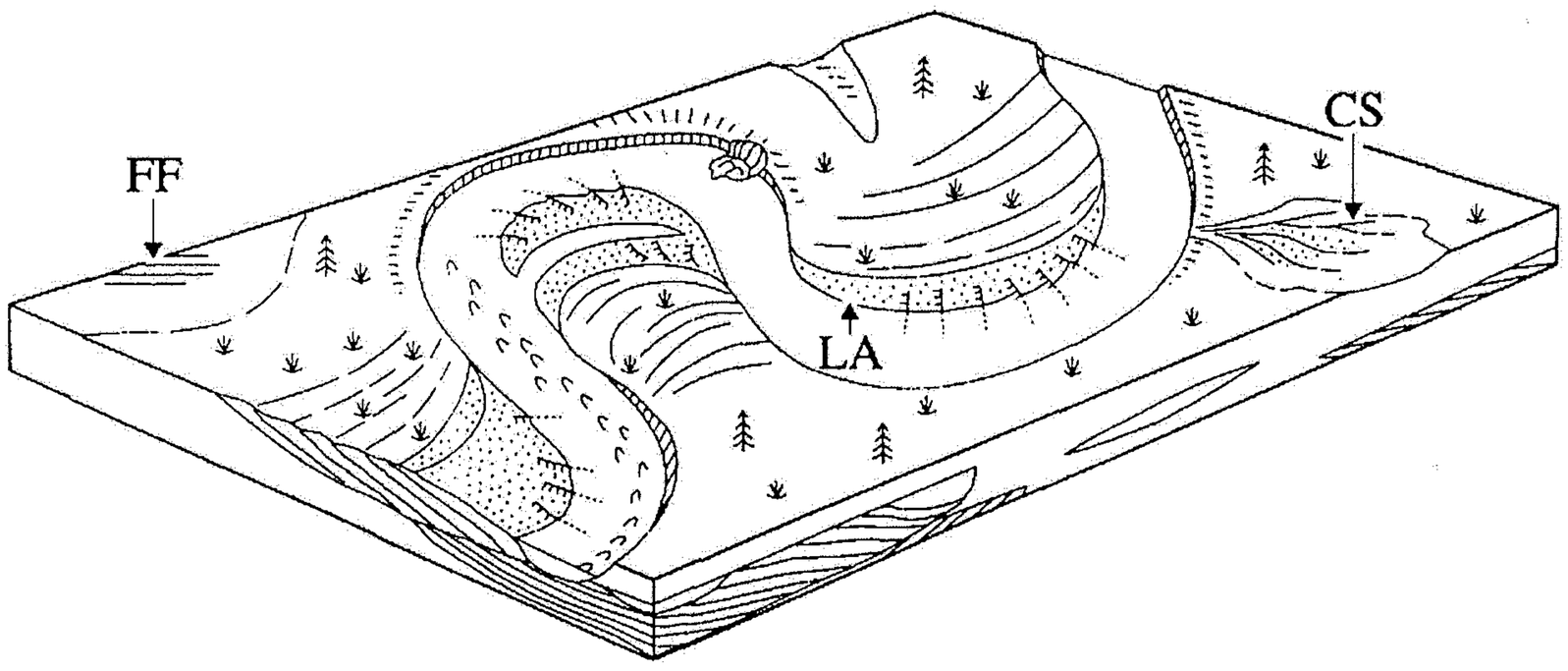

FIGURE 12–19
Idealized flow pattern of a typical meander. Left: *The velocity vectors downstream for five cross sections of the curve* (*arrows on blank background*) ; *lateral components of velocity indicated by the triangular hatched areas.* Right: *Streamlines at the surface of the meander.* (*After Luna B. Leopold and W. B. Langbein, "River Meanders." Copyright © June 1966 by Scientific American, Inc. All rights reserved.*)

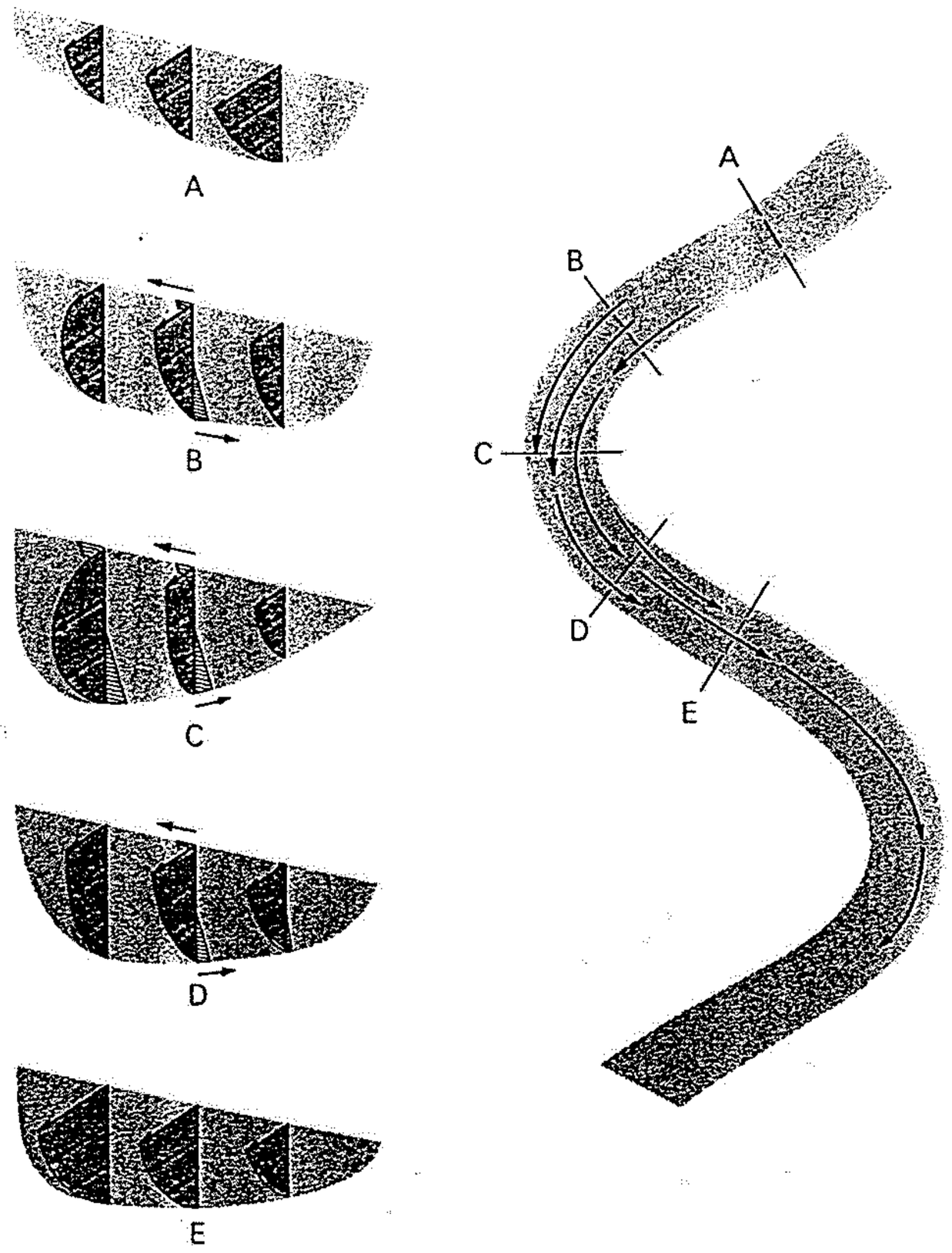

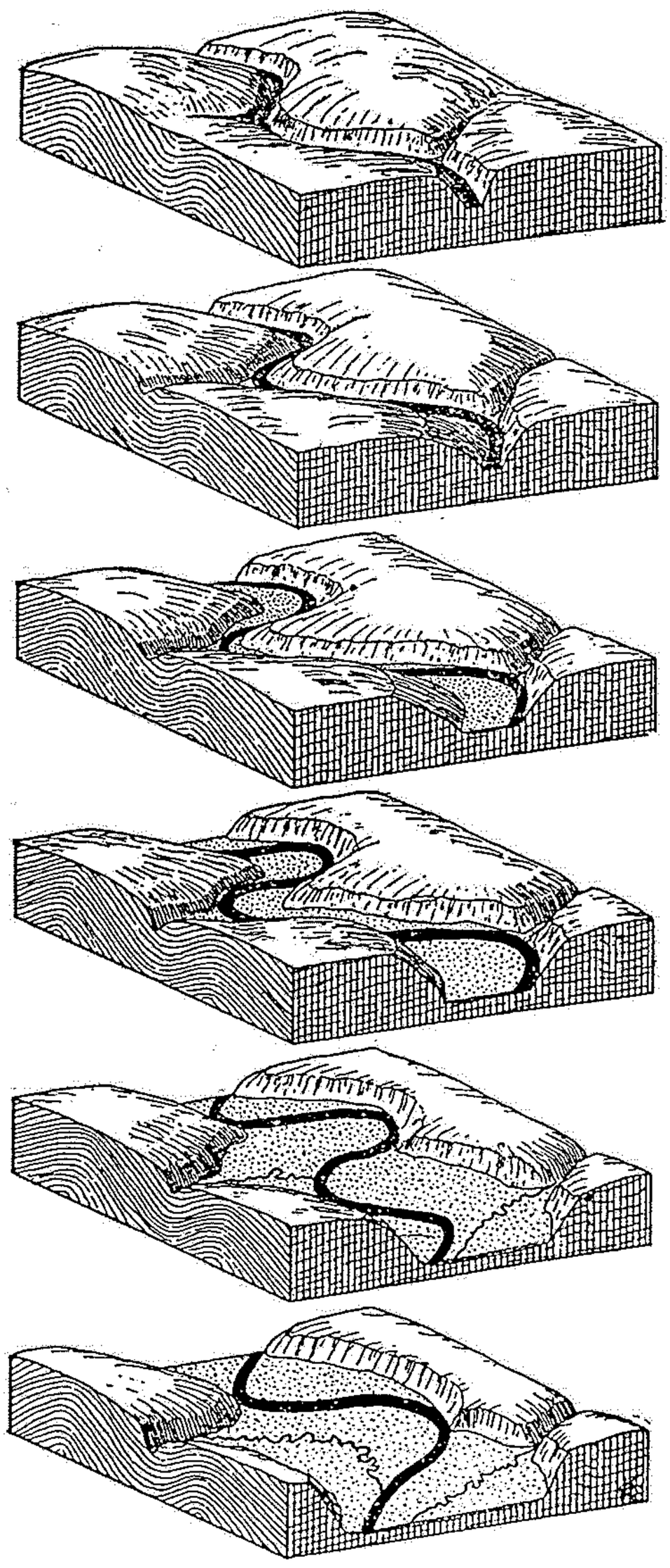

Obr. 53. *Prohlubování a rozšiřování údolí meandrující řekou. Účinky bočné erose a vznik údolní nivy.* (Sestavil autor.)

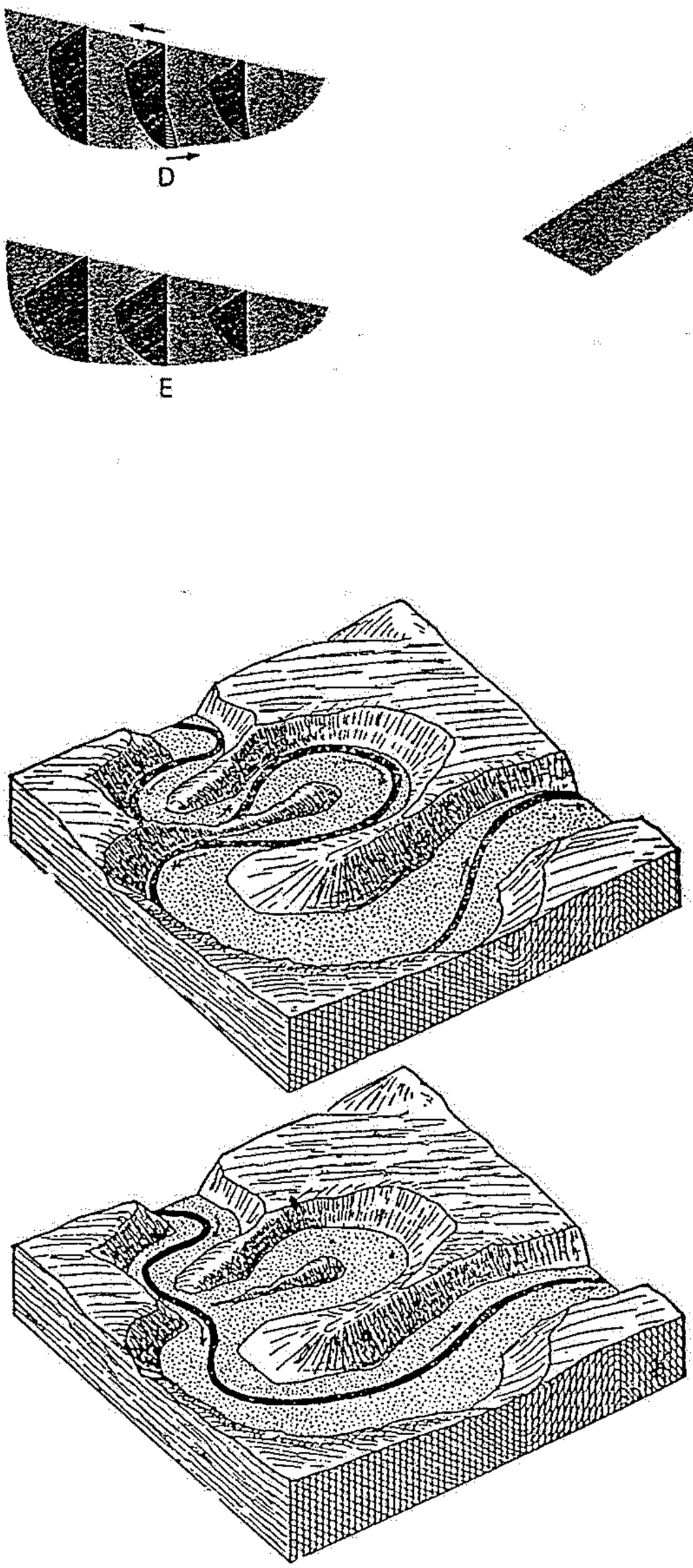

Obr. 54. *Vznik opuštěného meandru. Blokdiagram meandru u Masečína na Kocábě* (srv. obr. 119); originál.

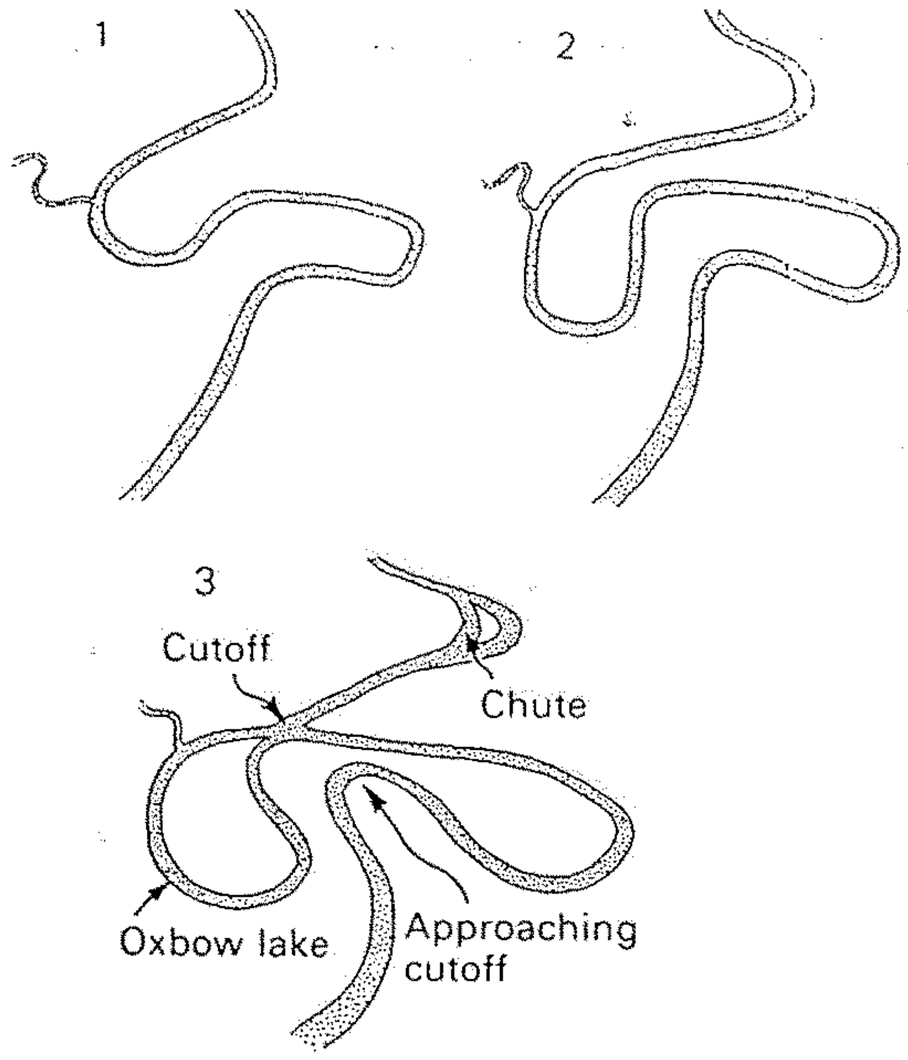

FIGURE 12–27 Top: *A river meandering on a broad floodplain. Note the lowridged deposits on the insides of bends and the abandoned meander channels, including oxbow lakes.* Bottom: *Possible stages in the evolution of the meander cutoff that has recently taken place in the center of the view. (Photo by U.S. Air Force.)*

FIGURE 12–18 *Entrenched meanders of the San Juan River, Utah. (Photo by Tad Nichols, Tucson, Arizona.)*

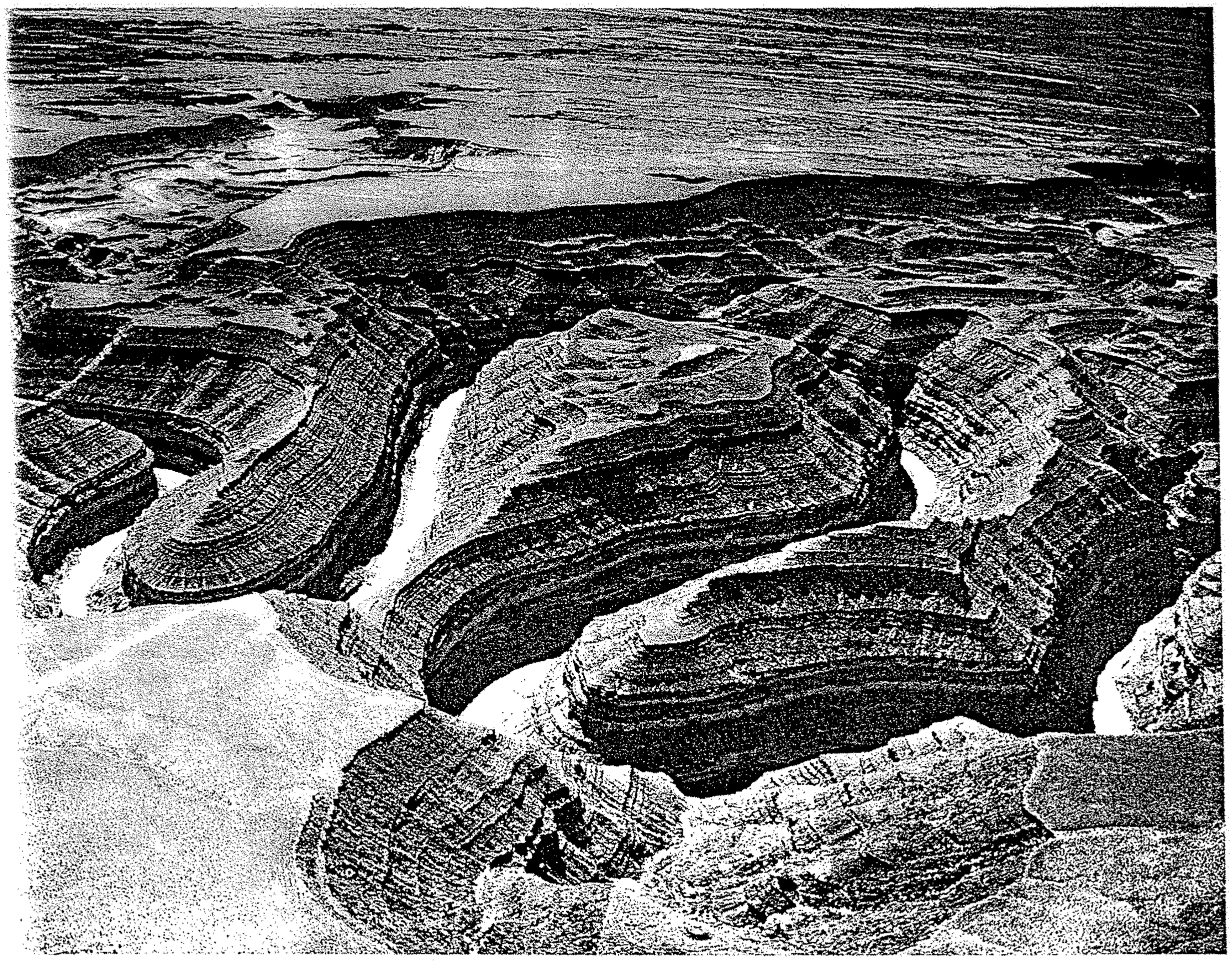

Fig. 3.24. The classical point bar model for a meandering stream (after Allen, 1964, 1970b).

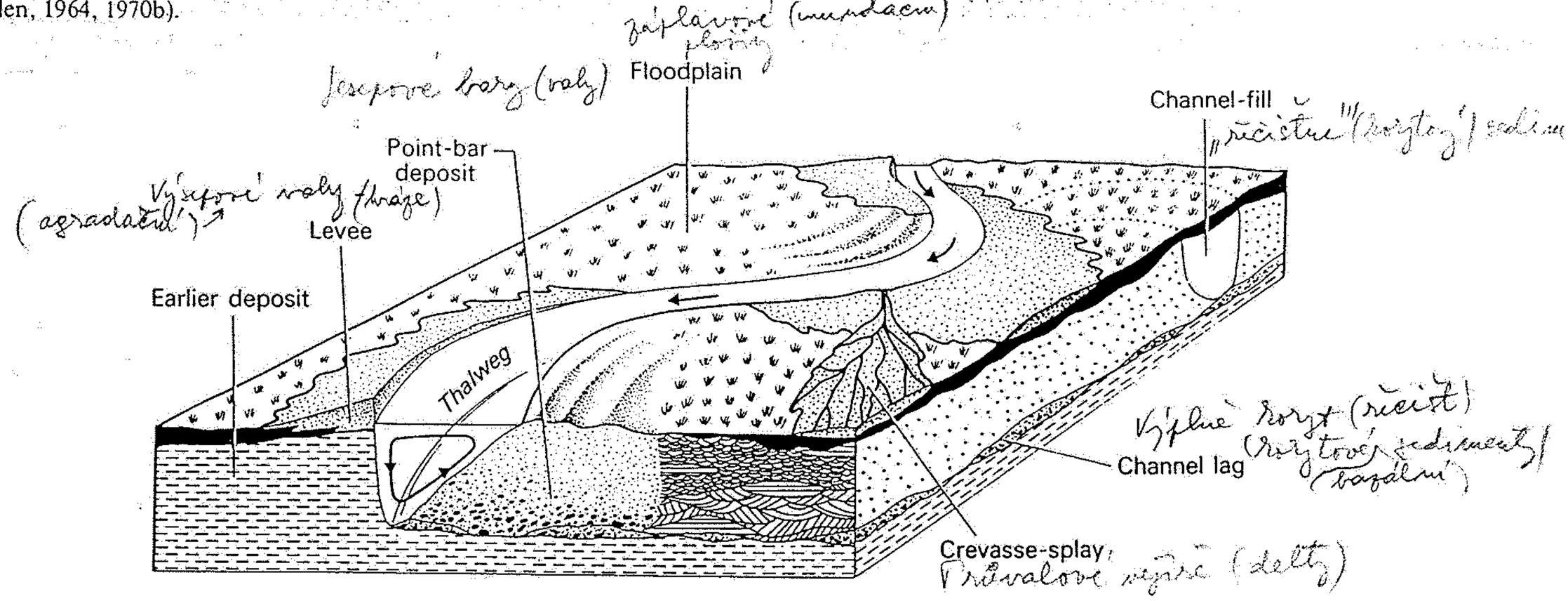

OVERBANK FLOODING

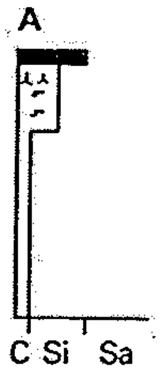

Deposition of fine sediment from suspension

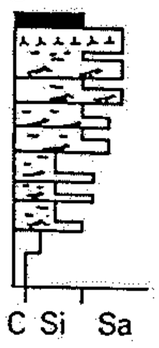

Alternating sand laden currents (overbank floods and minor crevasse splays), and deposition of fine suspended sediment. Results in levee progradation

CREVASSE SPLAY

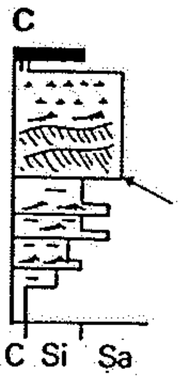

Ponded sediment

Sudden incursion of sand laden current – major crevasse splay lobe

Sheet erosion

Levee progradation

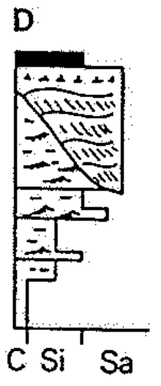

Lenticular channel units of crevasse splay origin, with unidirectional palaeocurrents

Levee progradation

MINOR SAND SPIT

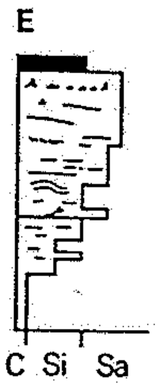

Wave reworking of crevasse supplied sediment, wave-produced structures predominate

Levee progradation

MINOR MOUTH BAR – CREVASSE CHANNEL

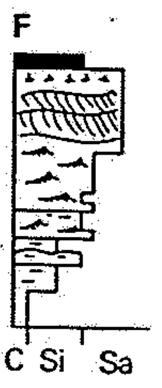

Ripple and dune migration by river currents

Minor mouth bar

Interaction of sand laden river currents, wave reworking and deposition of suspended sediment

Crevasse channel – with unidirectional currents of fluctuating velocity

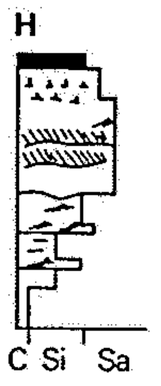

Crevasse channel

Minor mouth bar

AVULSION

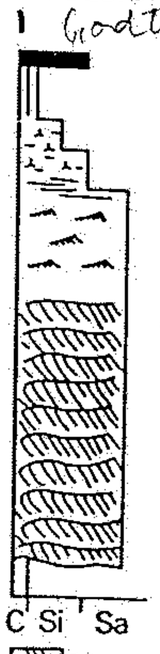

Deposition of fine sediment from suspension-overbank facies

Waning flow of unidirectional currents in point bar of fluvial-distributary

BAY MOUTH SEQUENCE

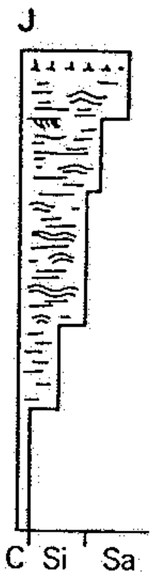

Dominance of wave-produced structures in beach or sand spit sequence

Bay mouth facies

Key

Trough cross beds
Asymmetrical ripples
Symmetrical ripples
Flat laminations
Accretion surfaces
Rootlets
Carbonaceous
Coal
Irregular erosive contact
Planar erosive contact
Gradational contact

C – Clay
Si – Silt
Sa – Sand
Vertical scale:
A–H – 2–10 m
I–J – 6–14 m

Fig. 6.8. Sequences produced in fluvial-dominated interdistributary areas (after Elliott, 1974b).

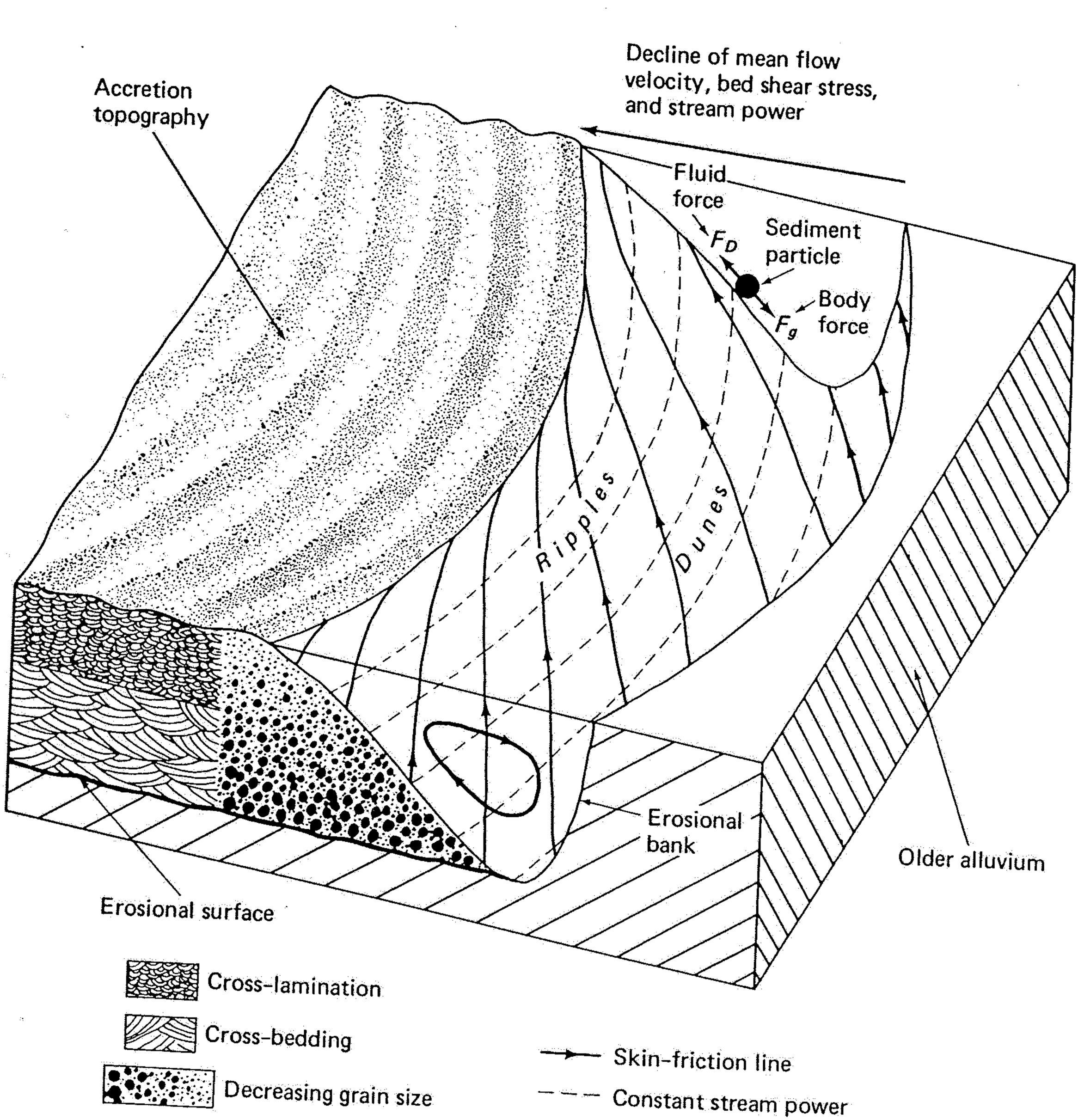

Figure 8–15 Meander bend diagram showing fining-upward lateral accretion deposits of the point-bar and fluid flow patterns. (From Allen, 1970a, Figure 4.5.)

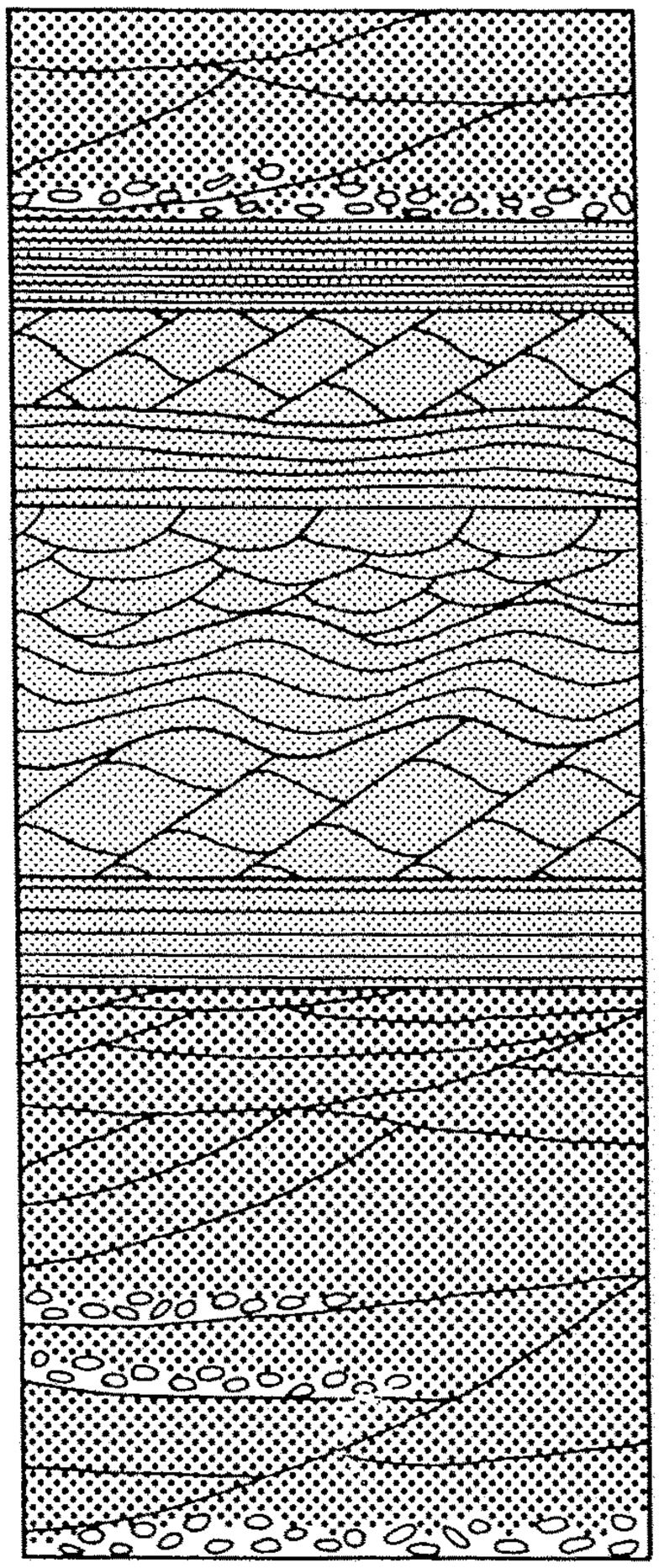

(a)

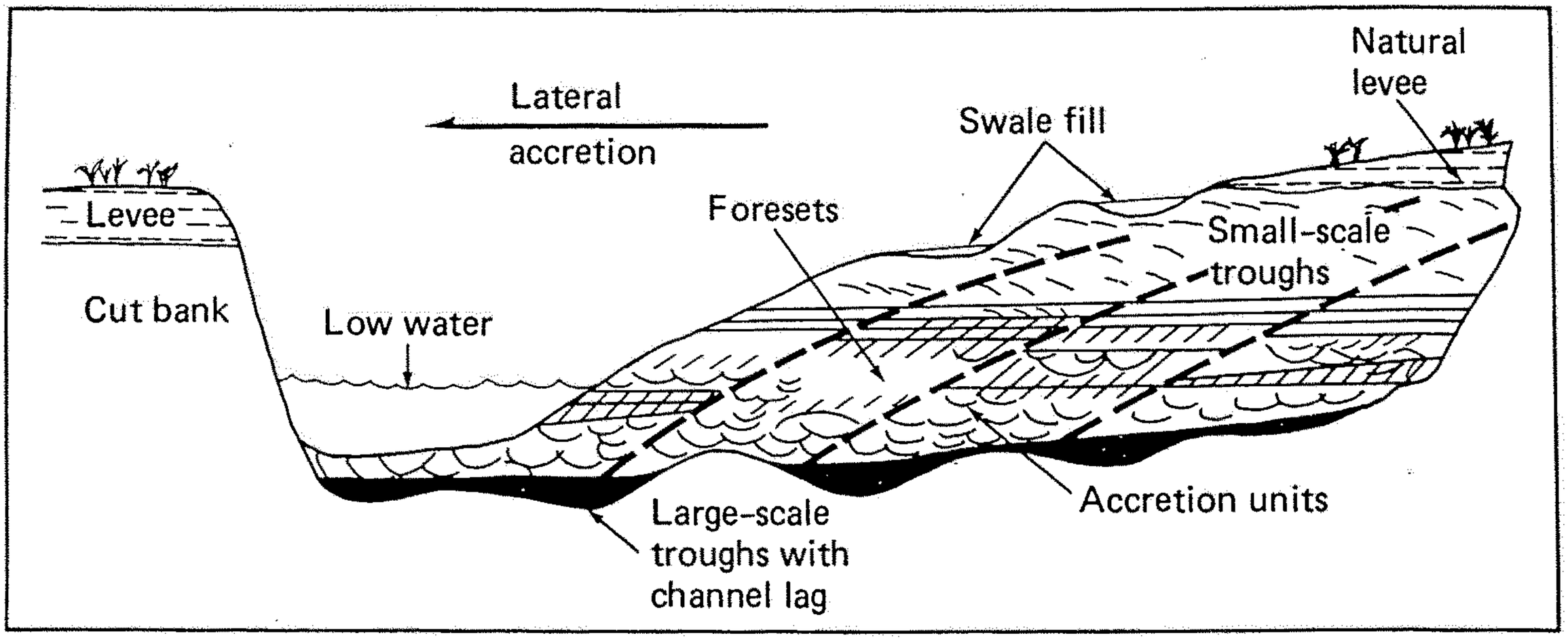

(b)

Figure 8–20 (a) Sequence of sediments and structures for the idealized, fining-upward point-bar deposit. (After Reineck and Singh, 1980, Figure 394, p. 277.) (b) Diagrammatic cross section of point bar and its contained strata with adjacent environments. (Modified after Bernard et al., 1963.)

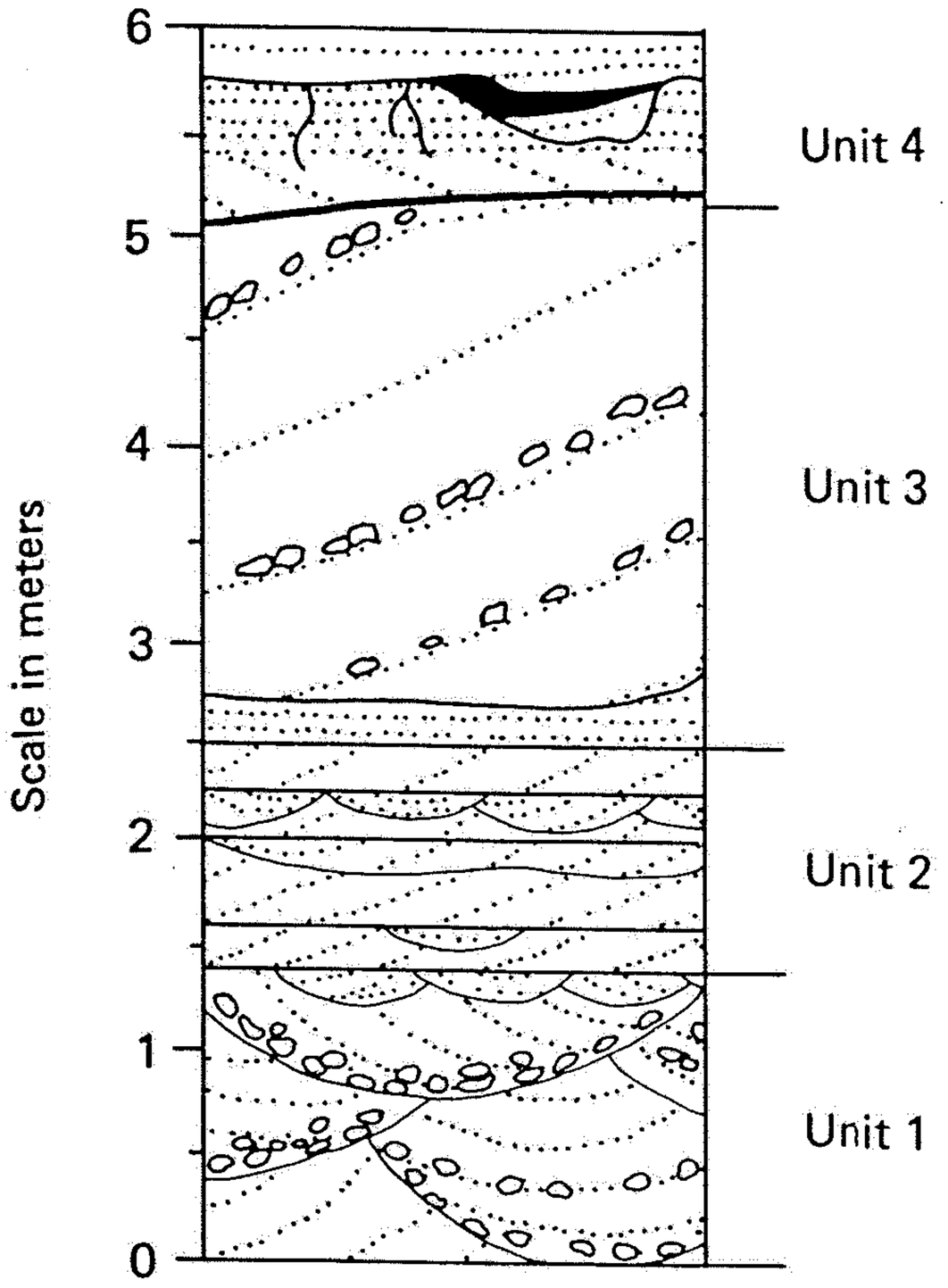

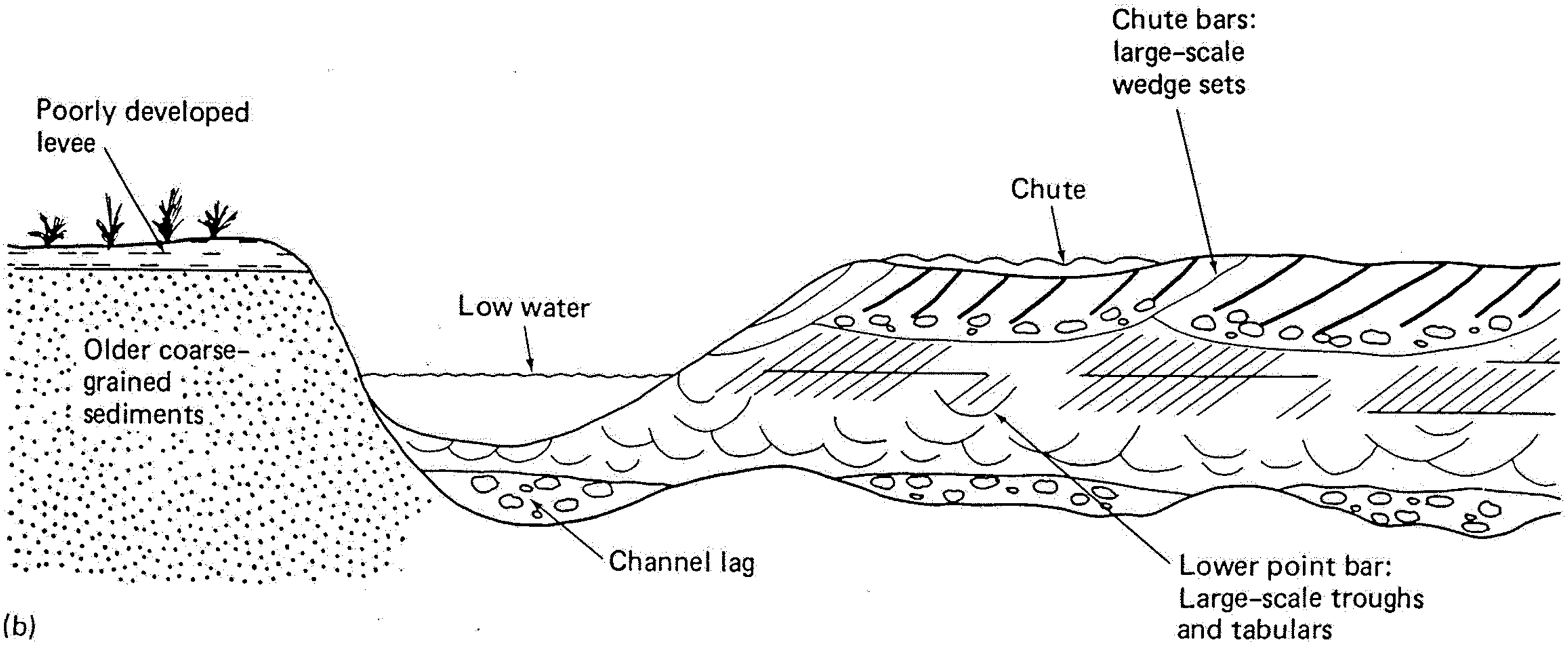

Figure 8–21 (a) Vertical sequence that characterized coarse-grained point bars. The four units represent scour pool deposit (1), lower point bar (2), chute bar (3), and floodplain (4). (Modified from McGowen and Garner, 1970.) (b) Generalized cross section shows a transverse profile across the coarse-grained point bar. (Modified from Brown et al., 1973.)

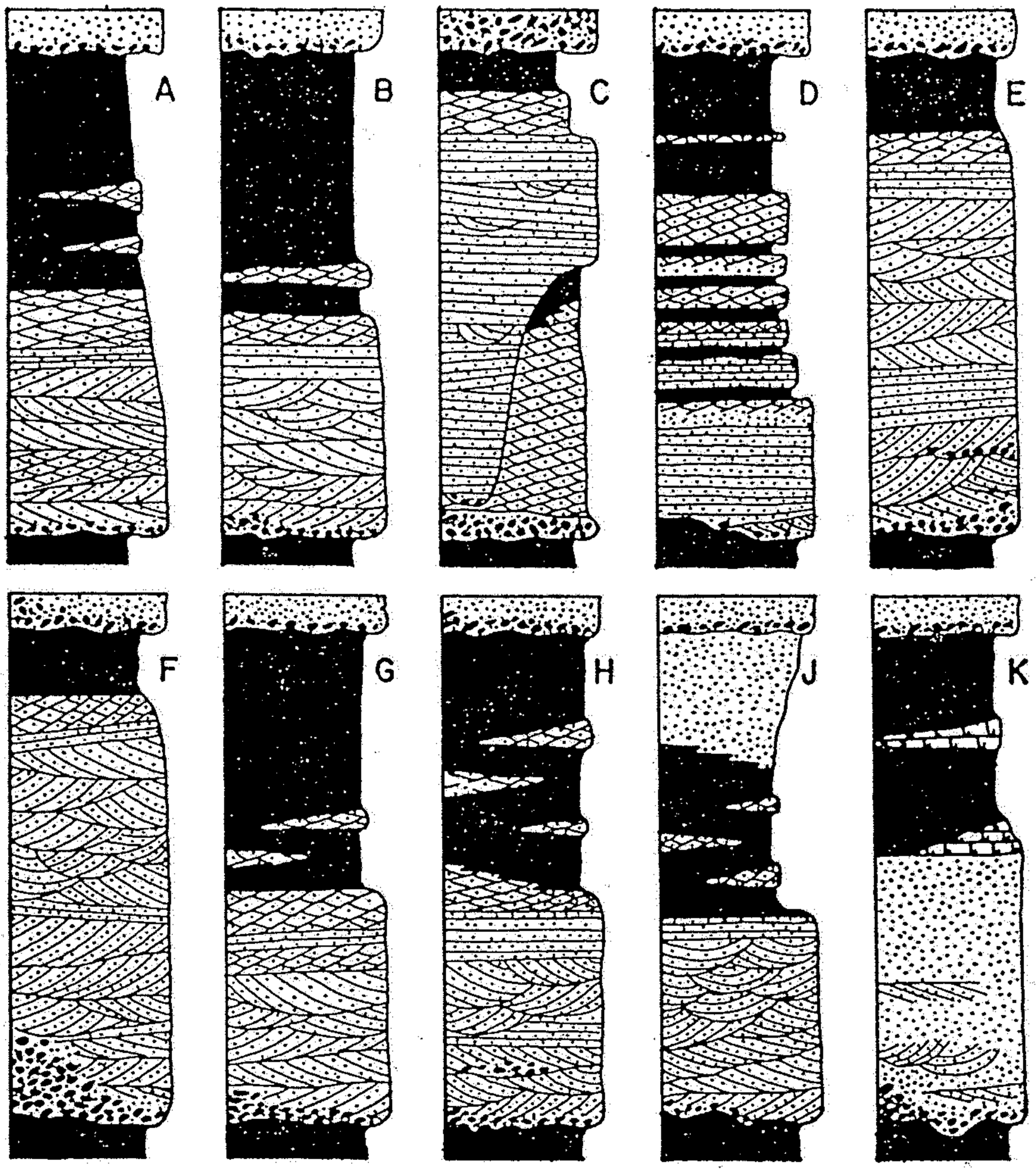

Fig.16. "Standard" and "representative" "fining-upwards" cycles: *A* = Standard cycle (thickness 2–15 m), Red Downton-Temeside Shale Groups (Lower Old Red Sandstone), Welsh Borders; *B* = Standard cycle (thickness 5–10 m), Holdgate Sandstones Group (Lower Old Red Sandstone), Welsh Borders; *C* = Cycle from Ditton Series (Lower Old Red Sandstone), near Tugford, Clee Hills (thickness of cycle 9.3 m); *D* = Cycle from Brownstones (Lower Old Red Sandstone), near Mitcheldean, Gloucestershire (thickness of cycle 8.1 m); *E* = Standard cycle (thickness 1–11 m) (Upper Old Red Sandstone), Gloucestershire; *F* = Standard cycle (thickness range uncertain but average probably several metres) (Upper Old Red Sandstone), Clee Hills, Shropshire; *G* = Standard cycle (average thickness 15 m) (Lower Devonian), Vestspitsbergen; *H* = Standard cycle (average thickness order of 5–20 m), Catskill facies, Appalachian Mountains region; *J* = Standard cycle (characteristic thickness 10–20 m), Salt Wash member, Morrison Formation, Colorado Plateau; *K* = Standard cycle (thickness 2–15 m), Molasse, Swiss Plain and Aquitaine Basin. (After J. R. L. ALLEN, 1965a.)

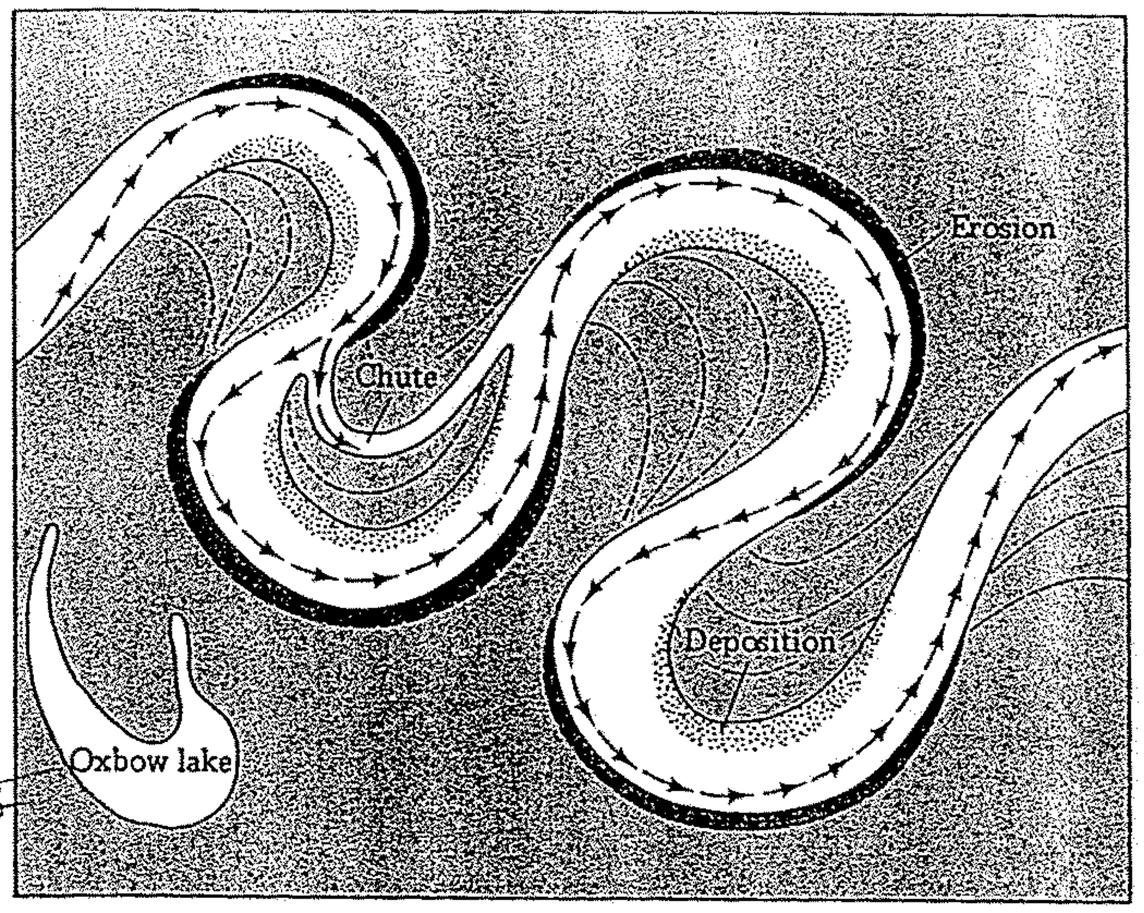

13.33 Erosion takes place on the outside of a meander bend, whereas deposition is most marked on the inside. If the neck of a meander is eroded through, an oxbow forms. A chute originates along the inside of a meander where irregular deposition creates ridges and troughs as the meander migrates.

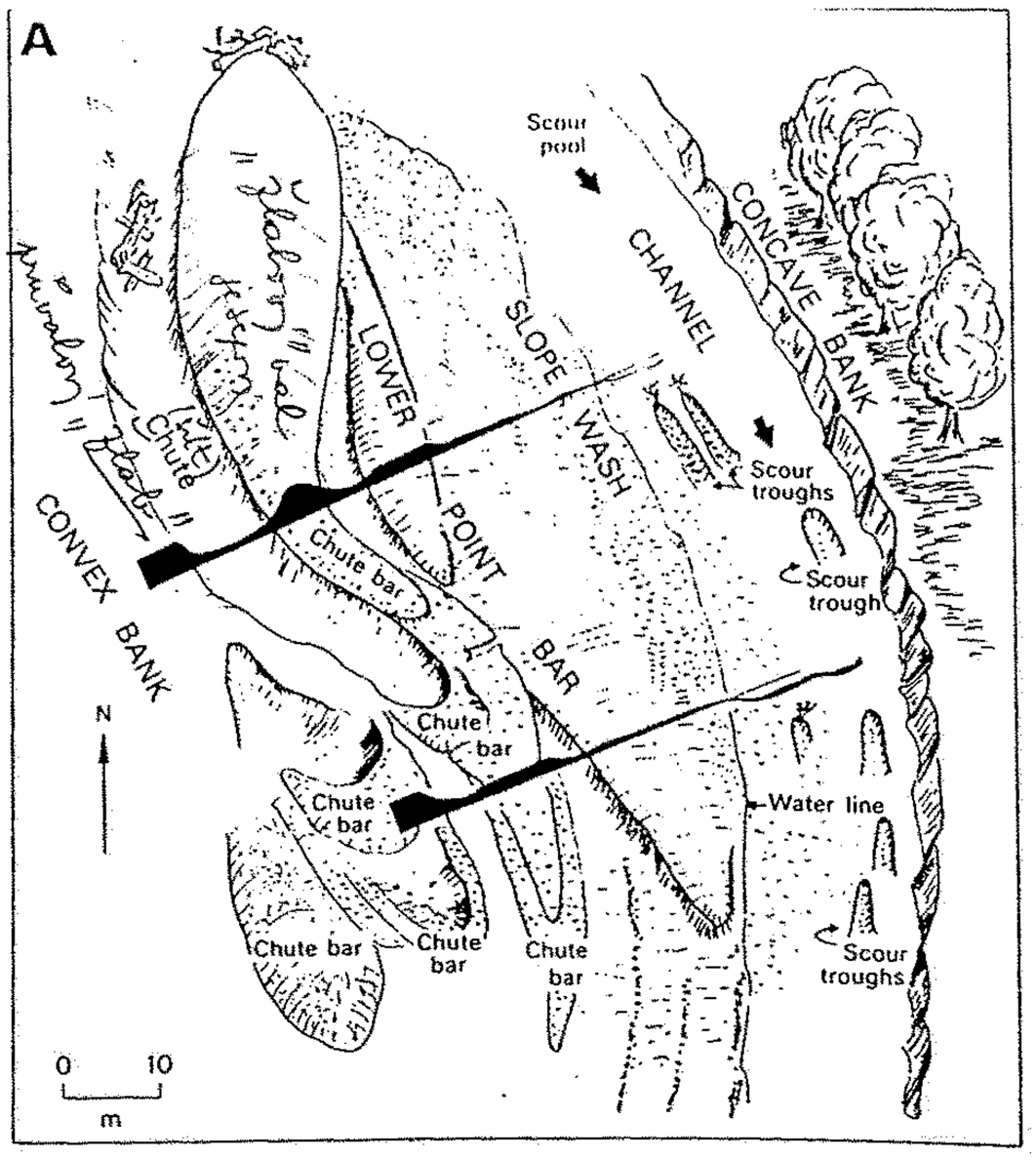

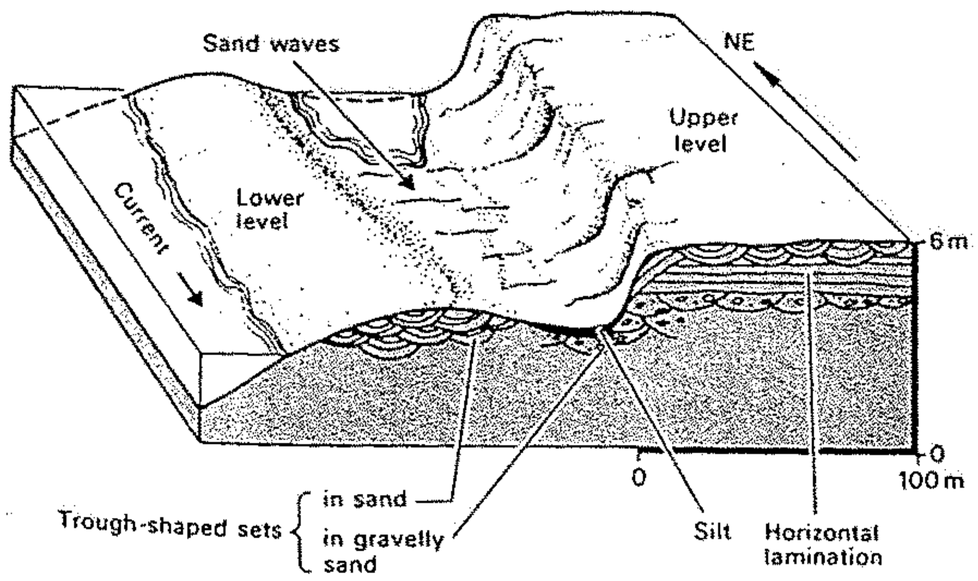

Fig. 3.25. Upstream part of Beene point bar showing the stepped profile and the associated internal structures (after Harms *et al.*, 1963).

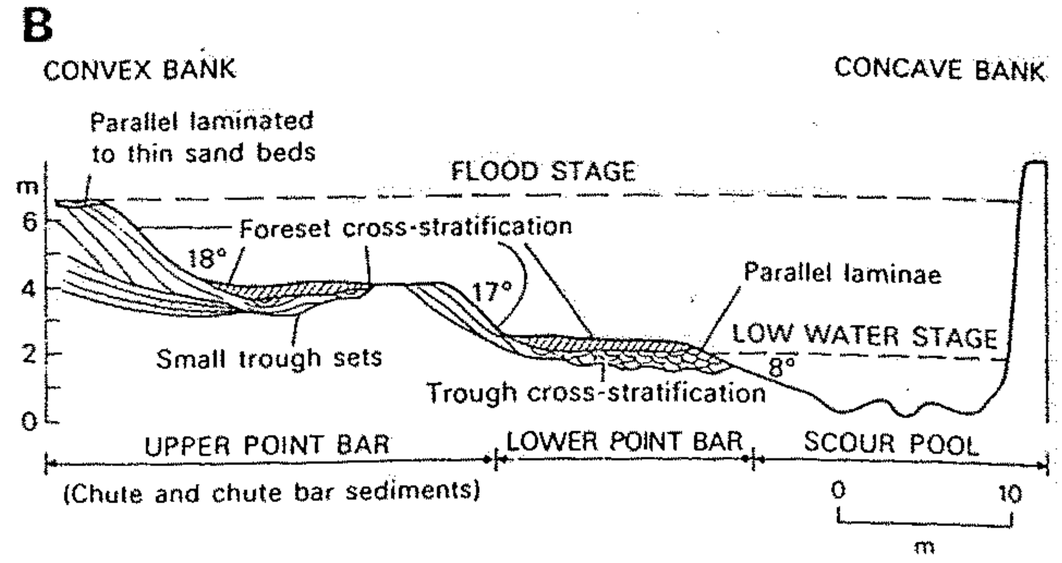

Fig. 3.26. Topographic features and internal structure of a coarse-grained point bar. (A) Plan, (B) cross-section (after McGowen and Garner, 1970).

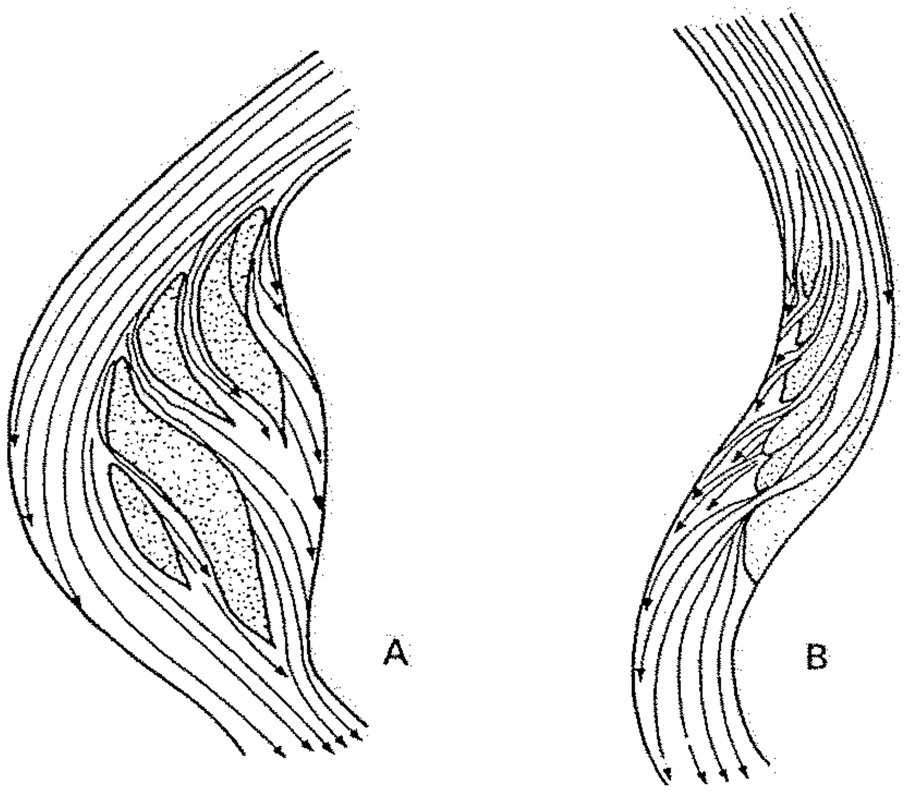

Fig. 3.10. Diagonal bars in curved channel reaches; A, attached to the inside bank; B, attached to the outside bank (after Krigström, 1962).

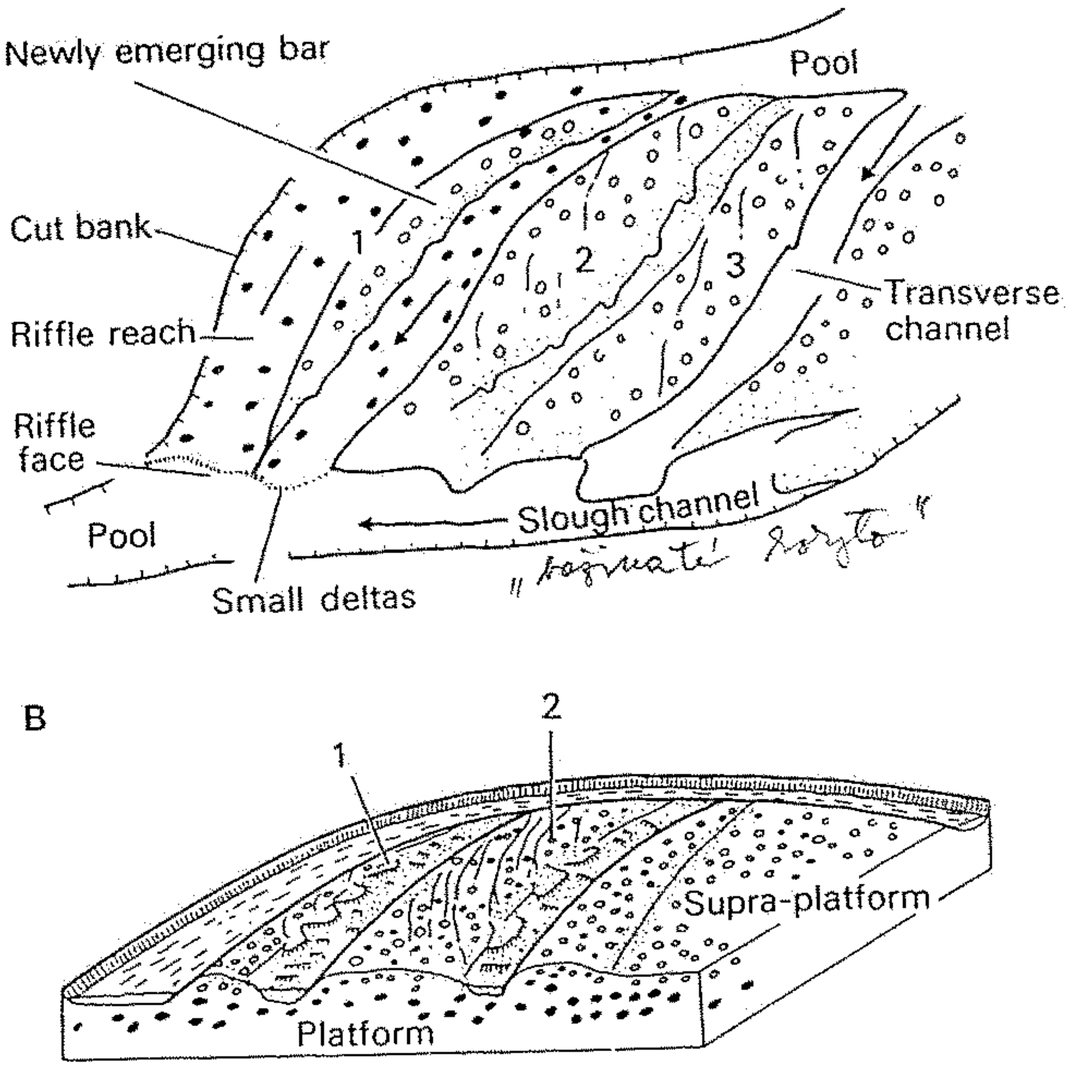

Fig. 3.11. Morphology, terminology and structure of a typical diagonal bar. (1), (2) and (3) are individual units of the bar where (1) is the newly emerging bar which will eventually become attached to (2) (after Bluck, 1974).

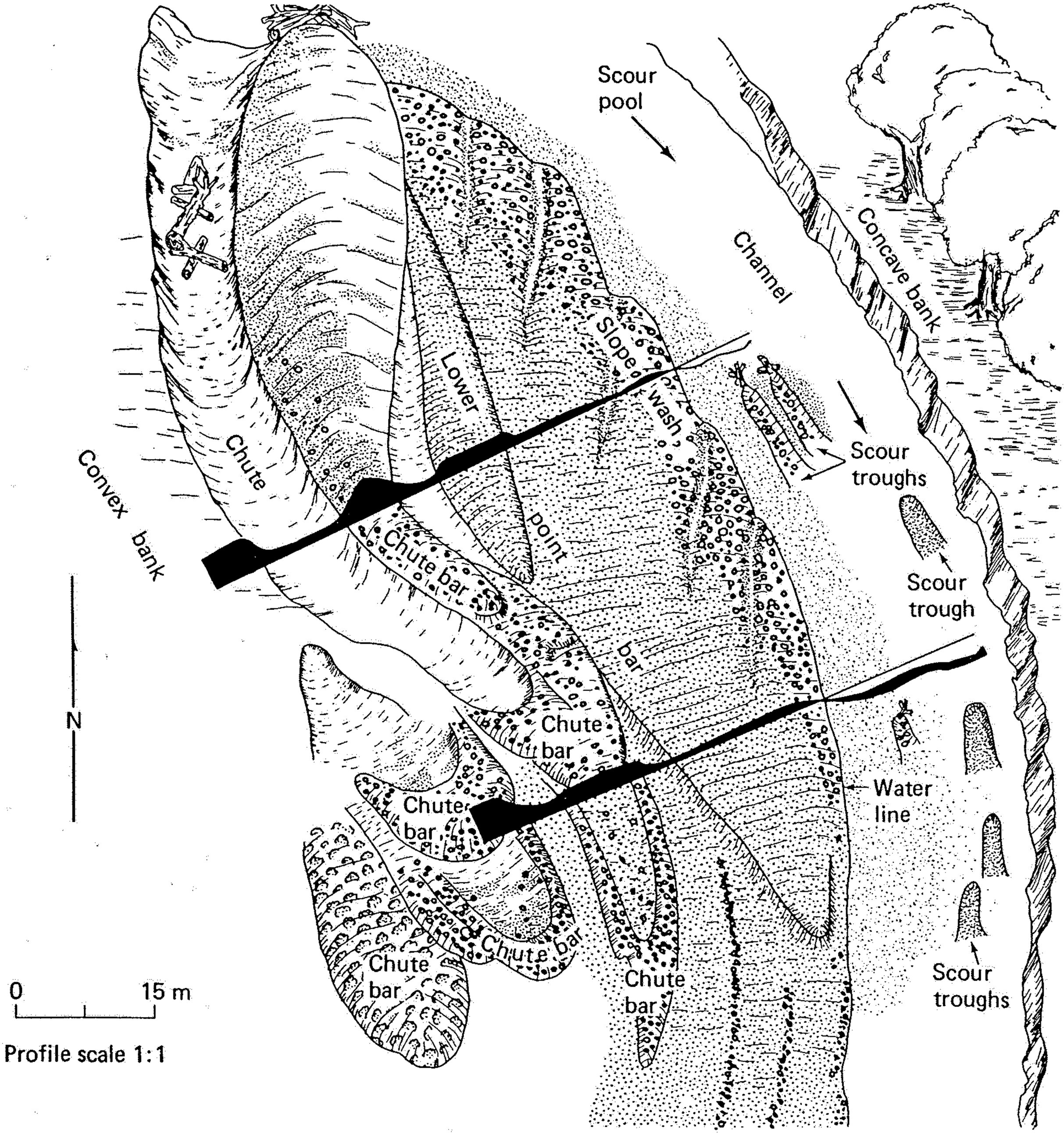

Figure 8–19 Coarse-grained point bar, showing sediment bodies and related features. (After McGowen and Garner, 1970, p. 31.)

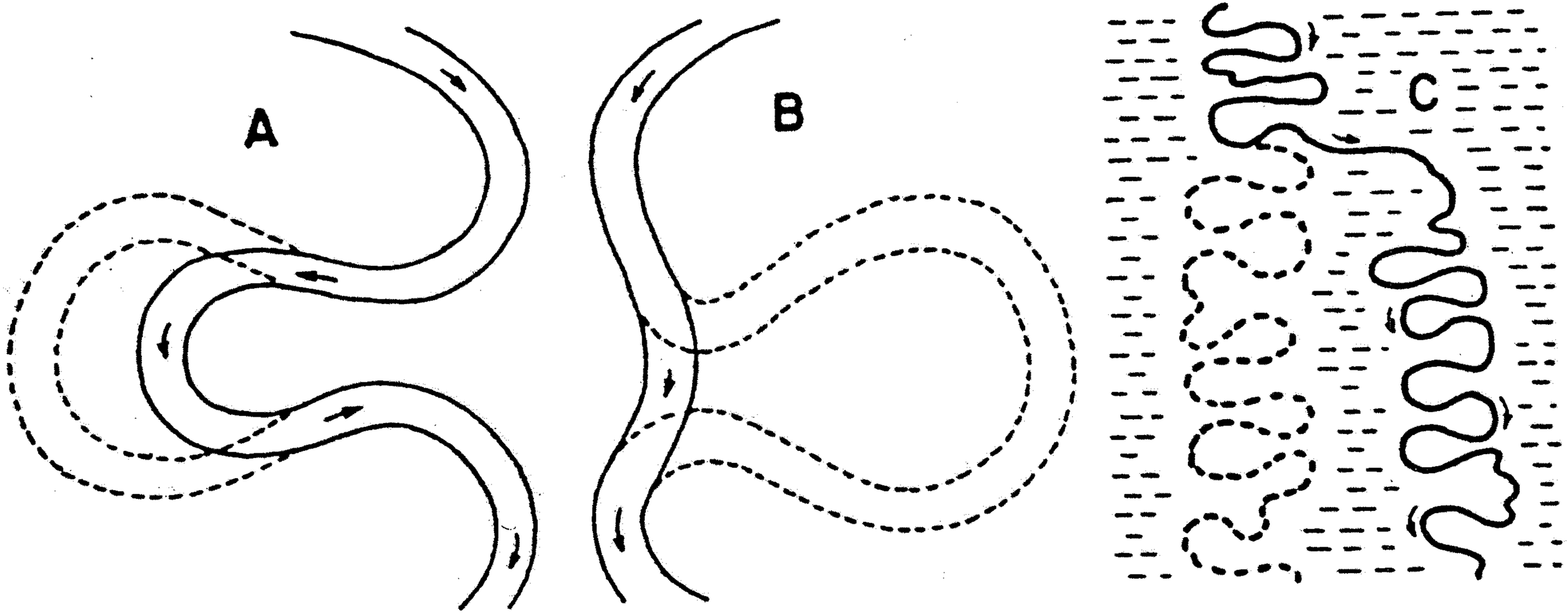

Figure 8–14 Various styles of channel shifting: (a) chute cutoff; (b) neck cutoff; (c) new meander belt after avulsion. (From Allen, 1965d, p. 119.)

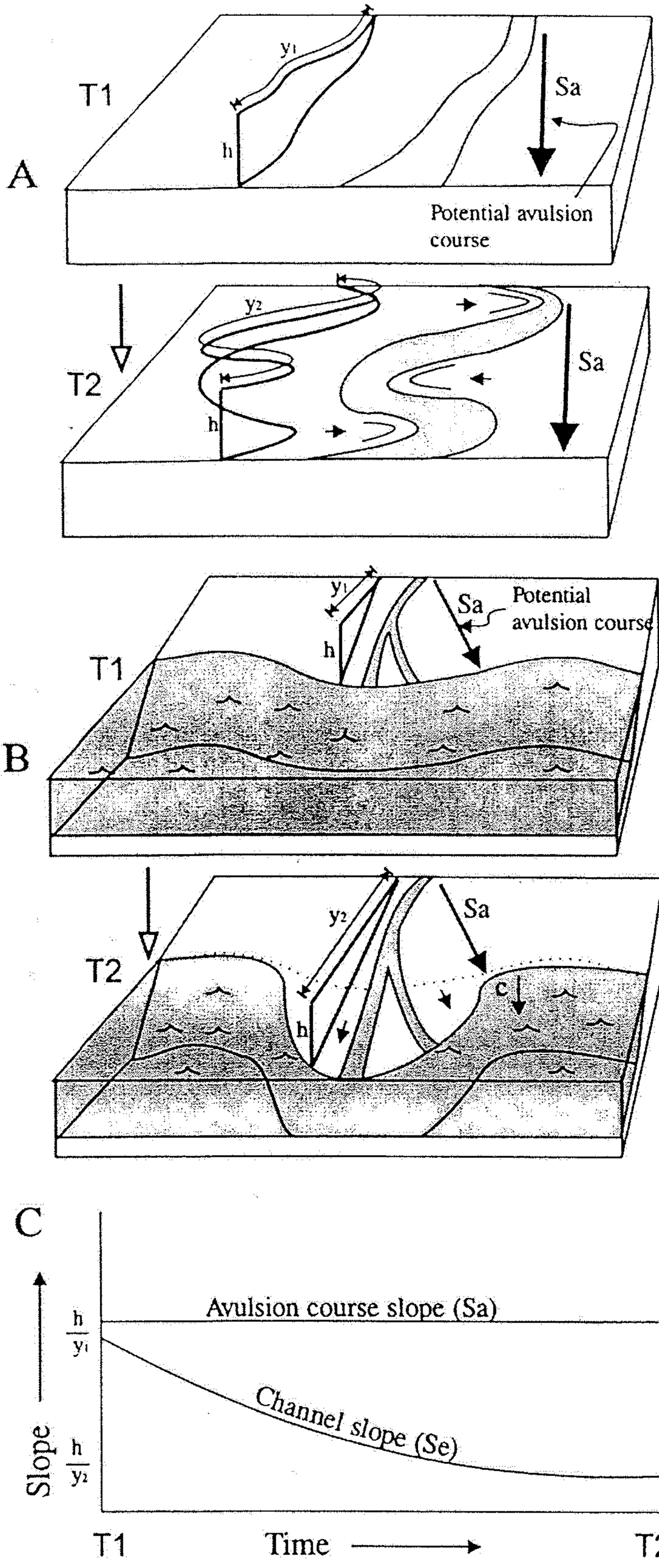

Fig. 3. Schematic block diagrams and graph demonstrating slope changes with time for sinuosity and deltaic avulsions (Table 1, 1a, 1b). (A) As sinuosity increases from time 1 (T1) to time 2 (T2), length y_1 increases to y_2 causing a decrease in channel slope, S_c, from h/y_1 to h/y_2. (B) As the delta lobe progrades from T1 to T2 at constant relative sea-level, length y_1 increases to y_2, causing a decrease in S_c from h/y_1 to h/y_2. (C) In both cases, the slope of a potential avulsion course, S_a, down the floodplain remains constant, and the ratio S_a/S_c increases. If, in (B) subsidence occurs at point c, the avulsion course slope, S_a, may simultaneously increase.

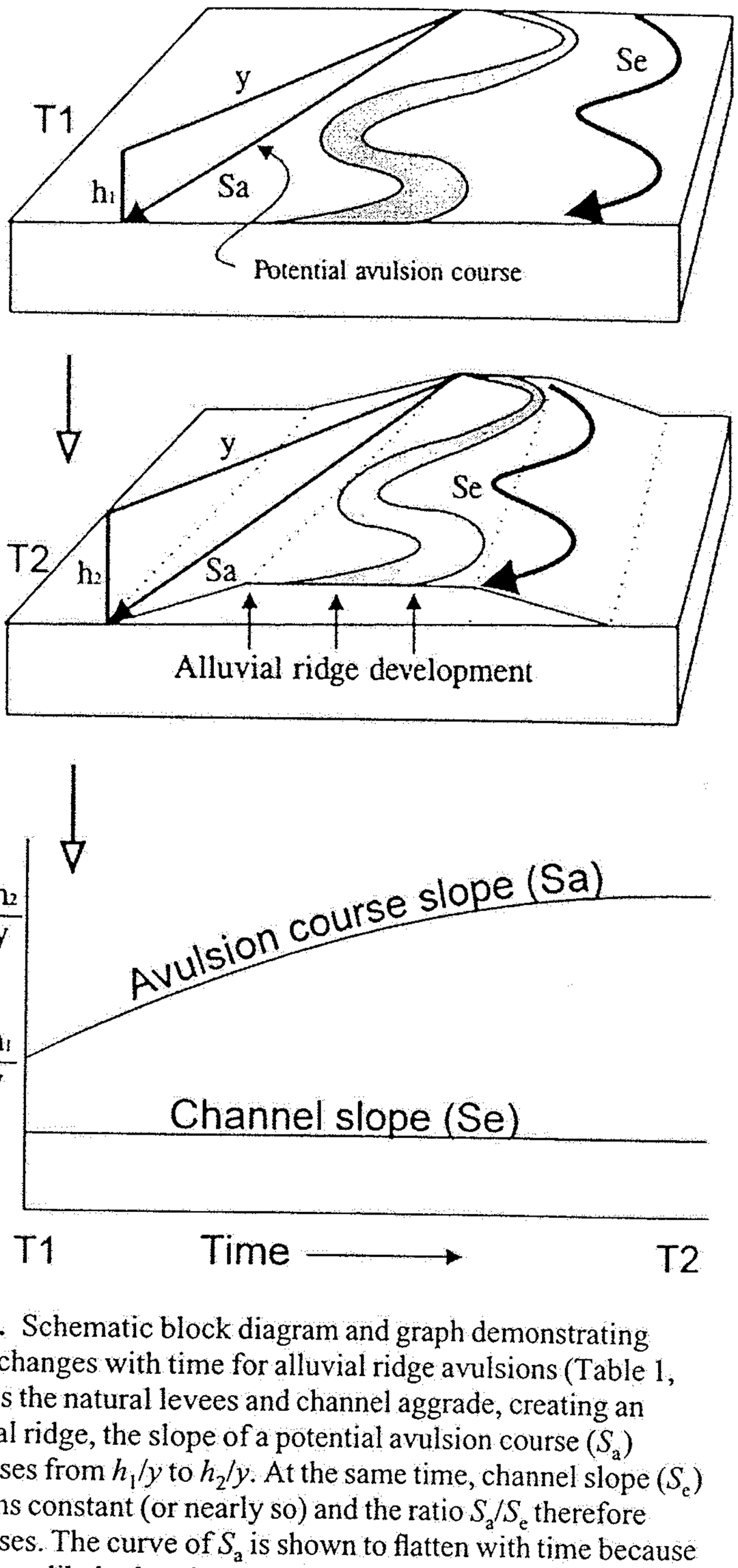

Fig. 4. Schematic block diagram and graph demonstrating slope changes with time for alluvial ridge avulsions (Table 1, 2a). As the natural levees and channel aggrade, creating an alluvial ridge, the slope of a potential avulsion course (S_a) increases from h_1/y to h_2/y. At the same time, channel slope (S_c) remains constant (or nearly so) and the ratio S_a/S_c therefore increases. The curve of S_a is shown to flatten with time because it appears likely that the net sedimentation rate on most natural levees decreases as levee relief increases owing to reduced sedimentation rate on the levee top and levee subsidence into floodplain muds (cf. Fisk, 1944). Compare graph with Fig. 3C.

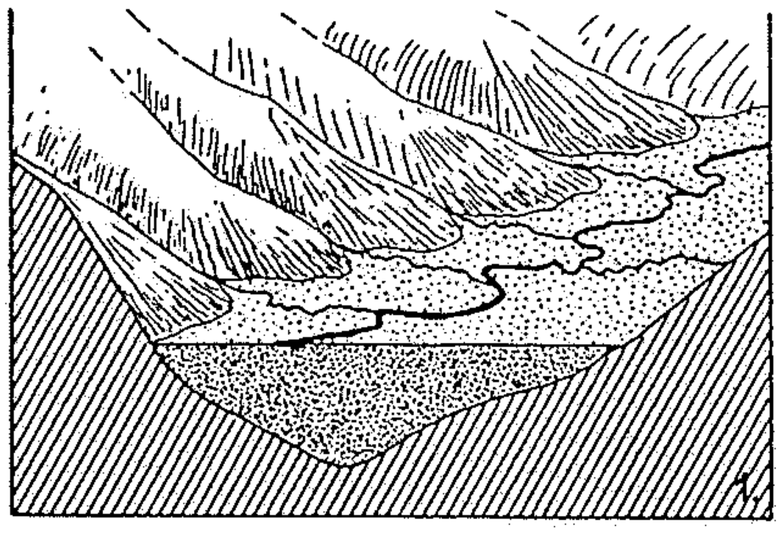

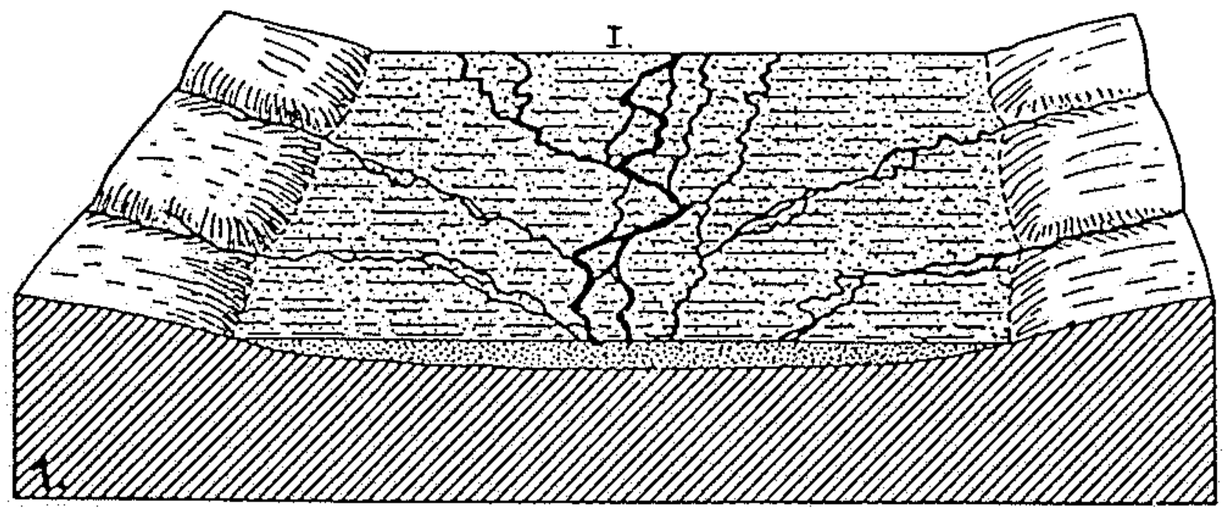

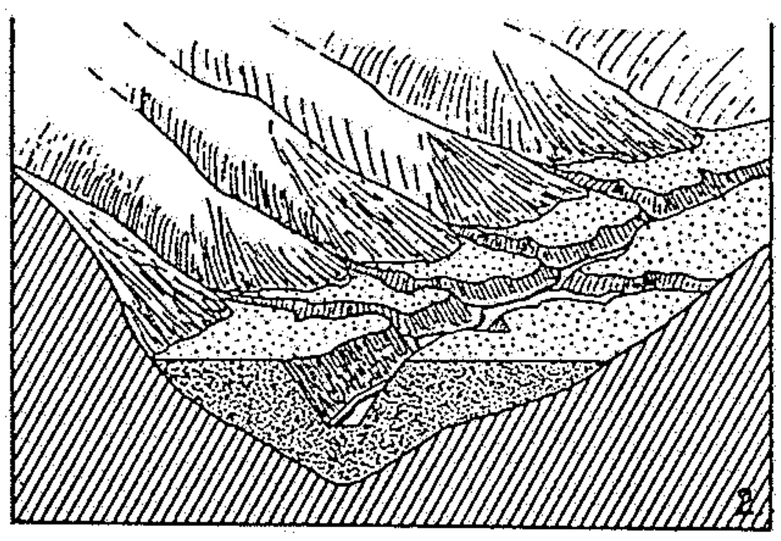

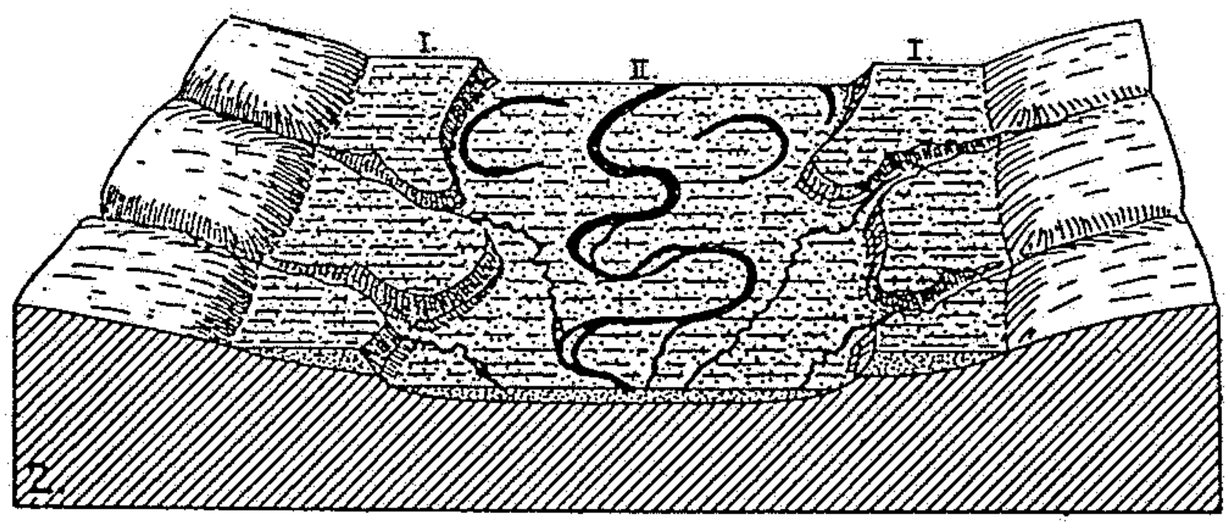

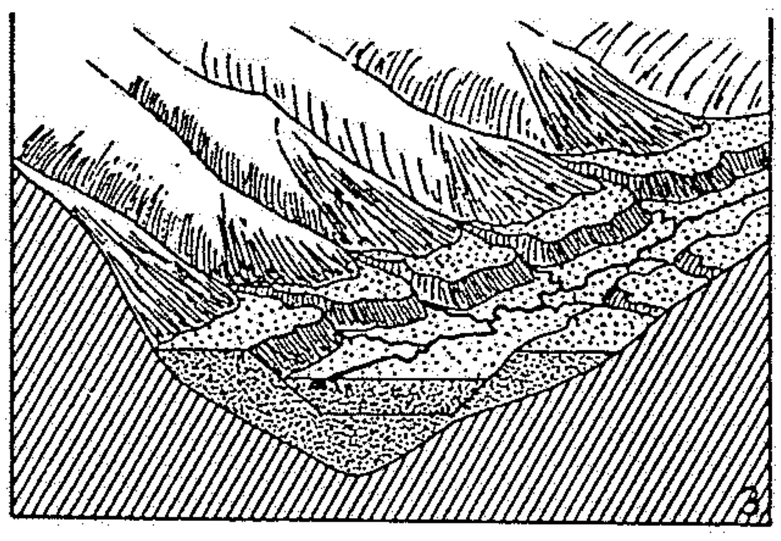

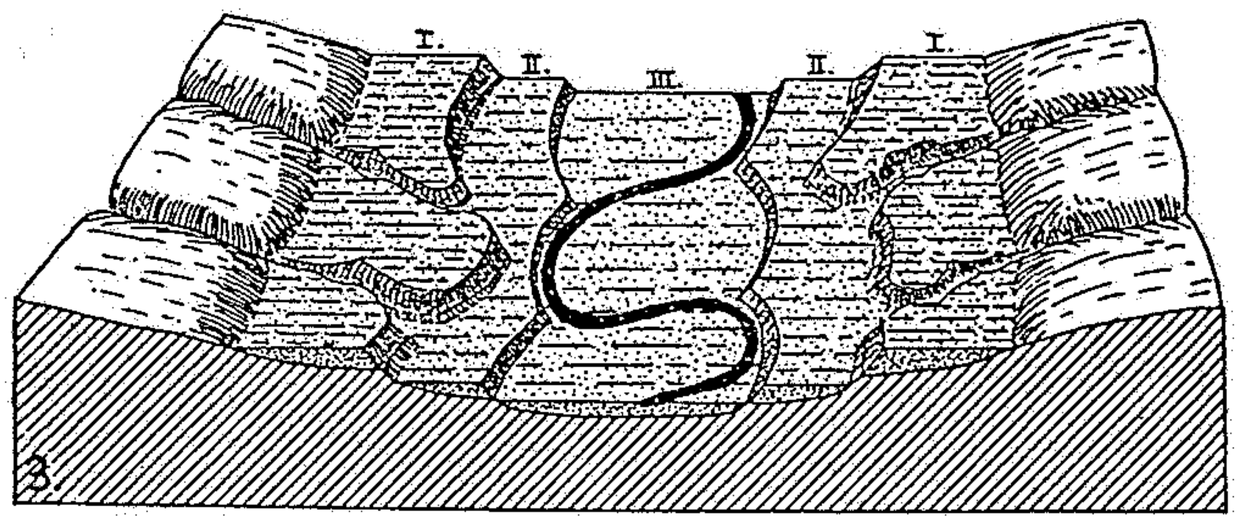

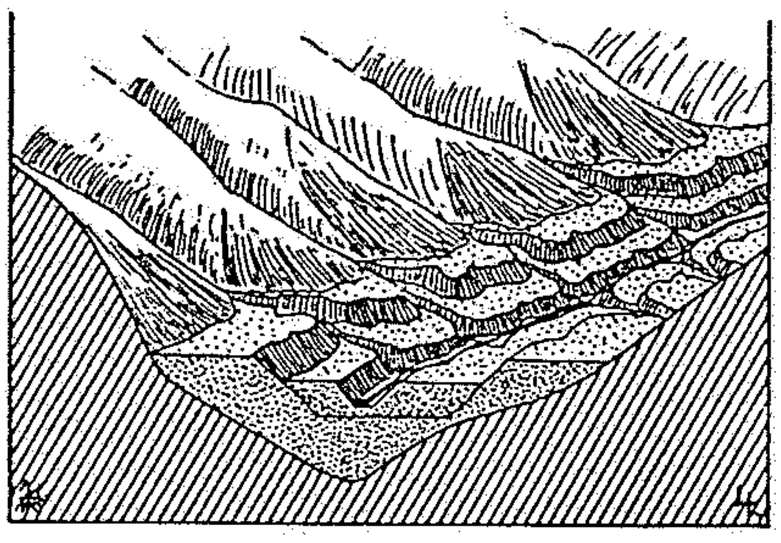

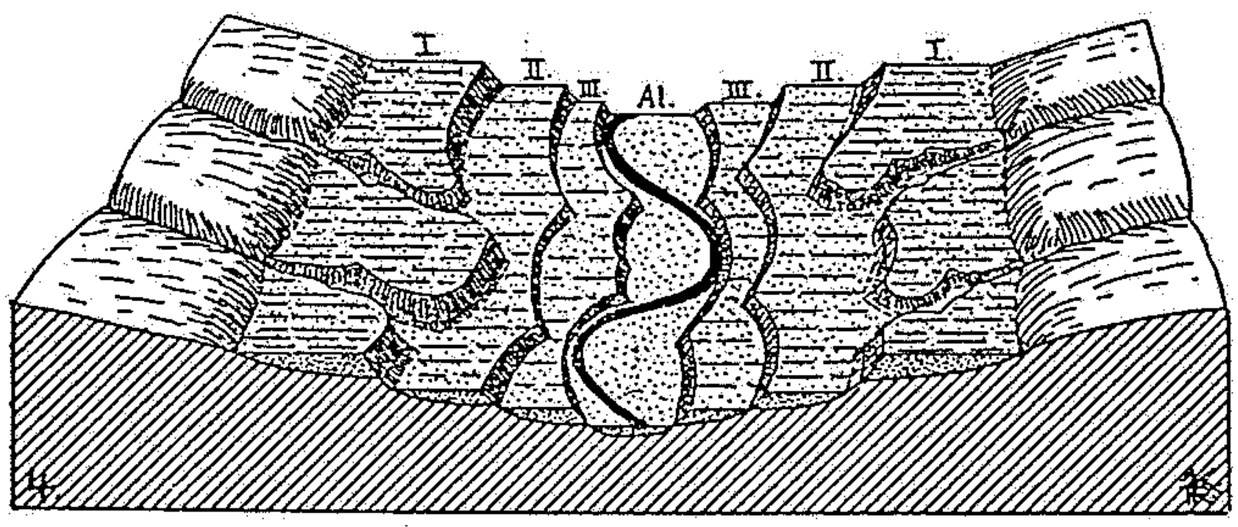

Obr. 103. *Schematické znázornění vývoje t. zv. vložených říčních teras, které se tvoří v údolí původně mocně zaneseném říčními plaveninami a spočívají na starších nánosech, nikoliv na erodovaném skalním podkladu.*
(Podle Em. de Martonna.)

Blokdiagramy znázorňující vývoj říčních teras uložených na skalním, říční erosí abradovaném podkladu. (Originál.)

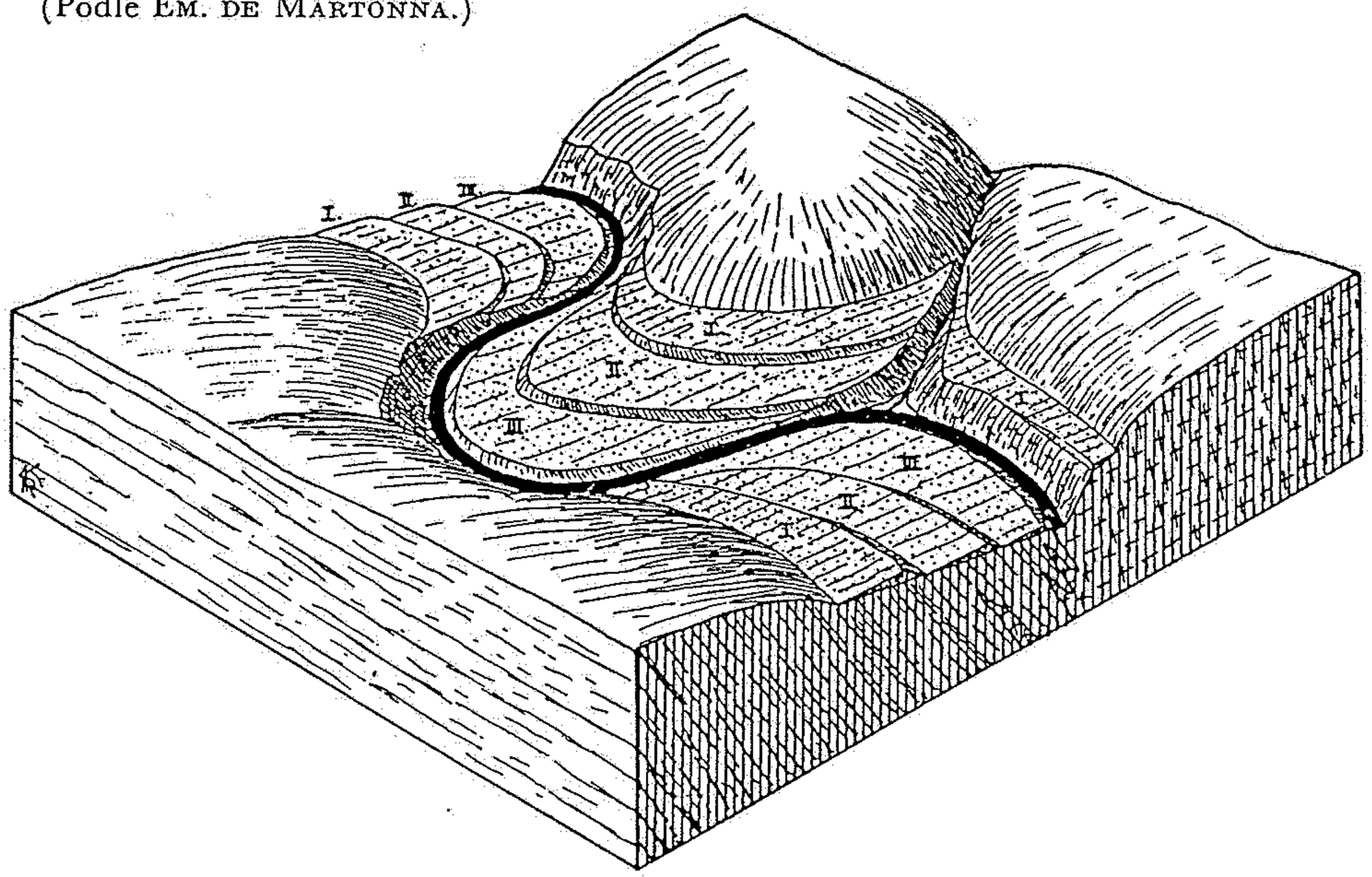

Obr. 104. *Blokdiagram znázorňující rozložení říčních teras v meandrech.* (Originál.)

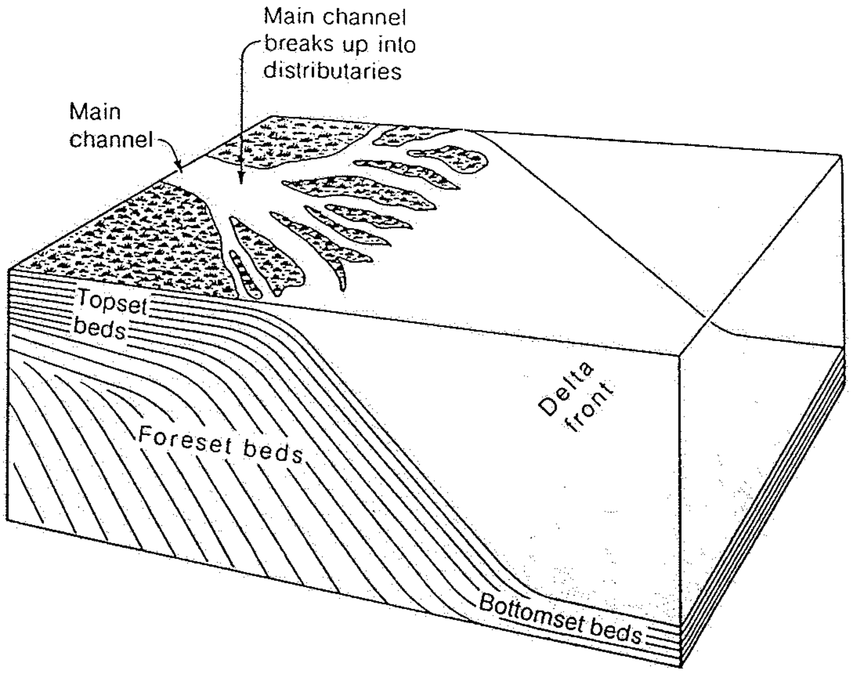

Figure 8-39

A typical freshwater delta, characterized by well-defined topset, foreset, and bottomset beds. The slope of the delta front is fairly steep, up to 25°. The main river channel may or may not break up into distributaries, depending on the stream discharge and the sediment load: The greater the load in relation to discharge, the greater the tendency to form distributaries.

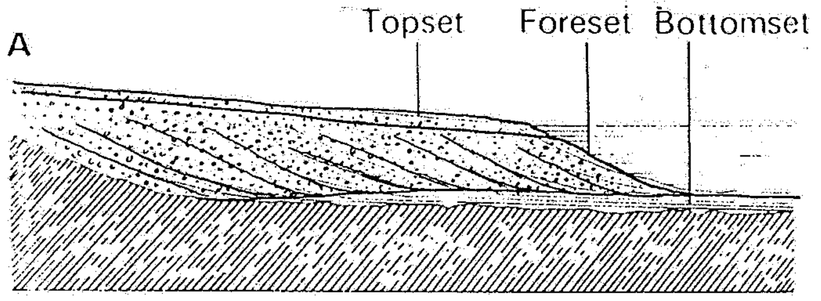

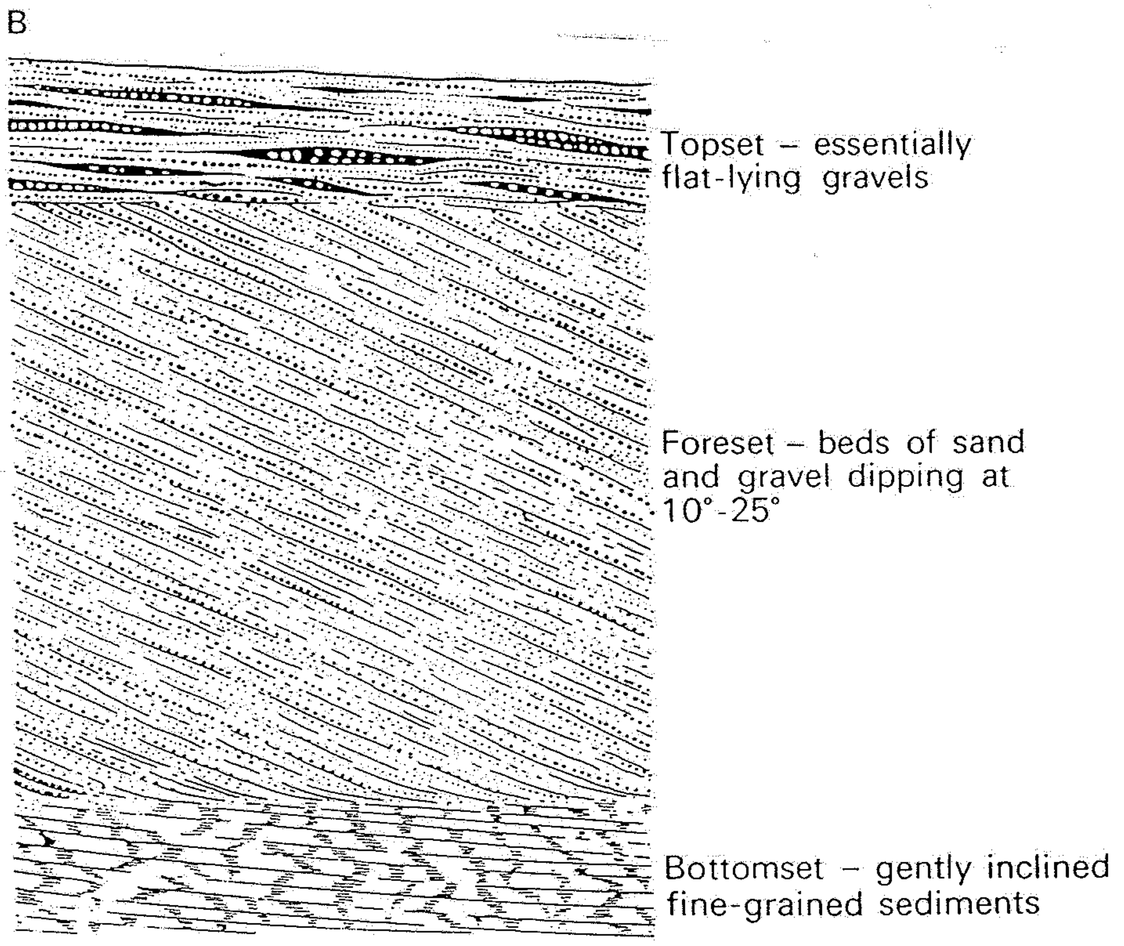

Fig. 6.1. (A) Section through a Pleistocene delta in Lake Bonneville; (B) Vertical facies sequence produced by delta progradation (after Gilbert, 1885; Barrell, 1912).

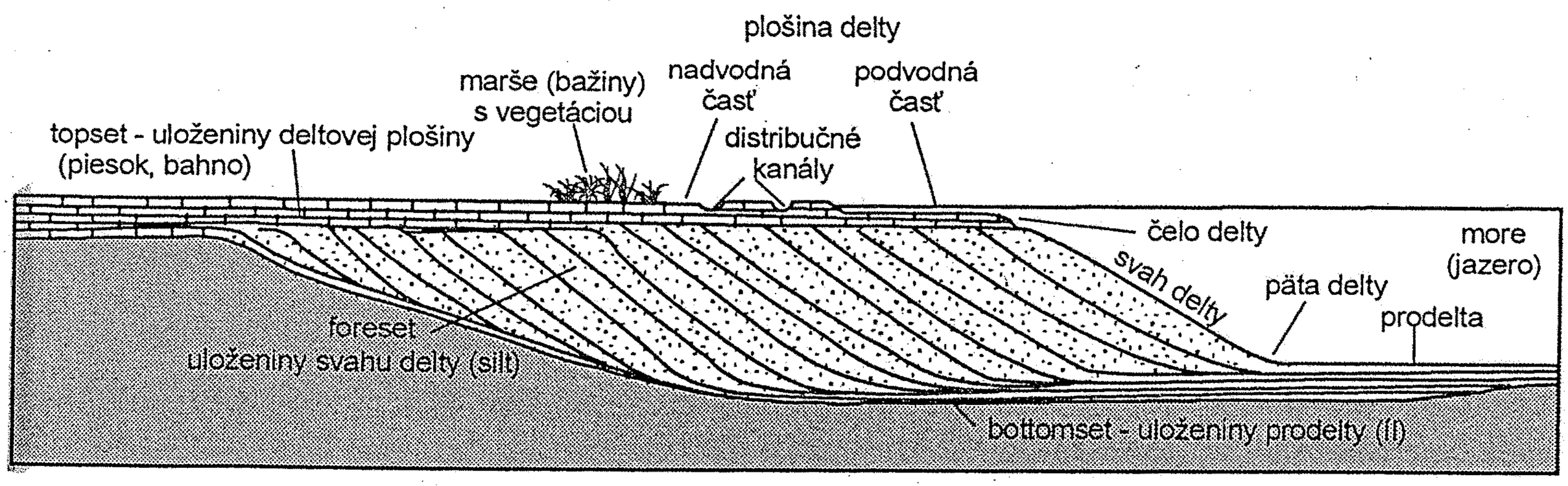

Obr. 16.17. Prierez riečnou deltou a názvoslovie. (upravené podľa Allisona – Palmersa 1980)

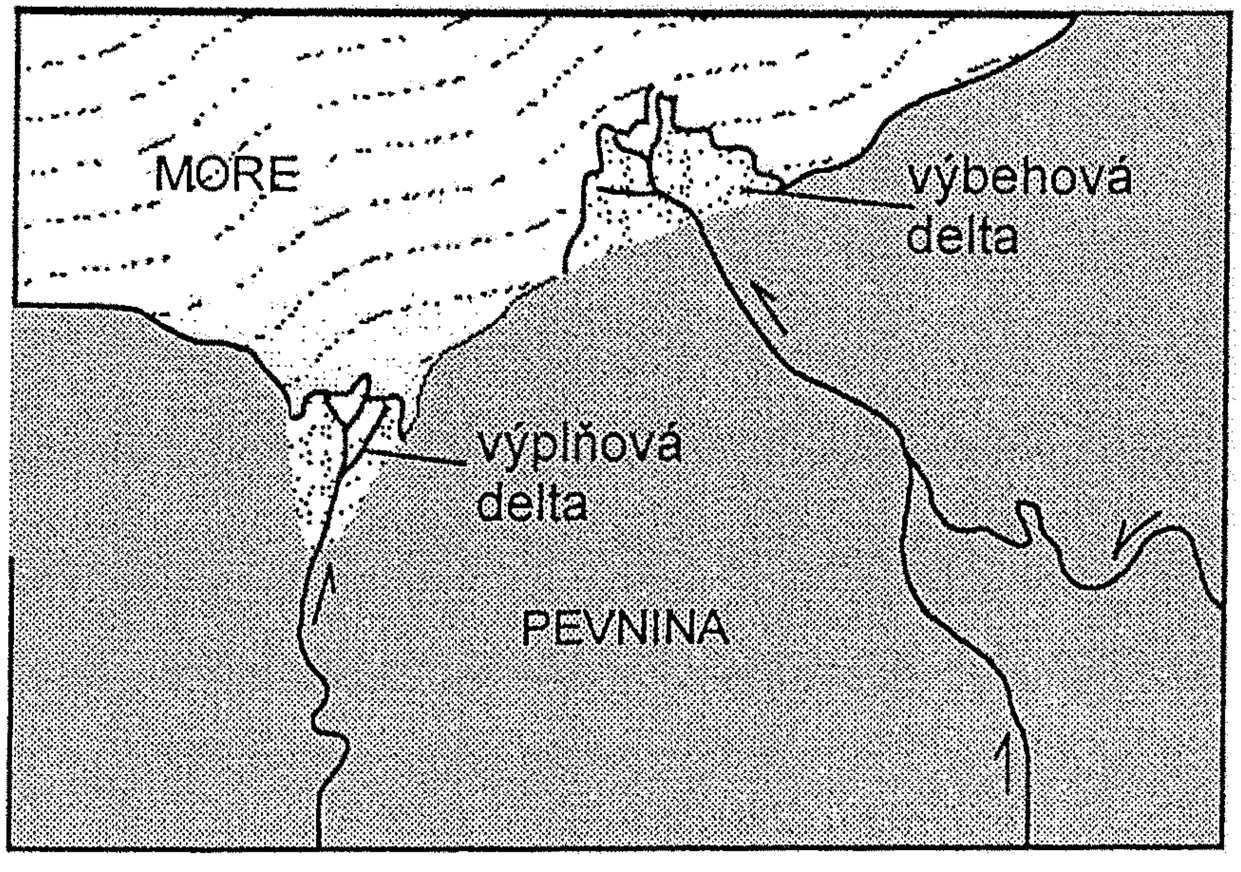

Obr. 16.18. Výplňové delty sa tvoria v zálivoch, výbehové na rovných úsekoch pobrežia. (upravené podľa Kettnera 1954)

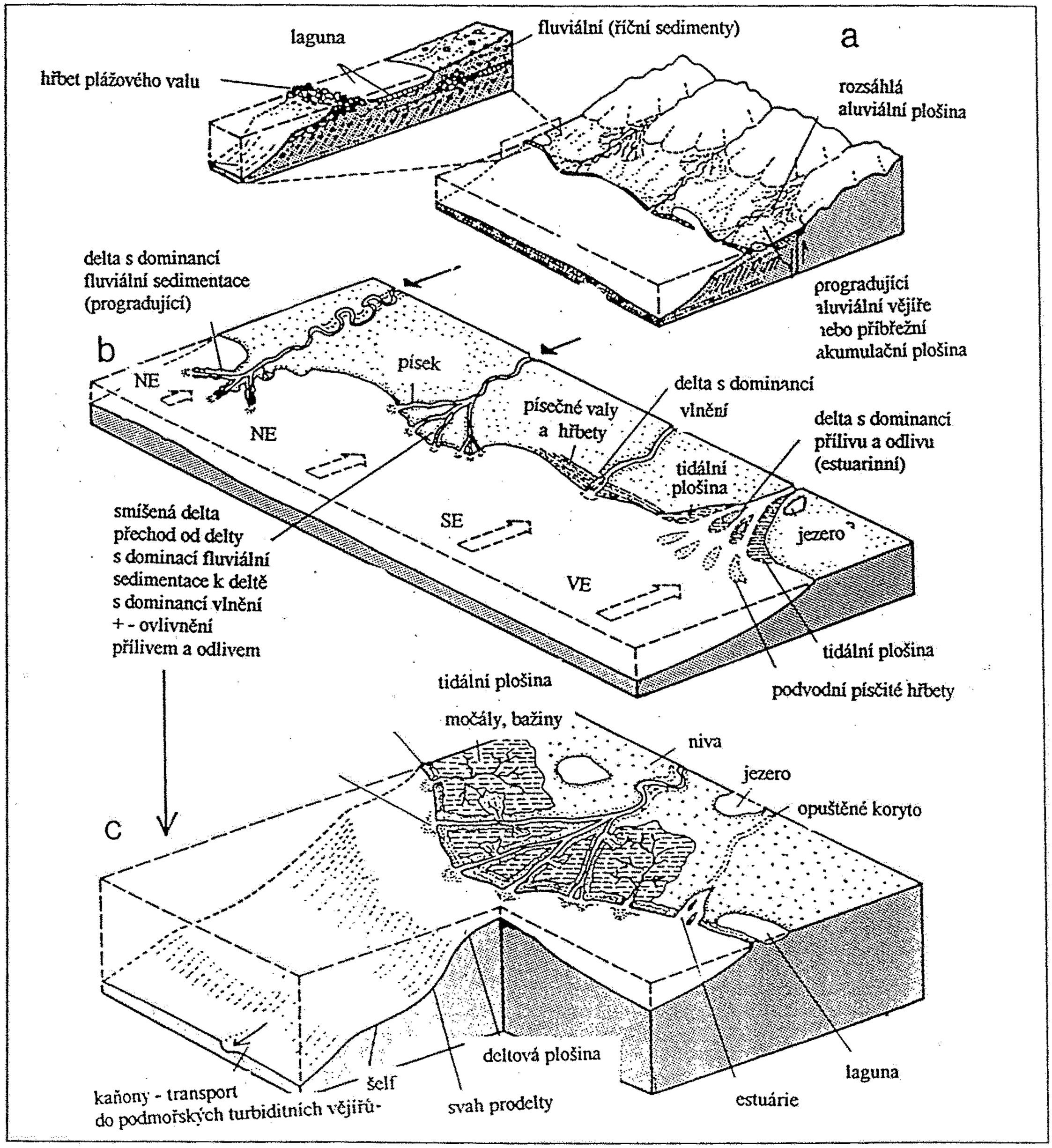

Obr. 140: Schematické znázornění základních typů delt: a) mořská delta vzniklá progradací aluviálních kuželů nebo výplavových plošin, b) různé typy velkých mořských delt (NE - nízká nergie vlnění, SE - střední energie vlnění, VE - vysoká energie proudů a vlnění). Dílčí prostředí velké delty (podle Einselle 1992), zjednodušeno.

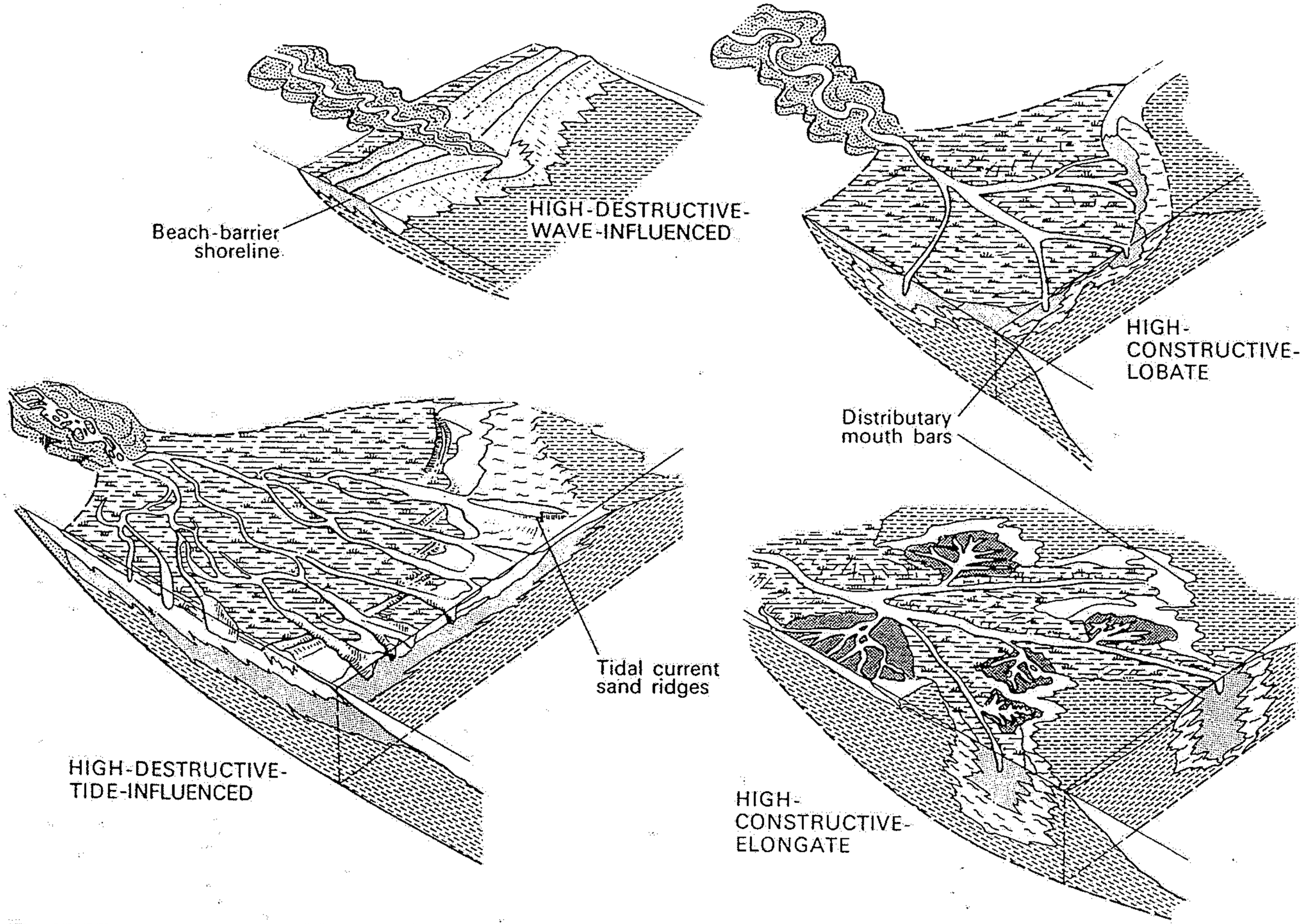

Fig. 6.3. High-constructive and high-destructive delta types as defined by Fisher *et al.* (1969).

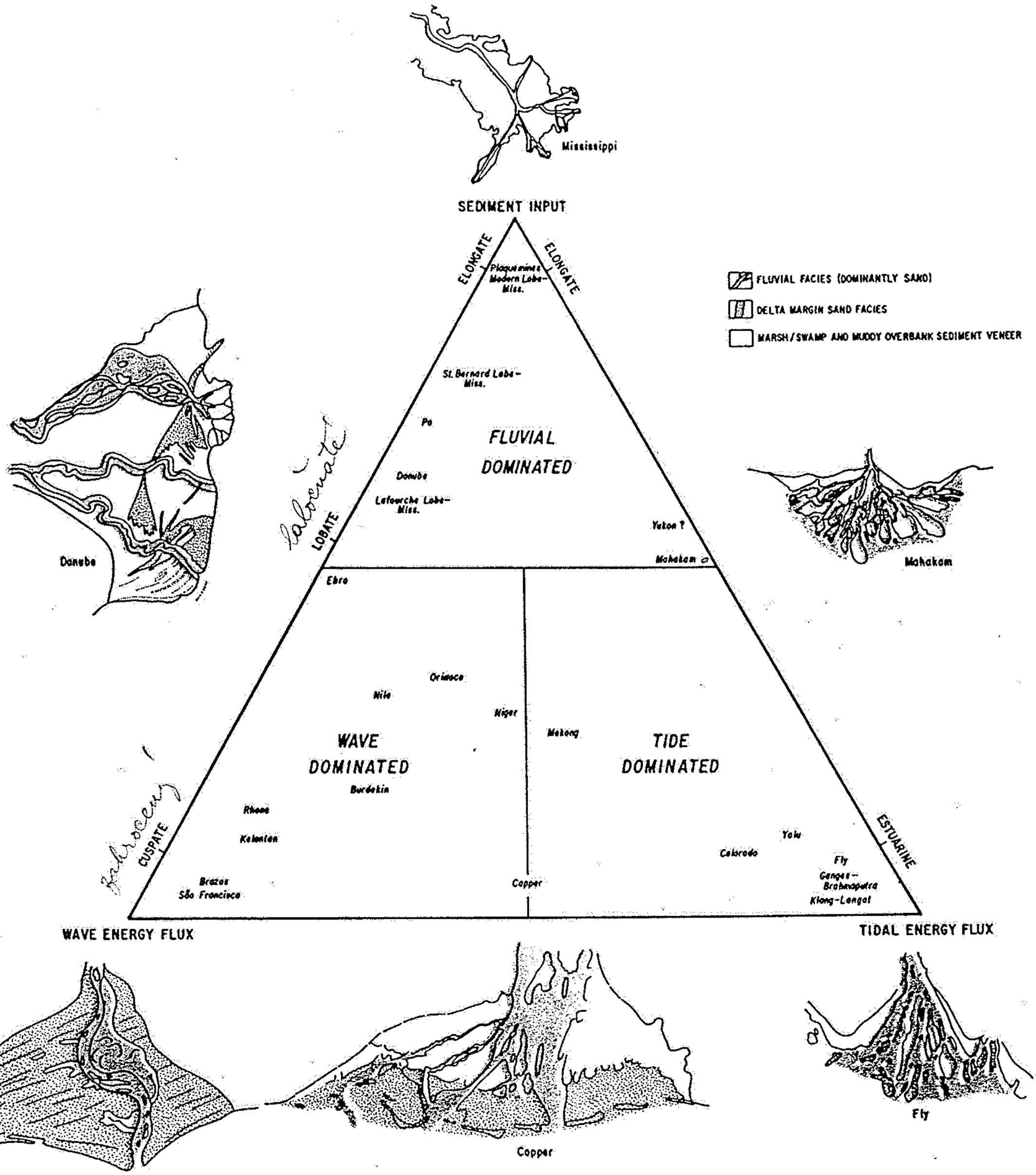

Fig. 446. Schematic diagram depicting the threefold division of deltas into fluvial-dominated, wave-dominated, and tide-dominated types. The relative importance of sediment input, wave energy flux, and tidal energy flux determine the morphology and internal stratigraphy of the delta. (After Galloway 1975)

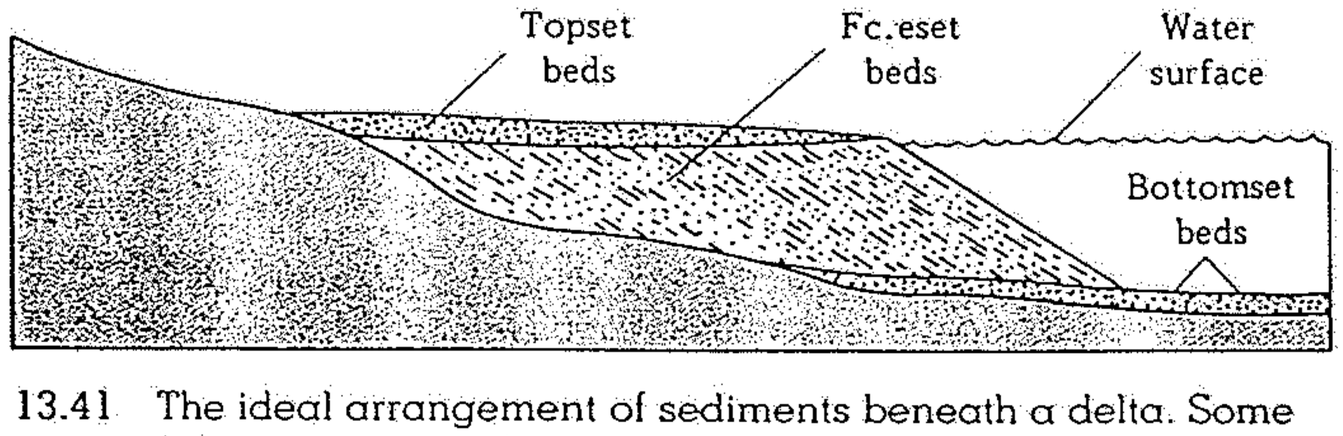

13.41 The ideal arrangement of sediments beneath a delta. Some material deposited in a lake or sea is laid on the bottom as bottomset beds. Other material is dumped in inclined foreset beds, built farther into the water and partly covering the bottomset beds. Over the foreset beds the stream lays down topset beds.

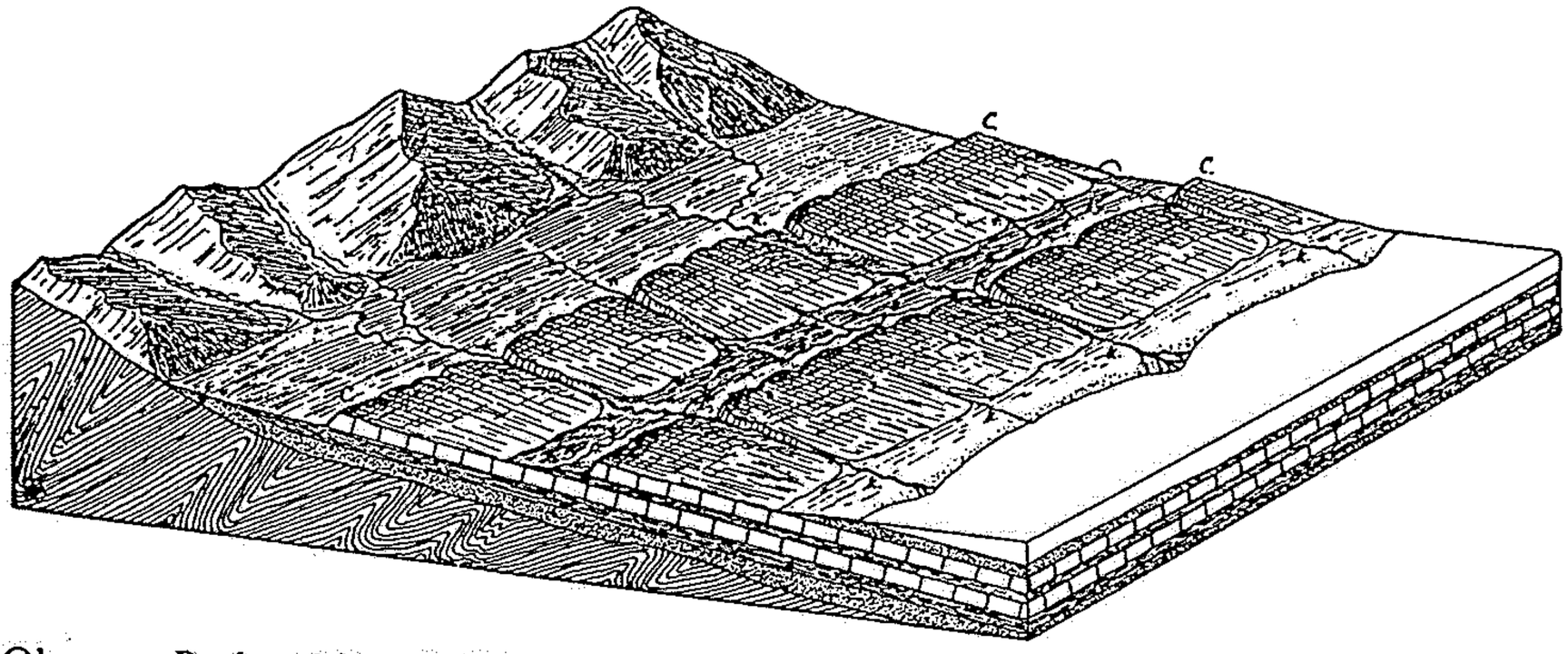

Obr. 90. *Druhy údolí podle jich orientace ke směru a sklonu vrstev.* k = *údolí svahová, souledná, konsekventní,* s = *údolí podélná, následná, subsekventní,* r = *údolí resekventní, t. j. údolí svahová, ústící do údolí subsekventních;* c = *nakloněné terénní stupně cuesty.* (Upraveno podle W. M. Davise.)

Figure 8-36

Typical drainage patterns. (a) A dendritic pattern is characterized by branching similar to that of the limbs or roots of trees. (b) In a typical rectangular drainage pattern developed on a strongly jointed rocky terrain, drainage tends to follow the joint pattern. (c) Typical trellis drainage develops in valley and ridge terrain, where rocks of varying resistance to erosion are folded into anticlines and synclines. (d) Radial drainage patterns develop on a large single peak, such as a large dormant volcano or a domal uplift.

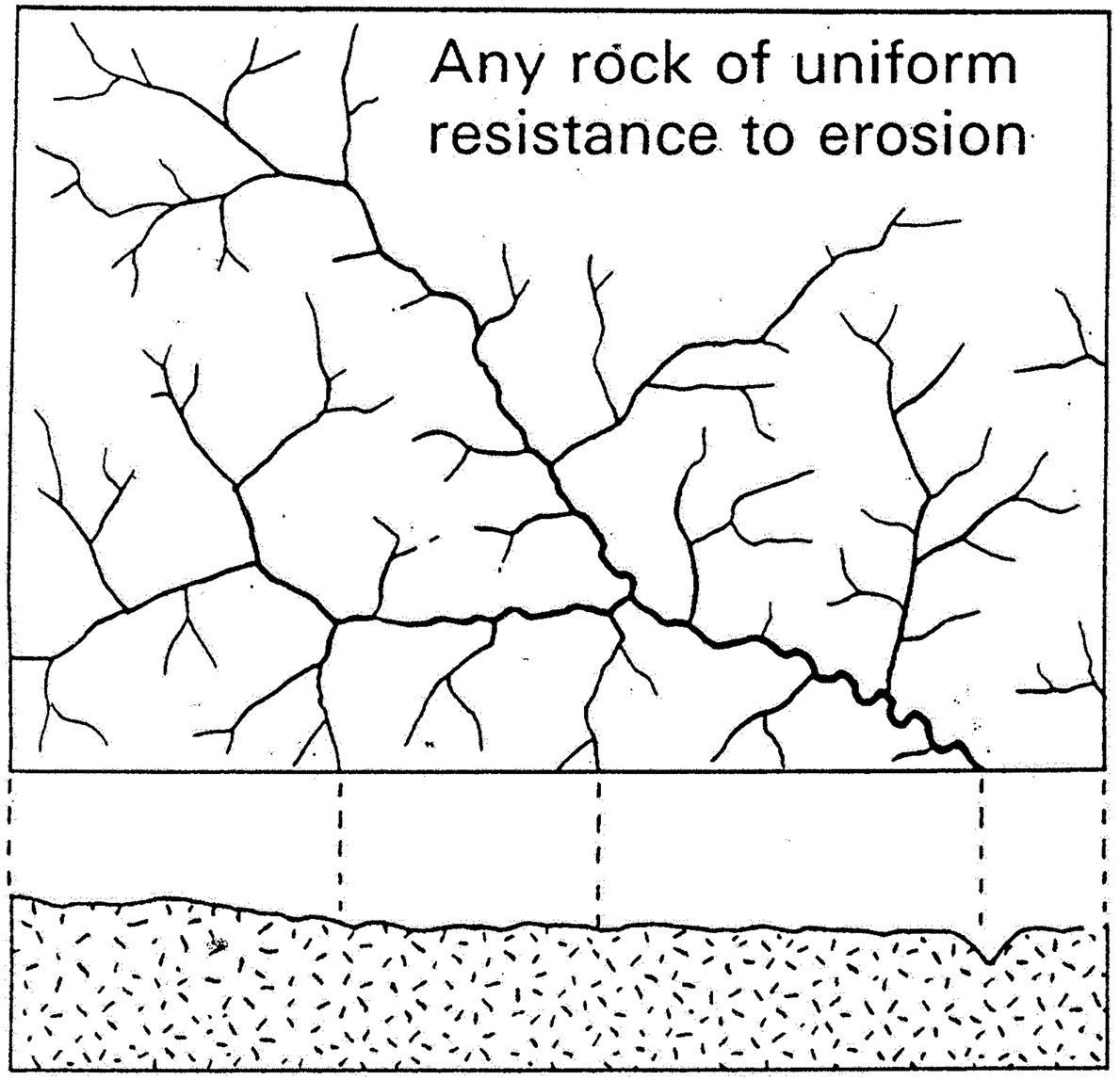

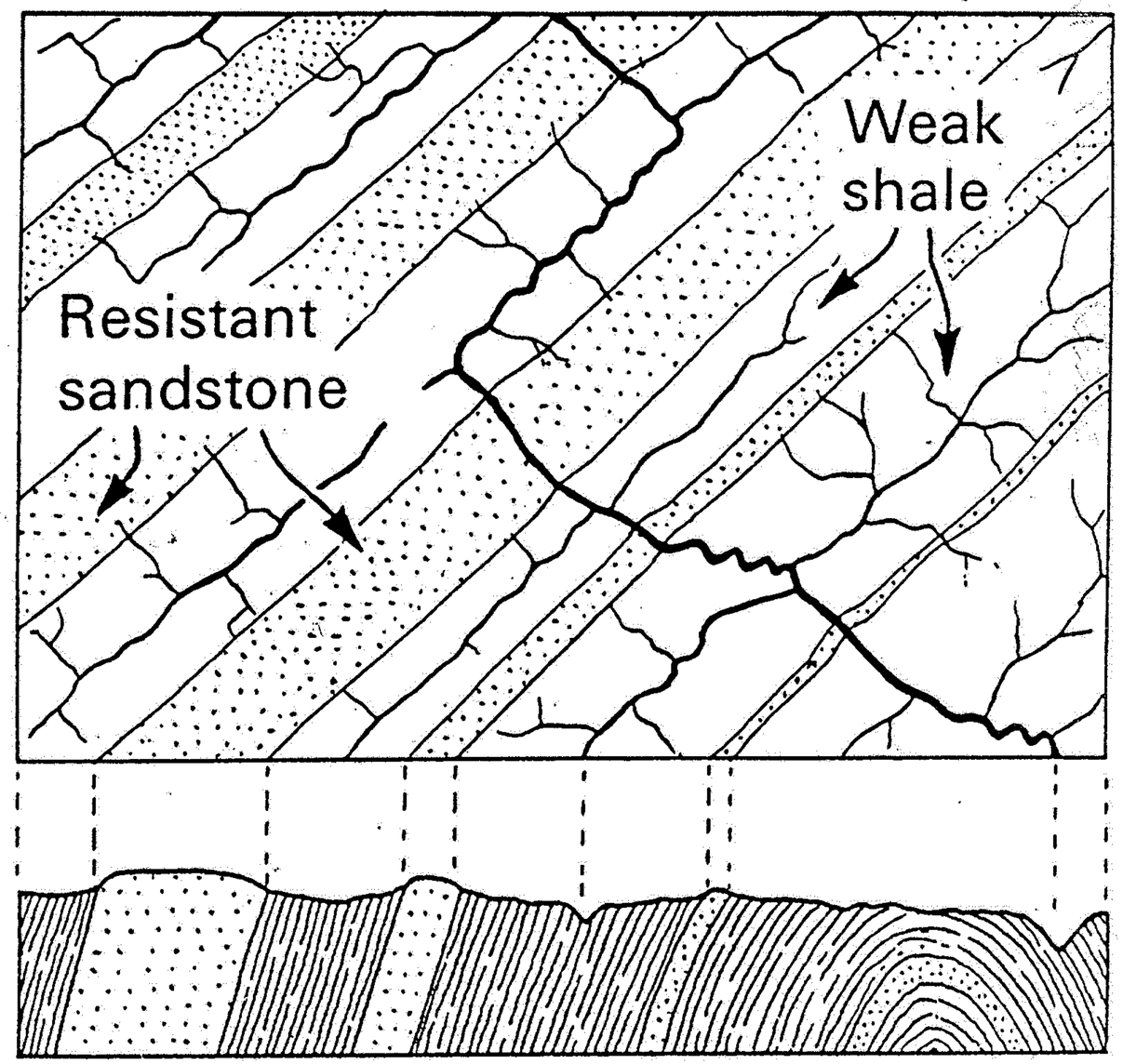

Structural control of stream patterns. Left: *Dendritic pattern.* Right: *Trellis pattern.*

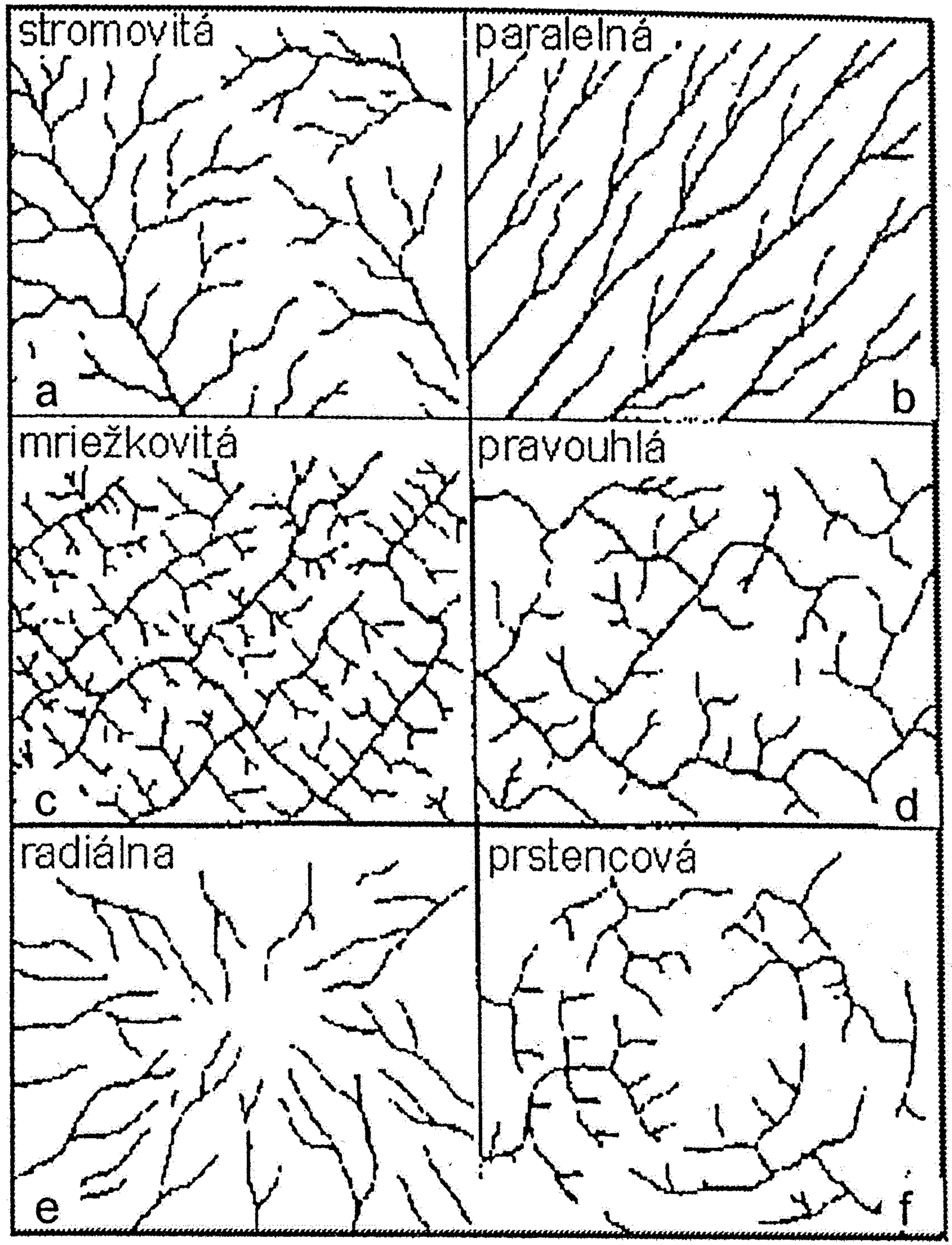

Obr. 16.21. *Vzory riečnej siete prezrádzajú geologickú štruktúru (stavbu) regiónu. Vzor: a – stromový, b – rovnobežný, c – mriežkový, d – pravouhlý, e – odstredný, f – prstencový. (prevzaté a upravené podľa Demeka 1987)*

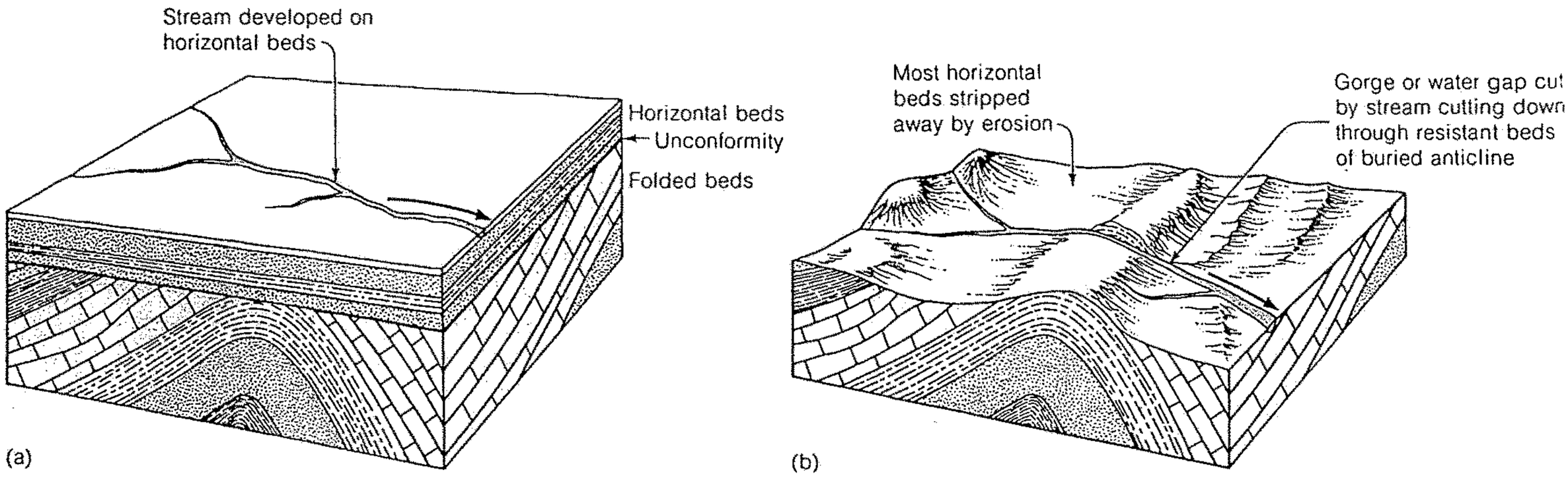

Figure 8-37

The development of a superposed stream by erosion of horizontal beds unconformably overlying folded beds of varying resistance to erosion. As the downcutting stream encounters the buried anticline, it erodes a narrow gorge, or water gap, in the resistant beds of the anticline.

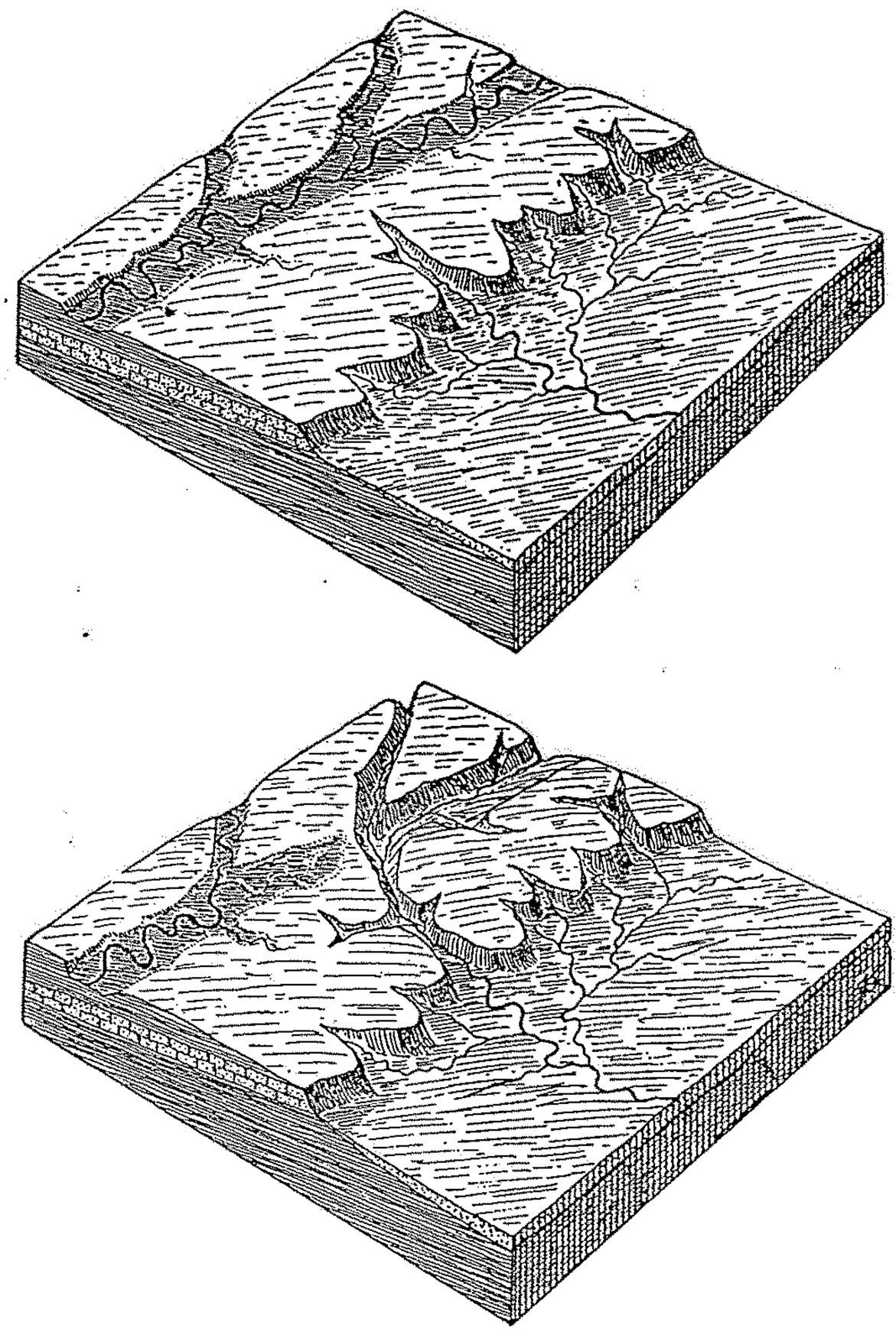

Obr. 64. *Schematické znázornění pirátství řeky. Řeka, která se značným spádem stéká doprava se stupňovité vyvýšeniny (cuesty), mocnou hloubkovou a zpětnou erosí přemisťuje své prameniště nazpět až k podélnému toku řeky druhé v (levé části blokdiagramu); podchycuje její vody a odvádí je novým korytem do prava. V místech podchyceni (načepování) vzniká nové rozvodí mezi oběma řekami.* (Orig.)

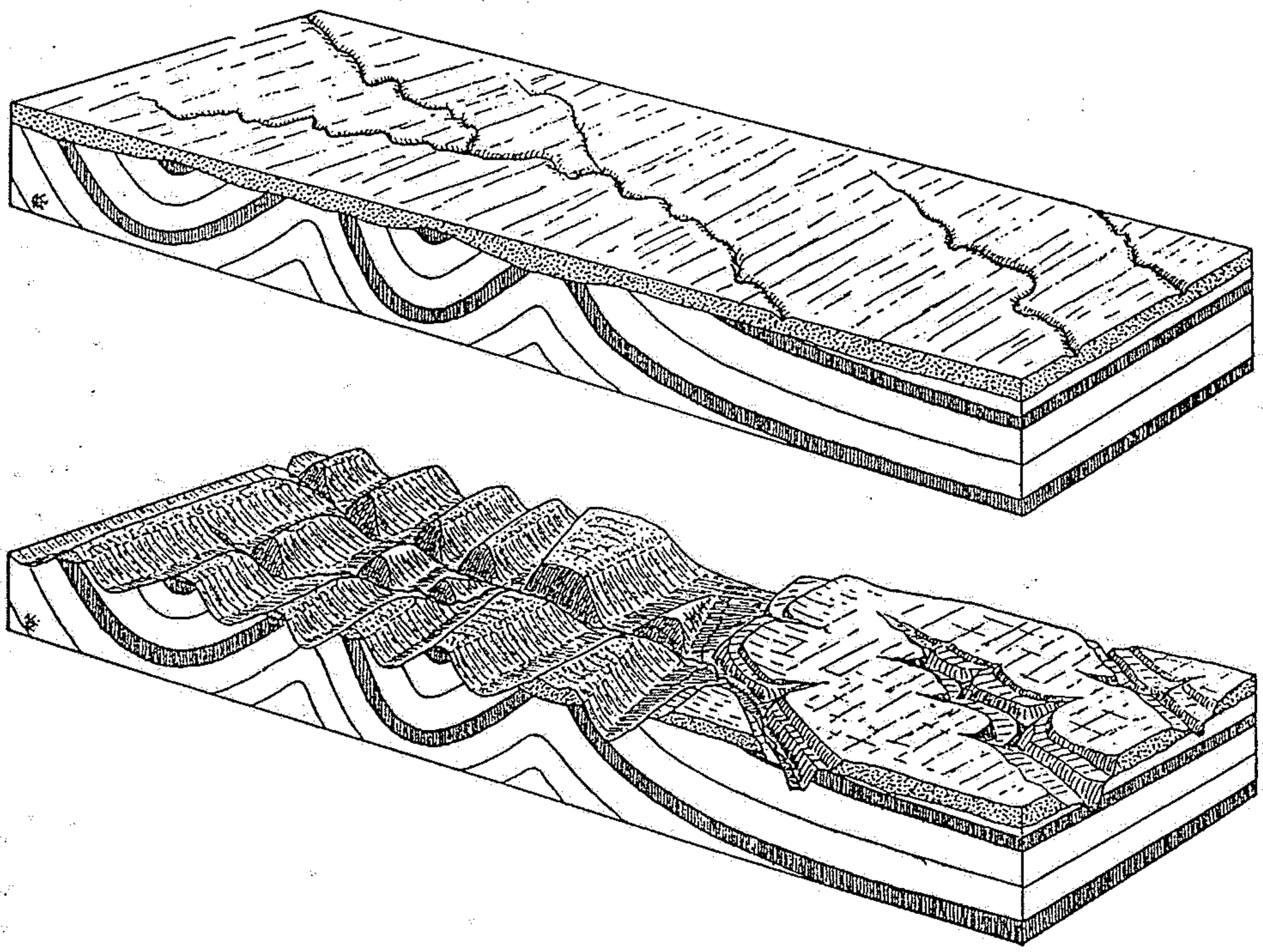

Obr. 98. *Vývoj epigenetických údolí. Nahoře vznik údolí v pokryvném útvaru. Údolí při postupném prohlubování setrvávají ve svém původním směru a zařízlou se posléze do podložních vrstev bez ohledu na jejich tektonické poměry (dole), takže probíhají napříč vrstvami.* (Podle R. F. Flinta.)

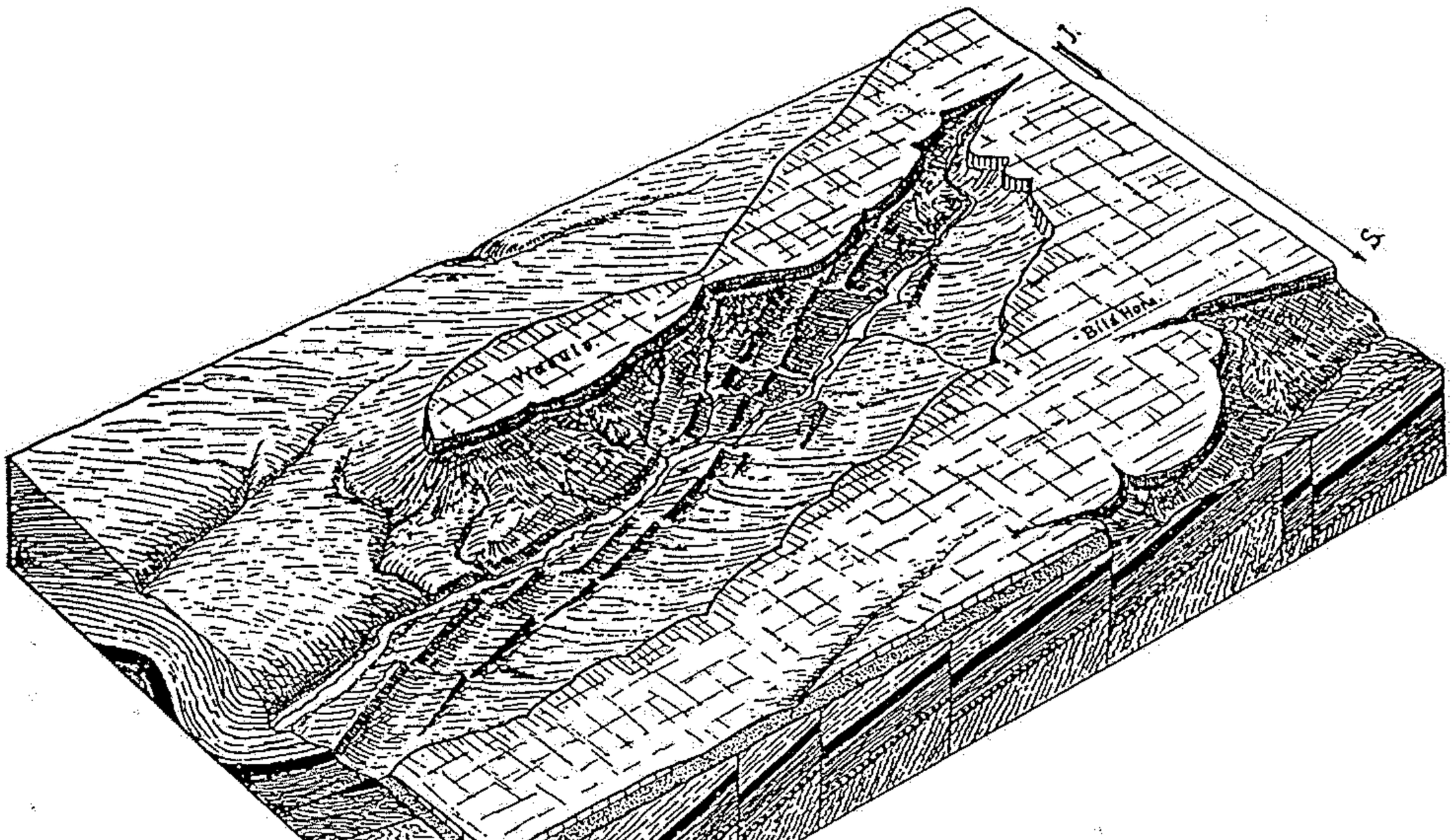

Obr. 99. *Blokdiagram Motolského údolí u Prahy, které se epigeneticky zahloubilo z křídové pokrývky do ordovických a zčásti silurských vrstev. Křídový útvar se zachoval v jižní části území v tabulové hoře Vidouli, v severní části je křídová pokrývka, skládající Bílou horu, souvislá. V údolí Motolského potoka vystupují hřbety tvrdých křemenců, které jsou porušeny četnými příčnými zlomy.* (Originál.)

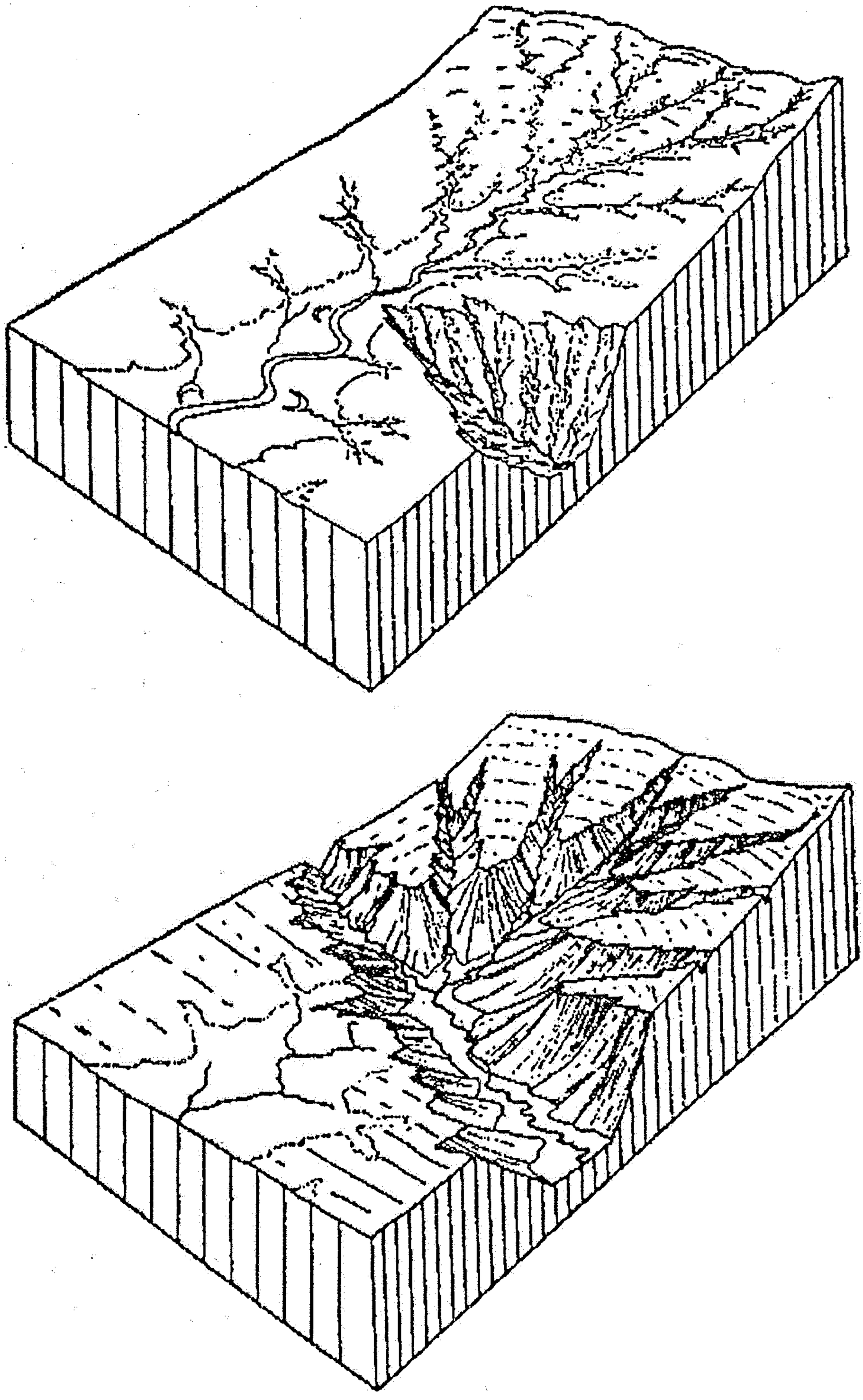

Obr. 16.24. Zmladenie reliéfu pri riečnom pirátstve. (podľa Kunského

BOX 13.2 Captured and Beheaded by Pirate

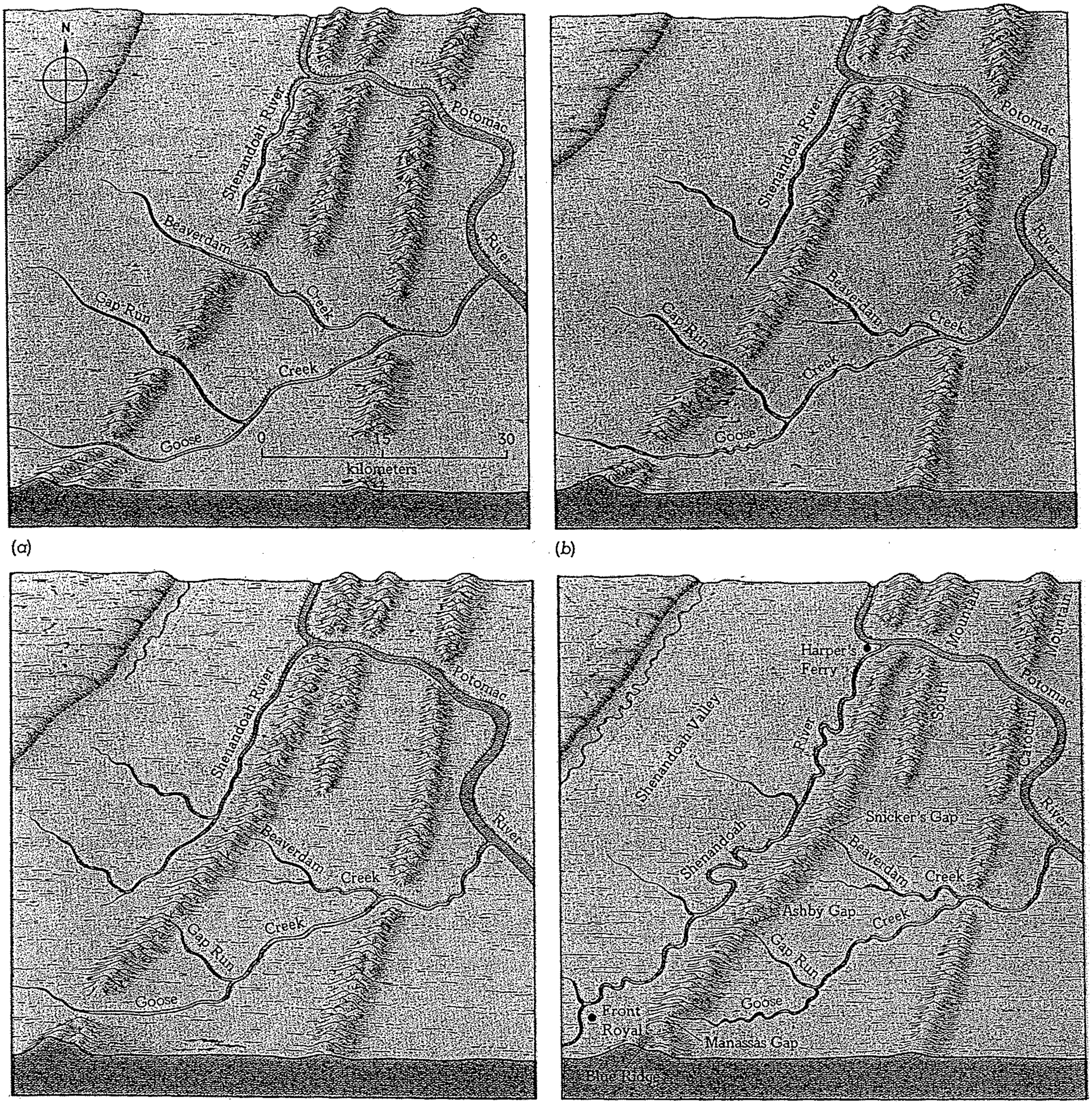

B13.2.1 The Shenandoah River has expanded its drainage basin at the expense of several other streams through a process of stream piracy. Along the way some old water gaps have become wind gaps.

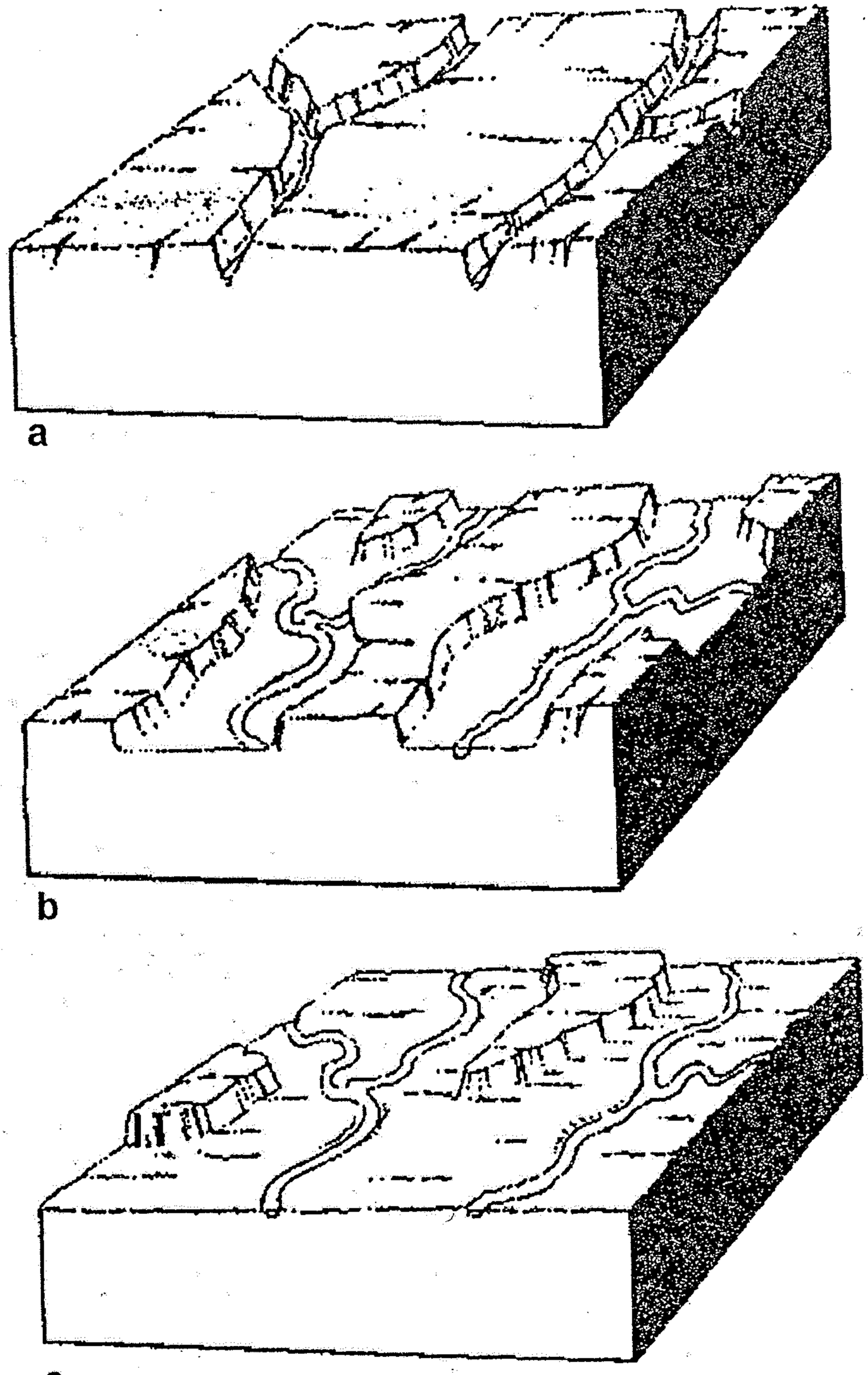

Obr. 16.32. *Zarovnávanie územia zboku – paralelným ústupom svahov. (podľa Plummera – McGearyho 1996)*

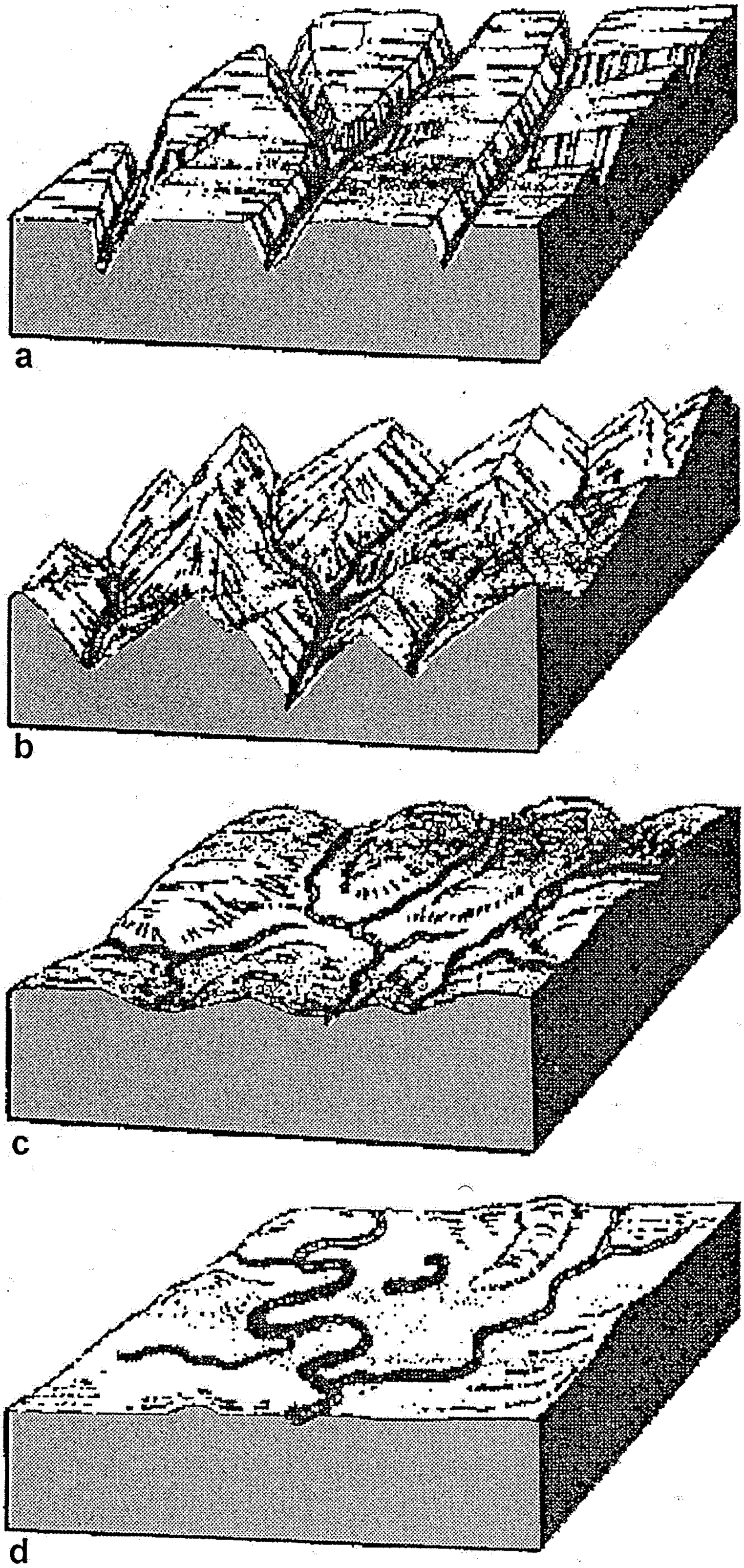

Obr. 16.31. *Štádiá vývoja riečneho reliéfu znižovaním a ústupom svahov (zarovnávanie zhora). a – štádium mladosti, b – štádium dospelosti (maturity), c – štádium neskorej dospelosti, d – štádium staroby (senility). (podľa Plummera – McGearyho 1996)*

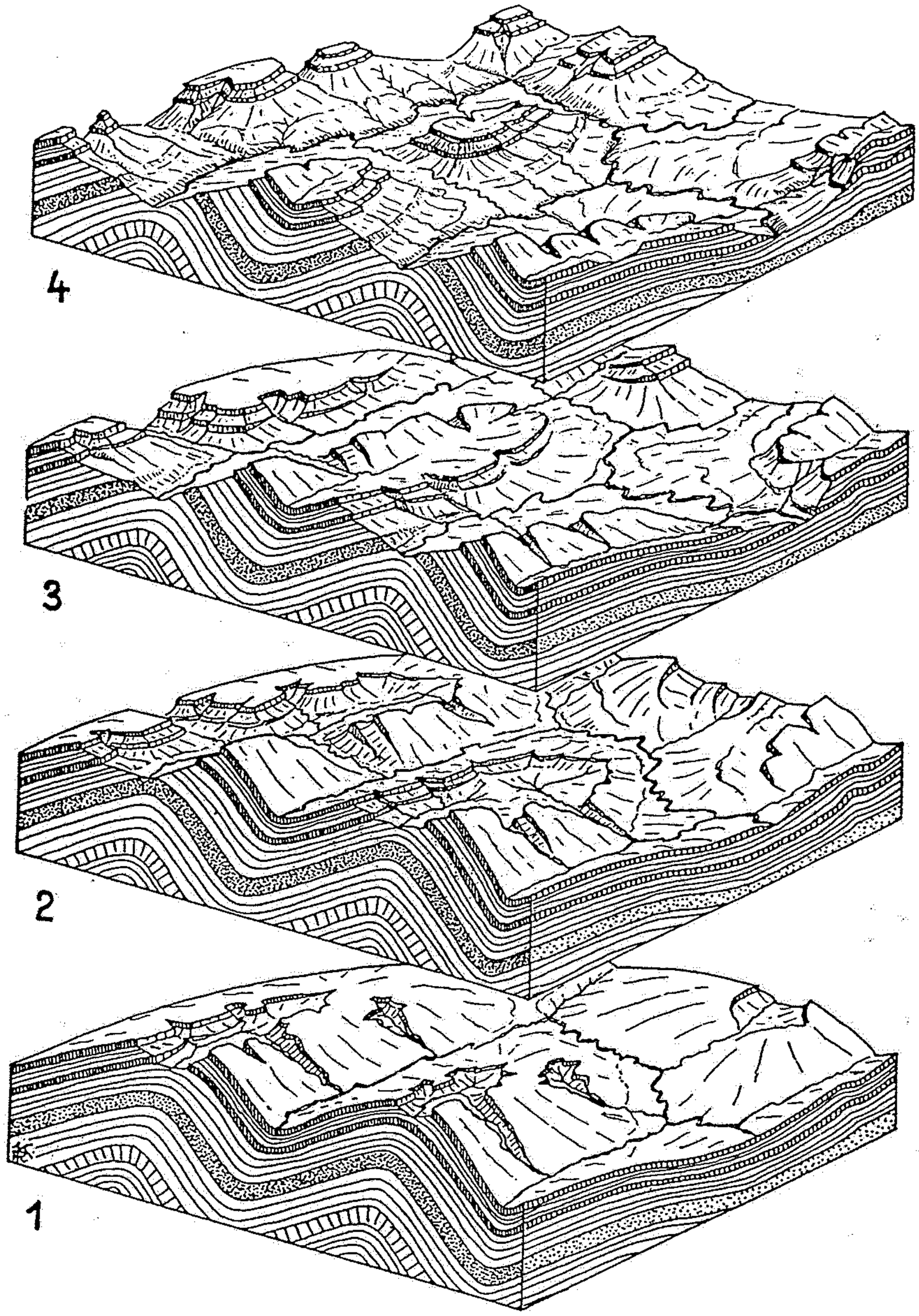

Obr. 94. *Postupné rozrušování jednoduše zvrásněného pohoří říční erosí. Kdežto na počátku (1) tekly hlavní podélné toky v osách synklinál, zaujímají posléze (4) podélné toky polohu v osách antiklinál a zbytky spodních částí synklinál tvoří pak nejvyšší místa horských hřbetů. Nastala tudíž inverse reliefu.* (Podle E. DE MARTONNA.)

Obr. 93. *Schematické znázornění postupného rozrušování zvrásněného pohoří říční erosí, při němž v jistém období vývoje nastane inverse reliefu (synklinály tvoří vrcholy horských hřbetů, údolí řek probíhají v osách antiklinál).* (Podle A. K. LOBECKA.)

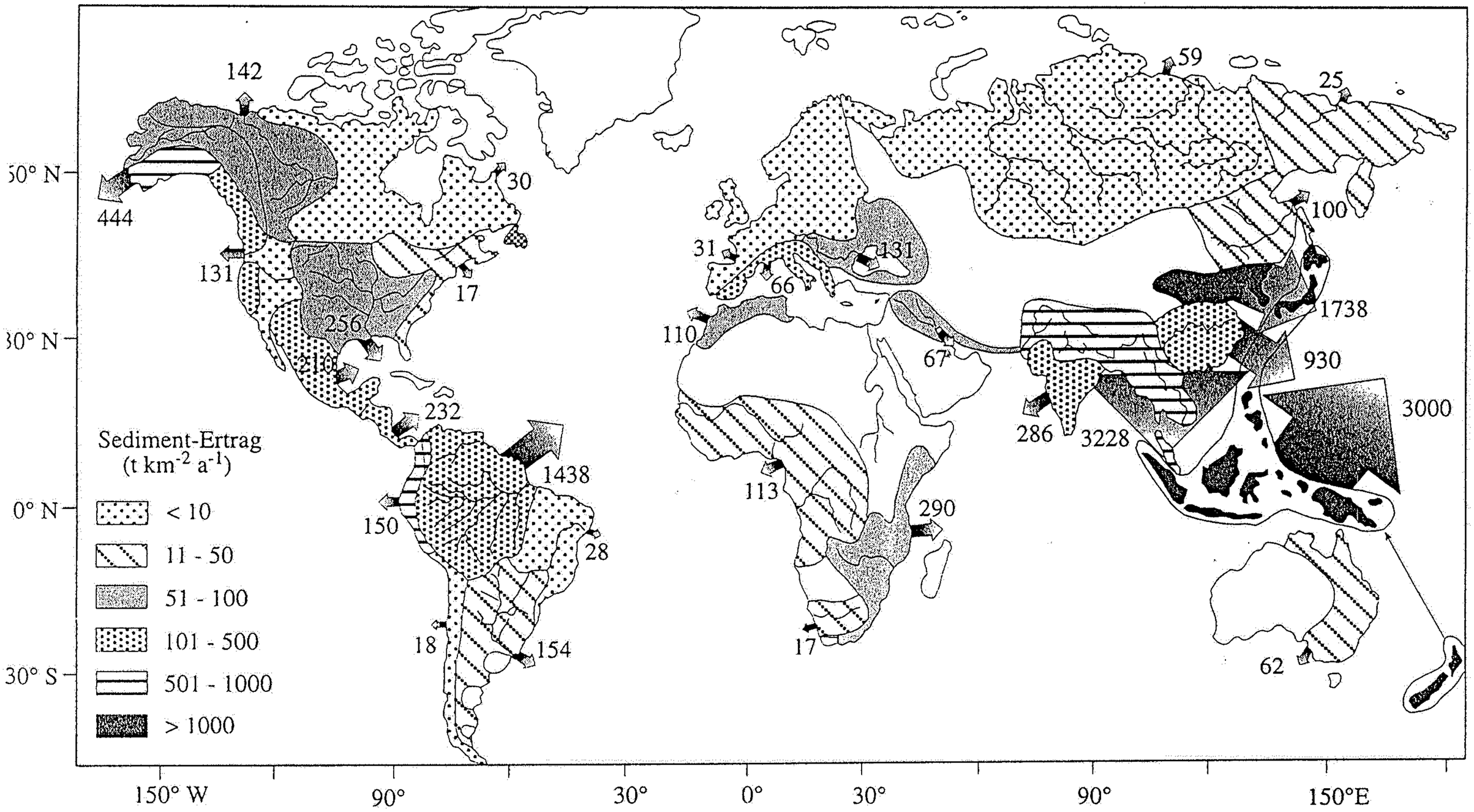

Abb. 5.3
Jährlicher Sediment-Eintrag der Festländer in die Ozeane. Die Breite der Pfeile veranschaulicht die eingebrachte Sedimentmenge, die nebenstehenden Zahlen geben den jährlichen Eintrag in Millionen t. Die flächigen Signaturen bezeichnen den jährlichen Sediment-Ertrag der wichtigsten Einzugsgebiete. Aus der Verteilung der Einzugsgebiete und der Richtung ihrer Entwässerung und damit des Denudationstransportes ergibt sich weiterhin die ungefähre Lage der wichtigsten kontinentalen Wasserscheiden (nach MILLIMAN & MEADE, 1983).

A stream hydrograph plots discharge of a stream against time. In this example rainfall is also shown.

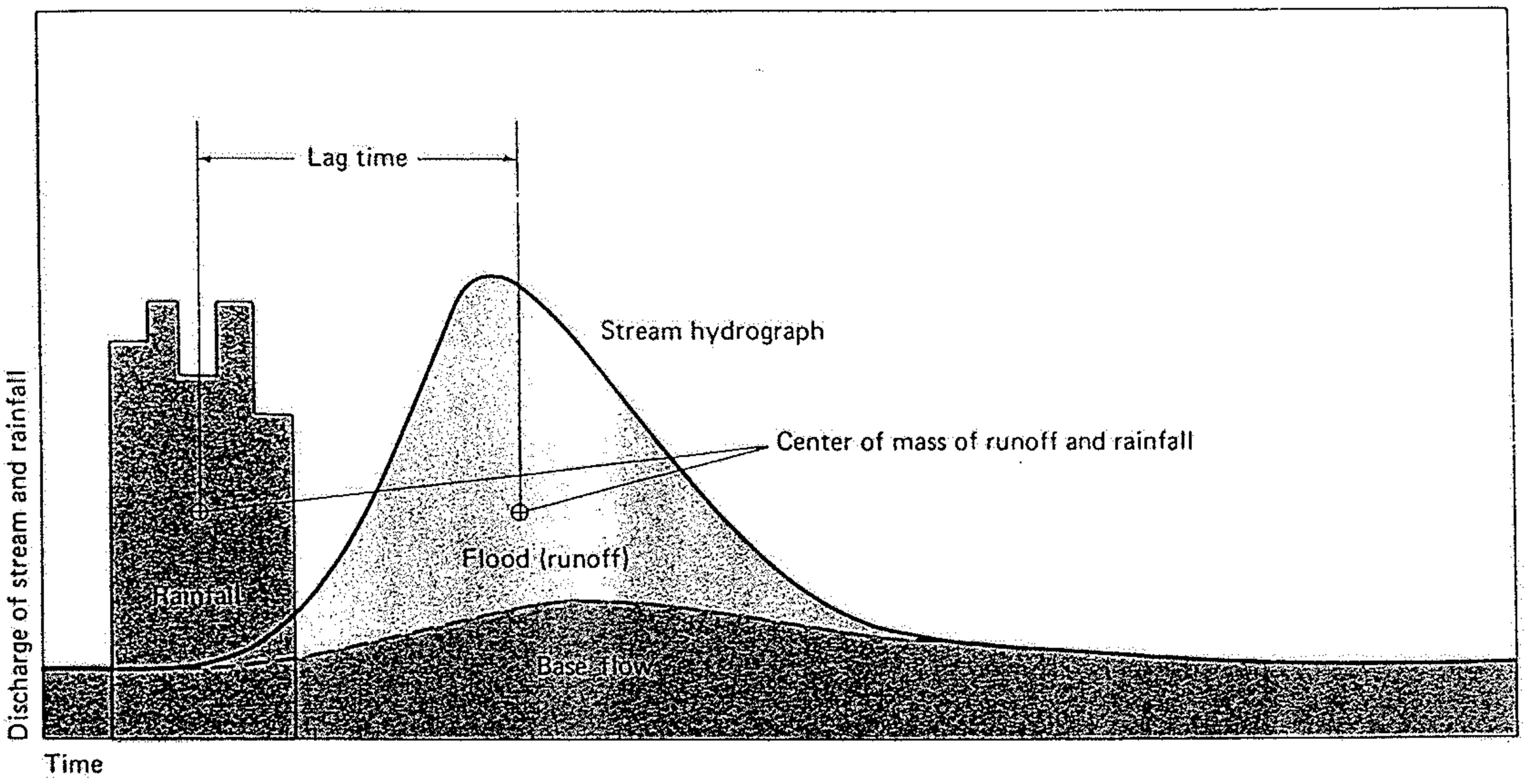

The hydrograph of Figure 13.14 is modified here by flood-control measures which tend to lower the crest of maximum discharge and spread the high water flow over a longer period of time.

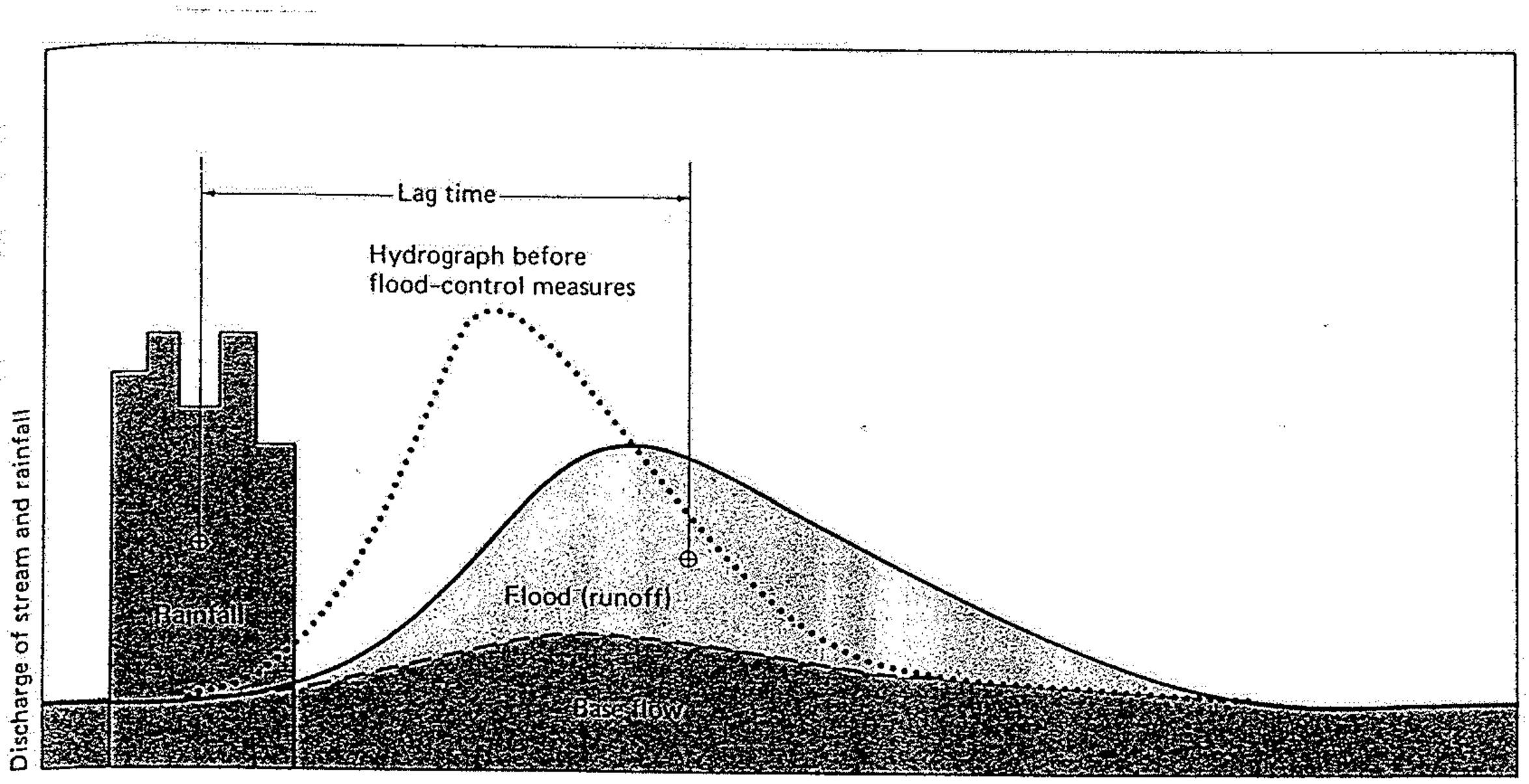

The hydrograph of Figure 13.14 is modified here by urbanization which increases runoff rate and decreases infiltration, thus giving a higher flood crest over a shorter period of time.

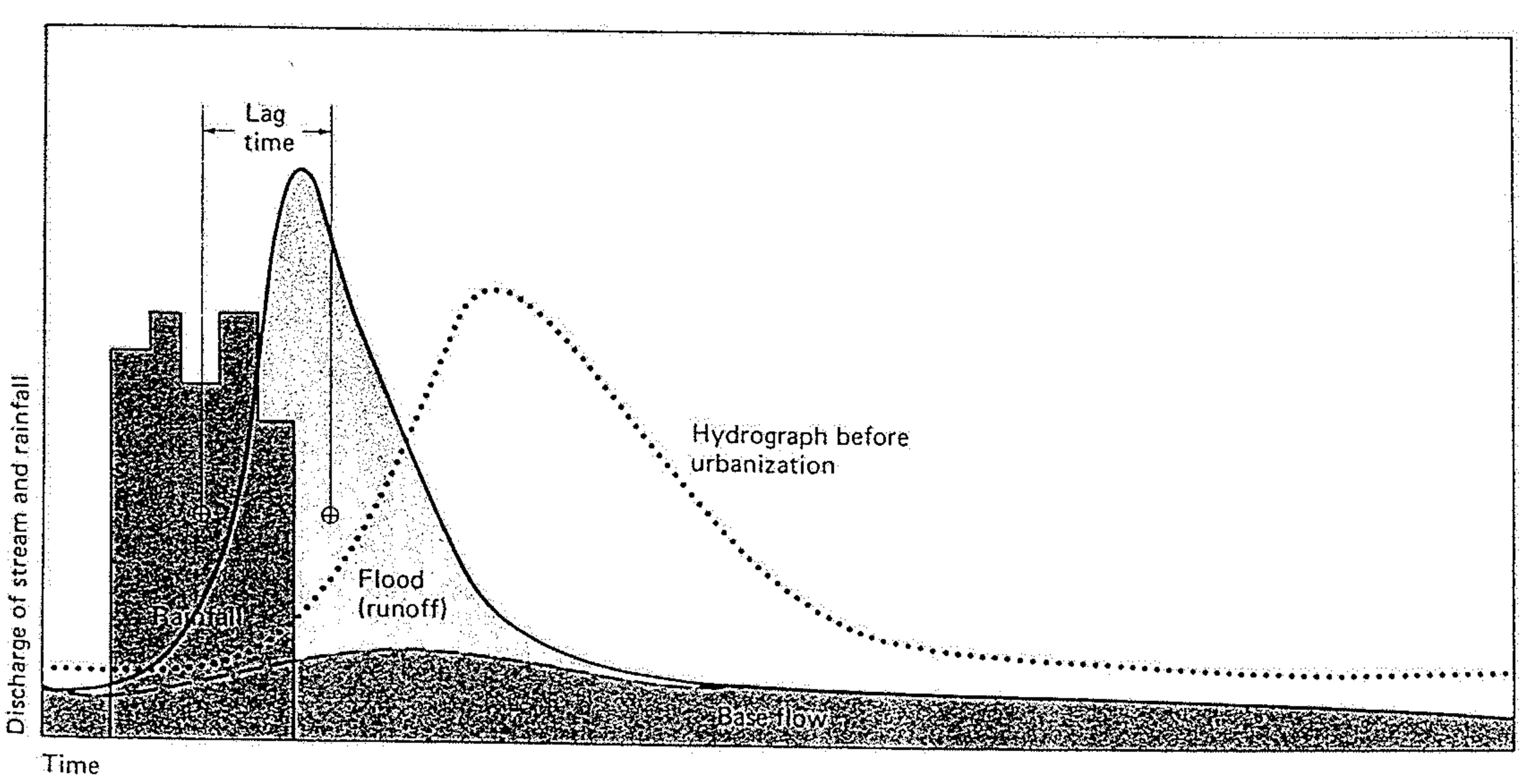

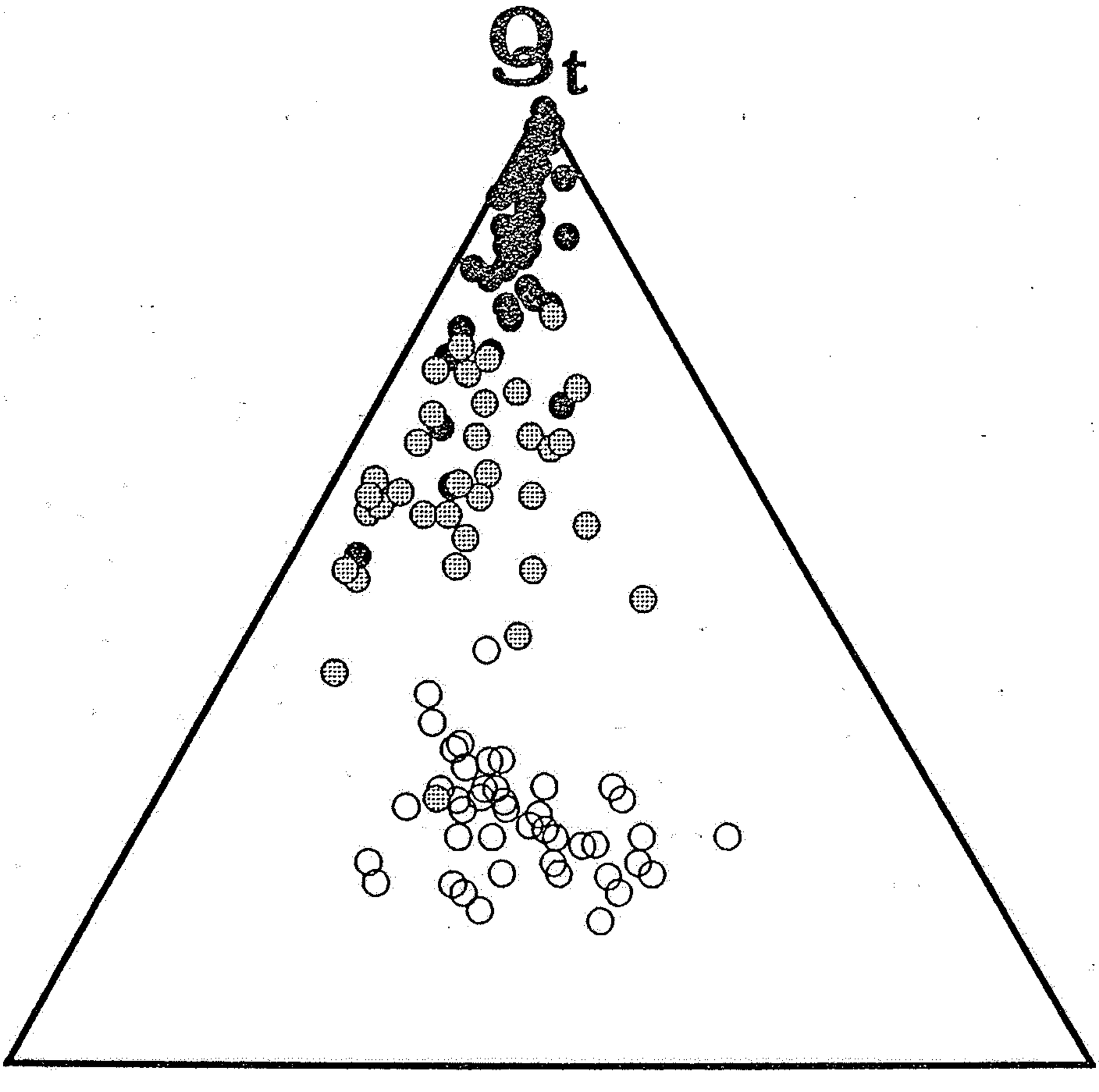

Figure 8.7. Composition of sands derived from granitic rocks in contrasting climatic regimes. Sand compositions are here expressed in terms of the relative proportions of quartz grains (Q_t), feldspar grains (F), and grains consisting of more than one mineral, or lithic fragments (L). These three components adequately describe the composition of most sandstones, and are plotted on a ternary diagram. Ternary diagrams are useful for portraying compositional information in terms of three components, one more component than can be conveniently expressed on most other types of diagrams. The proximity of a point to an apex of the triangle indicates the relative contribution of that component (e.g., pure quartz would plot at the Q_t apex, a 50–50 mixture of quartz and feldspar would plot midway between the Q_t and F apices, and an equal mixture of quartz, feldspar, and lithic fragments would plot at the center of the triangle). Sands produced in semiarid climates (indicated by open circles) are richer in feldspar and lithic fragments than are those from humid temperate climates (indicated by filled gray circles). Sands from tropical climates, indicated by filled black circles, are extremely quartz-rich. (*Source:* Adapted from A. Basu, Petrology of Holocene fluvial sand derived from plutonic source rocks: implications to paleoclimatic interpretation, *Journal of Sedimentary Petrology*, vol. 46, 1976; and M. J. Johnsson, R. F. Stallard, and N. Lundberg, Controls on the composition of fluvial sands froma tropical weathering environment: sands of the Orinoco River drainage basin, Venezuela and Colombia, *Geological Society of America Bulletin*, vol. 103, 1991.)

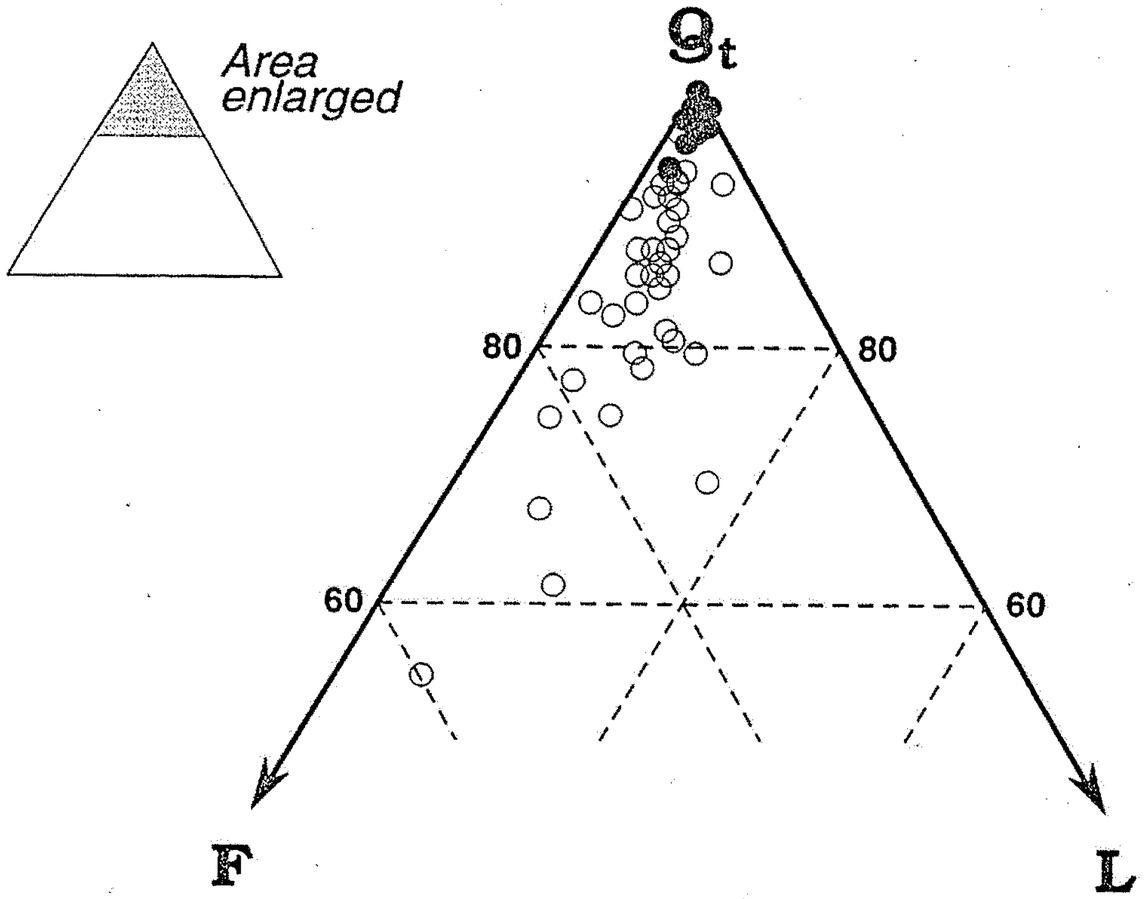

Figure 8.9. Compositions of sands derived from granitic rocks of the Guayana shield, Venezuela, expressed in terms of total quartz, feldspar, and lithic fragments. See Figure 8.7 for an explanation of ternary diagrams and abbreviations. The Guayana shield is divided into two regions of contrasting relief and erosion regime: a northern region of high relief undergoing both transport-and weathering-limited erosion; and a flat southern region experiencing only transport-limited erosion. Sands from rivers draining areas undergoing only transport-limited erosion (indicated by filled circles) are markedly more rich in quartz than are those from regions marked by both transport-and weathering-limited erosion (indicated by open circles). Only the upper (quartz-rich) portion of the ternary diagram is shown. (*Source:* Adapted from M. J. Johnsson, R. F. Stallard, and N. Lundberg, Controls on the composition of fluvial sands from a tropical weathering environment: sands of the Orinoco River drainage basin, *Geological Society of America Bulletin*, vol. 103, 1991.)

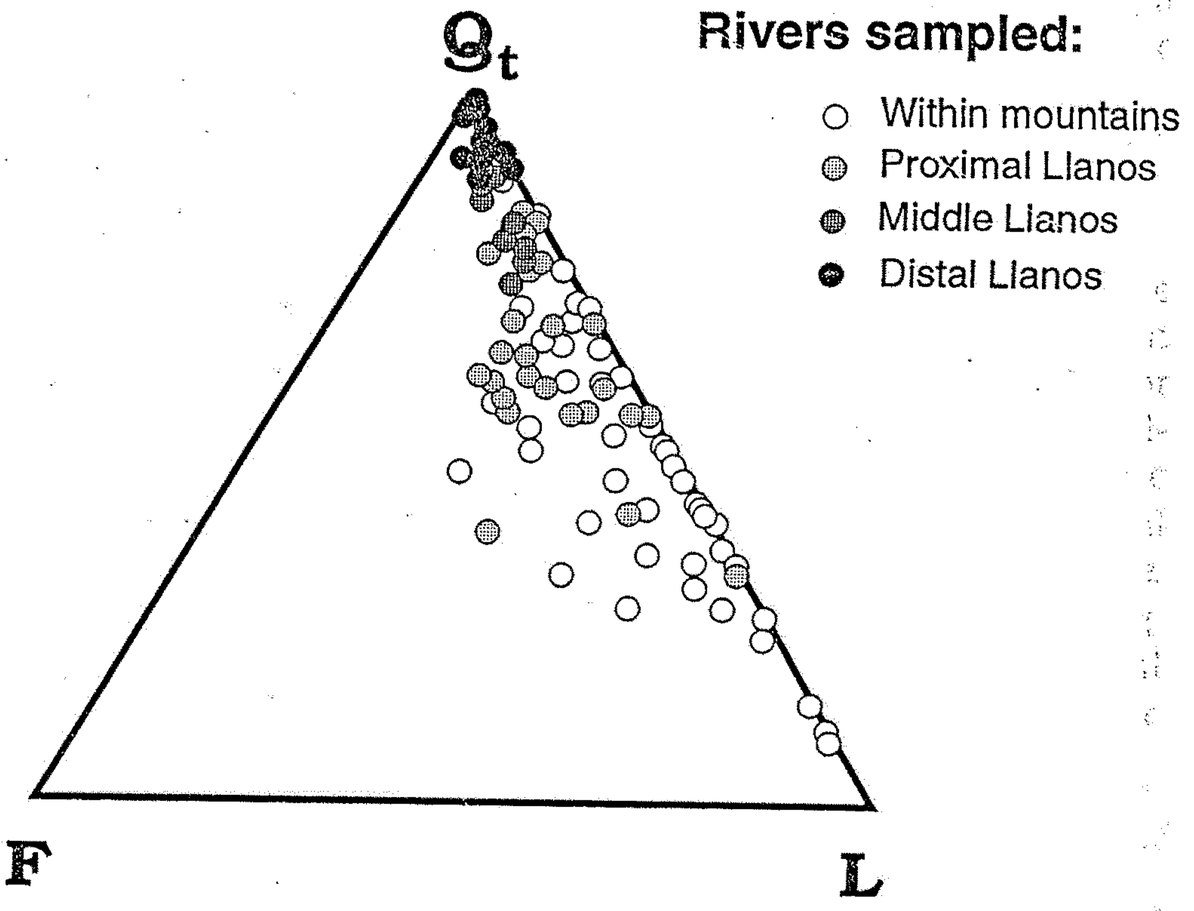

Figure 8.10. Compositions of sands from rivers reworking the broad alluvial plains of the Venezuelan Llanos, expressed in terms of quartz, feldspar, and lithic fragments. See Figure 8.7 for an explanation of ternary diagrams and abbreviations. Sands collected within the mountains where the streams originate are much poorer in quartz than those that have crossed the alluvial plains and reworked the material stored on them. (*Source:* Adapted from M. J. Johnsson, R. F. Stallard, and N. Lundberg, Controls on the composition of fluvial sands from a tropical weathering environment: sands of the Orinoco River drainage basin, *Geological Society of America Bulletin*, vol. 103, 1991.)